UNIVERSITY OF CALIFORNIA,
IRVINE

Investigating Protein Complex Dynamics: Analysis of Cullin-Ring Ligase Machinery through Development of Quantitative Cross-linking Mass Spectrometry Strategies

DISSERTATION

Submitted in partial satisfaction of the requirements
for the degree of

DOCTOR OF PHILOSOPHY

In Biological Sciences

By

Clinton Yu

Dissertation Committee:
Professor Lan Huang, Chair
Professor Todd Holmes
Professor Rongsheng Jin
Professor Feng Qiao

2017

TABLE OF CONTENTS

LIST OF FIGURES ..... **v**
LIST OF TABLES ..... **vii**
ACRONYMS & SYMBOLS ..... **viii**
ACKNOWLEDGMENTS ..... **ix**
CURRICULUM VITAE ..... **x**
ABSTRACT OF THE DISSERTATION ..... **xiv**
CHAPTER 1: Introduction **1**
1.1 Significance of Protein-Protein Interactions **1**
1.1.1 Traditional Methods for PPI Discovery 2
1.1.2 Traditional Methods for Structural Elucidation 3
1.2 Cross-linking Mass Spectrometry as a Tool for Studying PPIs **4**
1.2.1 Chemical Cross-linking Coupled with Affinity-Purification Mass Spectrometry 5
1.2.2 Chemical Cross-linking as a Hybrid Structural Methodology 6
1.2.3 Challenges in Cross-linking Mass Spectrometry Studies 7
1.3 The Ubiquitin-Proteasome System **9**
1.4 Cullin-Ring E3 Ubiquitin Ligases (CRLs) **13**
CHAPTER 2: Development of Isotope-coded, MS-cleavable Cross-linkers for Elucidating Protein Structures through Quantitative XL-MS **15**
2.1 Summary **15**
2.2 Introduction **16**
2.3 Experimental Procedures **19**
2.3.1 Materials and Reagents 19
2.3.2 Synthesis and Characterization of d_0-DMDSSO and d_{10}-DMDSSO 19
2.3.3 Cross-linking of Synthetic Peptides with d_0- and d_{10}-DMDSSO. 20
2.3.4 Cross-linking of Cytochrome C with d_0- and d_{10}-DMDSSO 20
2.3.5 Liquid Chromatography-Multistage Tandem Mass Spectrometry (LC-MS^n) 21
2.3.6 Data Analysis of Cross-linked Peptides 21
2.4 Results & Discussion **22**
2.4.1 Design and Synthesis of New Isotope-coded DSSO Derivatives 22
2.4.2 Expected CID Fragmentation Patterns of d_0- and d_{10}-DMDSSO Cross-linked Peptides 23
2.4.3 Characterization of DMDSSO Cross-linked Model Peptides by MS^n Analysis 25

2.4.4 Characterization of DMDSSO Cross-linked Cytochrome C by MS^n Analysis 27
2.4.5 Detection of d_0/d_{10}-DMDSSO Cross-linked Peptide Pairs 30
2.4.6 Quantitation of d_0-/d_{10}-DMDSSO Cross-linked Peptides 33
2.5 Conclusion 35
CHAPTER 3: Gln40 deamidation Blocks Structural Reconfiguration and Activation of SCF Ubiquitin Ligase Complex by Nedd8 39
3.1 Summary 39
3.2 Introduction 40
3.3 Experimental Procedures 42
3.3.1 Materials and Reagents 42
3.3.2 Preparation of Cul1-Rbx1 Protein Complexes 43
3.3.3 Ubiquitination Assays 44
3.3.4 DMDSSO Cross-linking and Digestion of Cul1-Rbx1 Complexes 45
3.3.5 Liquid Chromatography-Multistage Tandem Mass Spectrometry (LC MS^n) 45
3.3.6 Data Analysis, Identification and Quantification of Cross-linked Peptides 46
3.4 Results & Discussion 47
3.4.1 Reconstitution of SCF E3 Activity with Intact Proteins 47
3.4.2 Quantitative XL-MS strategy 50
3.4.3 Mapping XL-MS Data to Cul1-Rbx1 Complexes 53
3.4.5 Quantitation of DMDSSO Cross-linked Peptides 57
3.4.6 Comparison of Cul1-Rbx1 and Nedd8~Cul1-Rbx1 complexes 59
3.4.7 Comparison of Nedd8~ and Nedd8(Q40E)~Cul1-Rbx1 complexes 65
3.5 Conclusion 68
CHAPTER 4: Developing a Multiplexed Quantitative Cross-linking Mass Spectrometry Platform for Comparative Structural Analysis of Protein Complexes 72
4.1 Summary 72
4.2 Introduction 73
4.3 Experimental Procedures 76
4.3.1 Materials and Reagents 76
4.3.2 DSSO Cross-linking of Cytochrome C 76
4.3.3 TMT2 labeling of Cross-linked Cytochrome C Peptides 77
4.3.3 Liquid Chromatography-Multistage Tandem Mass Spectrometric (LC-MS^n) Analysis 77
4.3.4 Identification and Quantitation of TMT2 Labeled DSSO Cross-linked Peptides 78
4.4 Results and Discussion 79

4.4.1 Development of A New Multiplexed QXL-MS Strategy 79
4.4.2 Fragmentation of TMT-labeled, DSSO-cross-linked peptides 81
4.4.3 MS^n Analysis of TMT-labeled Cytochrome C Cross-linked Peptides 84
4.5 Conclusion 89
CHAPTER 5: Describing the Molecular Mechanisms of Ubiquitination Inhibition through Targeting of E2 Ubiquitin-Conjugating Enzymes 91
5.1 Summary 91
5.2 Introduction 92
5.3 Experimental Procedures 95
5.3.1 Materials and Reagents 95
5.3.2 Preparation of Cullin-RING Protein Complexes 96
5.3.3 Preparation of Cdc34 and Ub-charged Cdc34 96
5.3.4 Preparation of Samples for Analysis of Cdc34-SCF (E2-E3) Intermediates 97
5.3.5 Preparation of Samples for Analysis of CC0651-induced Inhibition of Cdc34 98
5.3.6 Liquid Chromatography-Multistage Tandem Mass Spectrometric ($LC-MS^n$) Analysis 99
5.3.7 Identification and Quantitation of Cross-linked CRL Peptides 100
5.4 Results and Discussion 101
5.4.1 Application of QMIX to Probe Topologies of Various Cdc34-CRL1 Complexes 101
5.4.2 Applying QMIX to Study the CC0651-dependent Inhibition of Cdc34 108
CHAPTER 6: Conclusions and Final Remarks 117
Bibliography 128

LIST OF FIGURES

Figure 2-1. Chemical synthesis schemes for d_0- and d_{10}-DMDSSO..... 20
Figure 2-2. Characteristic MS^2 fragmentation patterns for DMDSSO cross-linked peptides. 23
Figure 2-3. MS^n analyses of d_0- and d_{10}-DMDSSO inter-linked Ac-Myelin peptides. 25
Figure 2-4. MS^3 analyses of d_0- and d_{10}-DMDSSO inter-linked Ac-Myelin peptides. 26
Figure 2-5. General workflow for the analysis and identification of d_0/d_{10} DMDSSO cross-linked cytochrome C peptides..... 28
Figure 2-6. MS^n analysis of d_0/d_{10}-DMDSSO inter-linked cytochrome C peptides..... 28
Figure 2-7. MS^2 spectra of d_0/d_{10}-DMDSSO intra-link and dead-end cytochrome C peptides... 29
Figure 2-8. Examples of d_0/d_{10}-DMDSSO cross-link MS^1 quantitation..... 31
Figure 2-9. Cytochrome C DMDSSO cross-linking map. 32
Figure 2-10. Quantitative analysis of d_0/d_{10}-DMDSSO cross-linked cytochrome C peptides. ... 35

Figure 3-1. Biochemical assays for ubiquitin-ligase activity and general quantitative XL-MS experimental workflow. 49
Figure 3-2. d_0- and d_{10}-DMDSSO structure and cross-linking efficiency. 50
Figure 3-3. MS^n analysis of d_{10}-DMDSSO inter-linked peptides. 52
Figure 3-4. Mapping cross-link data onto current structural models of Cul1-Rbx1 complexes.. 54
Figure 3-5. Quantitative analysis of K-K linkages to determine neddylation-dependent structural changes in the Cul1-Rbx1 complex. 60
Figure 3-6. Quantitative analysis of intra-subunit Cul1 linkages to determine neddylation-dependent structural changes in the Cul1-Rbx1 complex..... 62
Figure 3-7. Describing the structural dynamics of various Cul1-Rbx1 complexes using QXL-MS. 66
Figure 3-8. Elucidation of structural dissimilarities between wt- and mt-neddylated Cul1-Rbx1 complexes by quantitative analysis of Cul1-Nedd8 inter-links. 67
Figure 3-9. Proposed model for Nedd8-dependent conformational changes of the Cul1-Rbx1 complex..... 70

Figure 4-1. The general MS^n analysis workflow for identifying and quantifying TMT-labeled, DSSO cross-linked peptides. 80
Figure 4-2. MS^n analysis of a selected TMT-labeled, DSSO cross-linked cytochrome c peptide. 82
Figure 4-3. Three MS^n acquisition methods utilized for analyzing TMT-labeled, DSSO cross-linked peptides. 85
Figure 4-4. Quantitation of TMT-labeled, DSSO cross-linked peptides from five premixed samples. 87
Figure 4-5. Distribution of raw cross-link quantitative ratios across five input mixings. 89

Figure 5-1. General workflow for QMIX sample preparation and MS^n analysis. 102
Figure 5-2. SDS-PAGE separation of cross-linked Cul1-Rbx1 and Cdc34 complexes. 103
Figure 5-3. Quantitative Analysis on the effect of Cul1 Neddylation on Structure of Cul1-Rbx1-Ub-Cdc34. 105
Figure 5-4. Quantitative Analysis on the effect of Ub-charging of Cdc34 on Structure of Nedd8~Cul1-Rbx1-Cdc34. 107
Figure 5-5. SDS-PAGE separation of cross-linked Cul4A- and Cul1-Cdc34 complexes. 108
Figure 5-6. Comparison of quantitative data for Cul1-Cdc34 cross-links obtained through single band and multi-band extraction. 111
Figure 5-7. Relative abundances of inter- and intra-subunit cross-links identified in CRL1-Cdc34 complexes before and after CC0651 modulation. 112
Figure 5-8. Relative abundances of inter- and intra-subunit cross-links identified in CRL4A-Cdc34 complexes before and after CC0651 modulation. 115
Figure 5-9. Cdc34-Ub cross-links mapped hCdc34-Ub-CC0651. 115

LIST OF TABLES

Table 2-1. Summary of Cytochrome C Cross-links Identified by d_0- and d_{10}-DMDSSO. 36

Table 3-1. Summary of CRL Cross-links Identified by d_0- and d_{10}-DMDSSO 58

ACRONYMS & SYMBOLS

AP-MS	Affinity purification mass spectrometry
CID	Collision-induced dissociation
CRL	Cullin-RING E3 ubiquitin ligase
^{CTD}	C-terminal domain
DMDSSO	Dimethyl succinimidyl sulfoxide
DSSO	Succinimidyl sulfoxide
HB	His-Biotin (affinity tag)
HCD	Higher-energy collisional dissociation
HDX	Hydrogen/deuterium exchange
LC-MS	Liquid chromatography-coupled mass spectrometry
MS	Mass spectrometry (field) or mass spectrometer (instrument)
MS^n	Multistage mass spectrometric analysis
m/z	Mass-to-charge ratio
NMR	Nuclear magnetic resonance
^{NTD}	N-terminal domain
PPI	Protein-protein interaction
QMIX	Quantitation of multiplexed, isobaric-labeled cross (x)-linked peptides
QTAX	Quantitative analysis of tandem-affinity purified cross-linked (x) proteins
QXL-MS	Quantitative cross-linking mass spectrometry
SCF	Skp1-Cul1-F-box E3 ligase
SILAC	Stable isotope labeling with amino acids in cell culture
SPS	Synchronous Precursor Selection
TAP	Tandem affinity purification
TMT	Tandem Mass Tags^{TM}
UPS	Ubiquitin-proteasome system
XL-MS	Cross-linking mass spectrometry

ACKNOWLEDGMENTS

First and foremost, I would like to thank my advisor, Prof. Lan Huang, for the years of support and direction during my time here as a graduate student at UCI. I could not have become the person (or the scientist) that I am today without your guidance, and for that I will always be grateful. It was truly fortunate for me to have had the opportunity to work in your lab.

I would also like to say thanks to the members of the Huang Lab, past and current: Dr. Robyn Kaake and Dr. Atet Kao for their instruction during the end of their time here, Yingying Yang, Dr. Sherry Wang, Alex Huszagh, and Craig B. Gutierrez for their contributions to not only my work but to the progress of the lab. I really appreciate your help over the years.

For years of fruitful collaborations and their contributions to the design and organic synthesis of our cross-linking reagents, I would like to thank Prof. Scott D. Rychnovsky and the members of his lab: Dr. Wynne Kandur, Dr. Eric J. Novitsky, and Sarah A. Block.

For their great contributions to our successful collaborations, including purification of proteins and scientific knowledge of the ubiquitin field, I would like to thank Prof. Ning Zheng and the members of his lab at the University of Washington, Howard Hughes Medical Institute, Department of Pharmacology: Dr. Haibin Mao, Dr. Xiaobo Tang.

For their continued support of Protein Prospector, which we have used as our primary protein database search engine, I would like to thank Prof. Alma Burlingame and the members of his lab at UCSF, Mass Spectrometry Facility: Dr. Robert Chalkley, Dr. Shenheng Guan, Dr. Peter Baker. Thanks for putting up with all my e-mails request for the things we needed.

I would like to thank the team at Thermo Fisher Scientific as well as their Field Service Engineers: Dr. Rosa Viner—for her hard work and dedication to always getting us the best data possible, Tonya Pekar Second, Rollie Singh, and Anjum Khan for their assistance in maintenance our mass spectrometer and LC when I was at the end of my wits.

To my committee members: Prof. Todd Holmes, Prof. Feng Qiao, and Prof. Rongsheng Jin—thank you for taking the time to read this thesis and provide advice over the years. Your input has been invaluable and I wish I would have sought out your guidance more frequently.

I would also like to thank Prof. Feng Qiao and the members of his lab (Jinqiang Liu, Xihan Hu, and J.K. Kim) for the years of collaborative efforts to expand the use of cross-linking mass spectrometry. Your insight has been greatly appreciated.

Thank you to all my collaborators over the years; it has been a pleasure to work with you and learn about the various aspects of science I would have missed along the way.

To the friends in our department that I've made along the way. Dr. Tobias X. Dong, Dr. Logan Roberts, and Lisa S. Baik, I want to say a big thanks. We've gone through some stressful times impacted by the work we do, but I appreciate the mutual support we've had for one another.

And last, but certainly not least, I would like to thank my family for their continued support during my time as a student. Thank you for pushing me to be who I am today and always being there when I needed the help.

This work was supported by the National Institutes of Health grants RO1GM74830-06A1 and R21CA161807 to Prof. Lan Huang, R01GM106003 to Prof. Lan Huang and Prof. Scott D. Rychnovsky, and R01AI099190-01 to Prof. Haoping Liu. Thank you as well to ACS Publications and the Nature Publishing Group for their permission to adapt my authored works for portions of Chapters 2 and 4 originally published in Analytical Chemistry, and Chapter 3 originally published in Nature Communications.

CURRICULUM VITAE

Clinton Yu

26522 Laurel Crest Dr.
Laguna Hills, CA 92653
Cell: (949) 302-8858
E-mail: 7yuc12@gmail.com

EDUCATION

2012-2017 Graduate program in Physiology and Biophysics, School of Medicine, University of California, Irvine, Irvine, CA
Thesis Title: Investigating Protein Complex Dynamics: Analysis of Cullin-Ring Ligase Machinery through Development of Quantitative Cross-linking Mass Spectrometry Strategies
Advisor: Prof. Lan Huang

2007-2011 **BSc. Degree in Biology**, University of California, Irvine, Irvine, CA
BSc. Degree in Chemistry, University of California, Irvine, Irvine, CA

RESEARCH EXPERIENCE

2012-2017 Graduate Research Assistant, Department of Physiology & Biophysics

University of California-Irvine, Irvine, CA

- Involved in the development of a novel *in vivo* cross-linking platform to define human interactomes in living cells using a novel multifunctional cross-linker (Azide-A-DSBSO) that allows the capture of protein interactions, enrichment of cross-linked peptides, and facile identification of protein interaction interfaces.
- Developed a novel quantitative cross-linking mass spectrometry approach based on new isotope-coded MS-cleavable homo-bifunctional cross-linkers: d_0- and d_{10}-labeled dimethyl disuccinimidyl sulfoxide (DMDSSO), for deciphering structural dynamics of protein complexes under different physiological conditions.
- Employed d_0/d_{10}-DMDDSO cross-linking strategy to quantify the neddylation-dependent structural changes of SCF complexes underlying substrate ubiquitination.
- Involved in the development and application of a novel strategy integrating cross-linking mass spectrometry and evolutionary analysis (MICro-MS) to study topologies and isolate separation-of-function mutations in shelterin (telosome) complexes.
- Developed a novel multiplexed quantitative cross-linking platform (QMIX) for

simultaneous comparisons of protein complex topologies in various states.

- Applied QMIX to study the E2-E3 interactions between Cdc34-SCF Cdc34-CRL4A , as well as the structural effect of CC0651 inhibition of Cdc34 on E2-E3 topology.
- Developed novel MS-cleavable cross-linking mass spectrometry platforms and reagents exploring various functionalities (e.g. residue reactivity, reagent length, MS-labile functional groups, enrichment strategies) to provide complementary information to existing technologies for improved integrative 3D modeling.

2009-2011 Undergraduate Researcher, Department of Physiology & Biophysics

University of California-Irvine, Irvine, CA

- Understanding the function and regulation of the 26S proteasome structure upon oxidative stress using mass spectrometry-based and biochemical approaches

---

TECHNICAL SKILLS

- Expert in proteomic techniques including:
  - Peptide sequencing and protein identification by MS
  - SILAC-based and label-free quantitation
  - Identification of post-translational modifications (e.g., phosphorylation, ubiquitination)
  - Characterization and development of novel reagent technologies for expanding the cross-linking mass spectrometry toolkit.
  - Application of cross-linking mass spectrometry to study protein interactions, topologies, and structural dynamics of multi-subunit complexes.
- Expert in peptide separation by liquid chromatography (SCX, RP-HPLC).
- Expert in the maintenance and operation of the lab's Thermo Scientific LTQ Orbitrap XL mass spectrometer and Thermo Scientific Easy-nLC 1000.
- Expert in biochemical methods including protein purification (tandem affinity, denaturing, native), SDS-PAGE, and immunoblot analysis.
- Experienced with *in vitro* enzymatic assays (e.g. proteasome activity assays)

PEER-REVIEWED PUBLICATIONS

1. Wang X*, Cimermancic P*, **Yu C***, Schweitzer C, Chopra N, Engel JL, Greenberg CH, Huszagh A, Beck F, Sakata S, Yang YY, Novitsky EJ, Leitner A, Nanni P, Kahraman A, Guo X, Dixon JE, Rychnovsky SD, Aebersold R, Baumeister W, Sali A and Huang L. Molecular Details Underlying Dynamic Structures and Regulation of the Human 26S Proteasome. *Mol Cell Proteomics* (2017). 16(5):840-854.

2. **Yu C**, Huszagh A, Viner R, Novitsky EJ, Rychnovsky SD, Huang L. Developing a Multiplexed Quantitative Cross-linking Mass Spectrometry Platform for Comparative Structural Analysis of Protein Complexes. *Anal Chem* (2016). 18;88(20):10301-1030

3. Gutierrez CB*, **Yu C***, Novitsky EJ, Huszagh AS, Rychnovsky SD, Huang L. Developing an Acidic Residue Reactive and Sulfoxide-Containing MS-Cleavable Homobifunctional Cross-Linker for Probing Protein-Protein Interactions. *Anal Chem* (2016). 88(16):8315-22

4. Fang L, Chen, D, **Yu C**, Li H, Brocato J, Huang L, Jin C. Mechanisms Underlying Acrolein-Mediated Inhibition of Chromatin Assembly. *Mol Cell Biol* (2016). 36:2995–3008.

5. **Yu C**, Yang Y, Wang X, Guan S, Fang L, Liu F, Walters KJ, Kaiser P, Huang L. Characterization of Dynamic UbR-Proteasome Subcomplexes by In vivo Cross-linking (X) Assisted Bimolecular Tandem Affinity Purification (XBAP) and Label-free Quantitation. *Mol Cell Proteomics* (2016). 15(7):2279-92

6. **Yu C**, Mao H, Novitsky EJ, Tang X, Rychnovsky SD, Zheng N, Huang L. Gln40 deamidation blocks structural reconfiguration and activation of SCF ubiquitin ligase complex by Nedd8. *Nature Communications* (2015). 6:10053

7. Liu J*, **Yu C***, Hu X, Kim JK, Bierma JC, Jun HI, Rychnovsky SD, Huang L, Qiao, F. Dissecting Fission Yeast Shelterin Interactions via MICro-MS Links Disruption of Shelterin Bridge to Tumorigenesis. *Cell Reports* (2015). 12(12):2169-80

8. Jiang L, Kosenko A, **Yu C**, Huang L, Li X, Hoshi N. Activation of m1 muscarinic acetylcholine receptor induces surface transport of KCNQ channels through a CRMP-2-mediated pathway. *J Cell Sci* (2015). 128: 4235-4245

9. Burke AM, Kandur W, Novitsky EJ, Kaake RM, **Yu C**, Kao A, Vellucci D, Huang L, Rychnovsky SD. Synthesis of two new enrichable and MS-cleavable cross-linkers to define protein-protein interactions by mass spectrometry. *Org Biomol Chem* (2015). 13(17):5030-7.

10. Kaake RM, Wang X, Burke A, **Yu C**, Kandur W, Yang Y, Novitsky EJ, Second T, Duan J, Kao A, Guan S, Vellucci D, Rychnovsky SD, Huang L. A new in vivo cross-linking mass spectrometry platform to define protein-protein interactions in living cells. *Mol Cell Proteomics* (2014). 13(12):3533-43.

11. **Yu C**, Kandur W, Kao A, Rychnovsky S, Huang L. Developing new isotope-coded mass spectrometry-cleavable cross-linkers for elucidating protein structures. *Anal Chem* (2014). 86(4):2099-106.

12. Kaake RM, Kao A, **Yu C**, Huang L. Characterizing the dynamics of proteasome complexes by proteomics approaches. *Antioxid Redox Signal* (2014). 21(17):2444-56.

These authors* made equal contribution towards these publications.

CONFERENCE PRESENTATIONS

1. **Yu C**, Mao H, Huszagh A, Viner RL, Novitsky EJ, Rychnovsky SD, Zheng N, Huang L. **Defining the Structural Dynamics of Cullin-RING Ligase Complex Using a Novel Multiplexed Quantitative Cross-linking Mass Spectrometry Strategy.** *65th ASMS Conference for Mass Spectrometry and Allied Topics. Indianopolis, Indiana. USA. 2017. (**Poster**)*

2. **Yu C**, Wang X, Viner RL, Huszagh A, Novitsky EJ, Second T, Rychnovsky SD, Huang L. **Developing a New Quantitative Cross-linking Mass Spectrometry (XL-MS) Strategy to Define *In Vivo* Structural Dynamics of Protein Complexes**. *64th ASMS Conference for Mass Spectrometry and Allied Topics. San Antonio, TX. USA. 2016. (**Selected Oral Presentation**)*

3. **Yu C,** Mao H, Huszagh A, Viner RL, Novitsky EJ, Second T, Rychnovsky SD, Huang L. **Developing a Novel Multiplexed Quantitative Cross-linking Mass Spectrometry Strategy to Define the Structural Dynamics of Cullin-RING Ligase Complex.** *64th ASMS Conference for Mass Spectrometry and Allied Topics. San Antonio, TX. USA. 2016. (**Poster**)*

4. **Yu C**, Mao H, Novitsky E, Rychnovsky SD, Zheng N, Huang L. **Understanding the Neddylation-dependent Structural Changes of Cul1-Rbx1 using Quantitative Cross-linking Mass Spectrometry.** *US HUPO 11th Annual Conference. Tempe, AZ. USA. 2015. (**Selected Oral Presentation**)*

5. **Yu C**, Mao H, Novitsky E, Guan, S, Rychnovsky, SD, Zheng N, Huang L. **Defining Structural Dynamics of Protein Complexes Using Quantitative Cross-linking Mass Spectrometry**. *62rd ASMS Conference for Mass Spectrometry and Allied Topics. Baltimore, MD. USA. 2014. (**Poster**)*

6. **Yu C**, Kandur W, Kao A, Rychnovsky SD, Huang L. **Development of Stable Isotope-Labeled CID-cleavable Cross-linkers for Structural Characterization of Protein Complexes**. *61st AMS Conference for Mass Spectrometry and Allied Topics. Minneapolis, MN. USA. 2013. (**Poster**)*

PROFESSIONAL SOCIETY MEMBERSHIPS

- American Society of Mass Spectrometry
- US HUPO (Human Proteome Organization)

ABSTRACT OF THE DISSERTATION

Investigating Protein Complex Dynamics: Analysis of Cullin-Ring Ligase Machinery through Development of Quantitative Cross-linking Mass Spectrometry Strategies

By

Clinton Yu

Doctor of Philosophy in Biomedical Sciences

University of California, Irvine, 2017

Professor Lan Huang, Chair

Protein assemblies represent the workhorses of the cell, forming the basis of all cellular processes. Their biological roles are intimately associated with their topologies, making the structural elucidation of proteins and protein complexes a critical requirement to understanding their function. While traditional structural biology approaches have greatly contributed to our current understanding of protein structure, they are ill-suited for analyzing the conformational dynamics associated with heterogenous protein complexes and their protein-protein interactions (PPIs). As a result, there is a growing demand for the development of new structural approaches to elucidate the impact of protein dynamics on the regulation of integral biological processes required for cell homeostasis. In particular, cross-linking mass spectrometry (XL-MS) has arisen in recent years as a popular hybrid structural technique for the topological determination of conformationally and compositionally heterogenous protein complexes. However, most studies utilizing cross-linking thus far have been limited to the determination of static protein structures.

Here, I focus on the development and application of quantitative cross-linking mass spectrometry (QXL-MS) strategies to determine how conformational dynamics of cullin-RING ligases (CRLs) dictate and regulate their ubiquitinating activity. Proteasomal dysregulation has been associated with a wide range of human pathologies, from diabetes and various forms of cancer to autoimmune and neurodegenerative disorders. As a result, the PPIs associated with CRL assemblies represent potential targets for therapeutic intervention. A comprehensive understanding of E3 ligase structure and conformational dynamics is critical for the development of pharmacological drugs that selectively inhibit or upregulate their function. However, such heterogenous assemblies are notoriously difficult to study using traditional structural biology techniques.

While this thesis focuses on the application of quantitative XL-MS strategies to study cullin-RING ligase machinery, these platforms represent versatile methodologies that can be universally employed for structural studies on a wide range of protein systems.

CHAPTER 1: Introduction

1.1 Significance of Protein-Protein Interactions

Proteins are the primary actors responsible for carrying out the biological functions necessary to maintain cell homeostasis. However, they seldomly act alone, rather in conjunction with other proteins through protein-protein interactions (PPIs) [1]. These interactions can be strong or weak, but are fundamentally characterized as being stable or transient [2]. Stable interactions often give rise to multi-protein complexes, macromolecular entities capable of performing sophisticated functions more diverse than the sum of its individual parts. Transient interactions typically effect regulatory changes in their protein participants, effectively modulating the assembly, structure and function of protein complexes. As a result, these macromolecular complexes readily dissociate and associate in response to environmental cues and stimuli to maintain the intricate equilibria necessary for cell viability [2]. The actions of PPIs are crucial for the diverse biochemical and signaling cascades that encompass all biological processes [3].

Due to their central role in cell biology, disruptions of endogenous protein-protein interactions can have deleterious consequences and are often associated with human diseases and cancers [3-8]. In recent years, a steadily increasing number of reports have demonstrated that targeting and modulating PPIs via their protein interaction surfaces represents a paradigm for drug therapy [9-15]. To this end, a comprehensive characterization of protein complex interaction networks, along with identification of their specific interaction interfaces, is a crucial necessity for identifying potential molecular targets for mechanism-driven drug discovery.

1.1.1 Traditional Methods for PPI Discovery

Common methodologies for identifying protein-protein interactions include yeast two-hybrid (Y2H) [16, 17], phage display, fluorescence complementation, co-immunoprecipitation (co-IP), and affinity purification (AP), of which the lattermost two strategies are often coupled with mass spectrometry (MS). Due to a recent surge of development in mass spectrometric technology and improvements in biochemical protocols and bioinformatics tools, affinity purification-mass spectrometry (AP-MS) has become a standard methodology utilized to identify protein-protein interactions at the systems level [18-21]. In comparison to other approaches, affinity purification permits the capture of proteins of interest and their interacting partners within an environment that mimics their physiological conditions. Furthermore, while other techniques are limited by the number of interactions that can be screened simultaneously, AP-MS experiments are capable of providing rich datasets of information that can be utilized to generate networks of diverse protein interactions. In this respect, the speed, sensitivity, and versatility offered by proteomic strategies makes AP-MS the optimal methodology for mapping proteome-wide interactome networks [22-25].

Despite the widespread success of AP-MS strategies to study protein-protein interactions, there are several drawbacks to this approach, including non-specific binding of proteins, loss of weak/transient interactions, and the potential reorganization of proteins and protein interactions during the sample preparation process. The unavoidable co-purification of background proteins through non-specific binding to the solid matrix is typically addressed through stringent wash steps as part of the purification process (e.g. salts and detergents). However, harsher purification conditions can also result in the undesirable loss of weak or transient interactions, perturbing the balance between removing background proteins and preserving *bona fide* interactions. Various

strategies have been developed to remove the contaminants from the sample prior to MS analysis. One popular strategy to reduce non-specific binding is employing tandem affinity tags (e.g. TAP, GS-TAP, His-Bio(HB)) which permit multiple enrichment steps during the purification procedure [26-29]. Each subsequent purification removes contaminant proteins that bind nonspecifically to the previous solid support, on the premise that resins attract different background proteins. While TAP (tandem affinity purification)-based strategies have been shown to significantly reduce background proteins, the increase in procedural steps can also result in the loss of weak but biologically relevant interactions. As a result, other strategies have been developed to tease apart true interactor from nonspecific proteins.

1.1.2 Traditional Methods for Structural Elucidation

Structural biology techniques have been utilized for decades to visualize the architectures of macromolecular protein assemblies, greatly contributing to the mechanistic understanding of their function. To date, the most broadly employed methods for the elucidation of protein structures are x-ray crystallography and NMR spectroscopy. These traditional approaches are both capable of providing high-resolution, atomic-detail macromolecular structures but are bottlenecked in their sample preparation processes due to their requirement for copious amounts of highly homogenous and concentrated protein samples—and in the case of x-ray crystallography, the crystallization process. These prerequisites often limit the range in which these classical methodologies can be employed, making the study of large or heterogenous protein complexes—particularly those that exist in multiple conformational or compositional states—recalcitrant. In recent years, single-particle cryo-electron microscopy (cryo-EM) has made strides in improvement, both in instrumentation and processing software, permitting the visualization of macromolecular protein complexes via near-atomic resolution 3D

reconstructions [30]. Compared to x-ray crystallography and NMR, the sample preparation process for cryo-EM is significantly less cumbersome. However, analysis of conformationally or compositionally heterogenous complexes still presents a problem, and the accurate localization of individual subunits within a protein complex is often unfeasible without other forms of structural information. In general, the biophysical structures obtained from rigid state data analyses such as x-ray crystallography, NMR, and cryo-EM represent static snapshots of protein complexes. While integral to our understanding of protein function, uncovering the dynamics and mechanistic details that govern individual protein-protein interactions remains elusive to such structural techniques. There is therefore a growing demand for the development of hybrid technologies that complement classical structural biology methods and expand the range of study for important biological complexes.

1.2 Cross-linking Mass Spectrometry as a Tool for Studying PPIs

Over the course of the last two decades, biological MS has evolved from its role as an auxiliary technique used for analysis of peptide fragments for protein identification to a major driving force in large scale proteomics [31-33], as well as a powerful approach for determining the structural architectures of intact protein complexes. Emerging mass spectrometry-based hybrid structural methodologies such as native MS [34-36], hydrogen-deuterium exchange (HDX) [37, 38], covalent-labeling “footprinting” [39, 40], and cross-linking mass spectrometry (XL-MS) [41-43] have proven their ability to provide orthogonal structural information to that obtained by traditional means. Compared to legacy structural approaches, hybrid MS techniques provide structural information at the “peptide-level”, describing the secondary tertiary structures of proteins, but not providing a true biophysical structure. However, the advantages of these

approaches are the versatility and throughput to which they can be utilized, which far exceeds the capacity of methods for static structure resolution. Of these methods, XL-MS appears to be the most promising hybrid approach for PPI analyses due to its ability to yield structural information on heterogenous protein structures and their conformational dynamics, while simultaneously improving the characterization of interactome networks through stabilization of PPIs [43, 49-51].

1.2.1 Chemical Cross-linking Coupled with Affinity-Purification Mass Spectrometry

While stable interactions persist through rigorous purification conditions and can be easily studied using native AP-MS strategies, weaker PPIs are more sensitive to experimental conditions and are often lost during purification. Thus, preserving endogenous interactions is critical towards a full understanding of PPI networks. The use of aldehydes (e.g. formaldehyde, paraformaldehyde, glutaraldehyde) as a chemical fixative has been studied for decades for the preservation of tissue and cell morphology [52]. These cell-membrane permeable reagents can be similarly used (albeit at significantly lower concentrations and incubation times) to stabilize protein interactions as they occur within intact cells and tissues by trapping proximal proteins through covalent linkages that persist through biochemical manipulations [53]. The added benefit of cross-linking protein complexes in their native environments is the preservation of interactions within their natural localizations, as lysis of cell compartments can result in reorganization and artifact interactions. Once cross-linking has been applied to intact cells, highly stringent conditions can be used during cell lysis and affinity enrichment, minimizing the potential for false positives. Applications of this method have shown improvements in PPI identification compared to traditional AP-MS, expanding the range of proteomic studies to identifying *in vivo* protein-protein and protein-DNA interactions [49, 54-57]. Mild formaldehyde cross-linking has also been shown to stabilize both the structure and enzymatic activity of protein complexes,

permitting subcomplex analysis of dynamic and heterogenous assemblies through incorporation with native purification approaches [58]. Additionally, cross-linking has also been used in conjunction with tandem affinity tags capable of withstanding denaturing conditions in order to capture and identify stable, transient, and weak interactions in a single analysis [49, 59]. Finally, integration of the cross-linking with quantitative MS (QMS) methods, i.e., SILAC, has culminated in the development of a general platform to study PPIs, denoted as QTAX (Quantitative analysis of Tandem Affinity purified *in vivo* cross-linked (X) protein complexes) [49, 60]. The combination of chemical cross-linking, tandem affinity purification under denaturing conditions, and quantitative mass spectrometry has greatly facilitated the study of *in vivo* protein-protein interactions.

1.2.2 Chemical Cross-linking as a Hybrid Structural Methodology

While cross-linking approaches utilizing formaldehyde have been successful in capturing various protein-protein interactions, determining the identities of binary-interacting proteins has proven to be challenging. Due to the difficulty in deciphering MS spectra of formaldehyde cross-linked peptides, differentiating between directly-interacting proteins and proteins that were purified through multiple associations to a given bait remained unlikely. The development of cross-linking reagents with residue-targeting specificity ushered in a new era for XL-MS as a hybrid structural strategy, facilitating not only the high-throughput identification of interacting proteins, but also the determination of the specific amino acid residues involved in their physical contacts. Identifying protein-protein contacts through XL-MS not only confirms physical proximity between subunits but provides structural information in the form of distance constraints that can be utilized for integrative structural modeling [43, 61-65]. Today, chemical cross-linking coupled with mass spectrometry is a well-established asset of the structural

biologist's repertoire, capable of yielding low-resolution structural information on the three-dimensional topologies of protein complexes and their interactions. XL-MS strategies offer distinct advantages when compared to traditional methods, largely due to their speed, sensitivity, and versatility. Specifically, the advantages of XL-MS over other structural techniques include its reduced demands for sample preparation and tolerance for sample heterogeneity, as well as its capability to sample multiple conformations of dynamic complexes. As a result, cross-linking mass spectrometry is one of few structural methodologies capable of describing the three-dimensional structures of protein complexes and their interactions as they occur in their native environments (e.g. in intact cells or tissues) [50, 65-67].

1.2.3 Challenges in Cross-linking Mass Spectrometry Studies

The general XL-MS strategy begins with the formation of covalent bonds between proximate residues of proteins in their native or native-like states. Cross-linked proteins are then digested into peptides prior to mass spectrometric analysis, and the cross-linked residues are identified through database searching. Over the years, many cross-linking reagents have been developed, each featuring unique chemical structures and combinations of functional groups. To date, the most commonly published cross-linkers are lysine-targeting reagents consisting of two *N*-hydroxysuccinimidyl (NHS) esters connected by an alkyl spacer arm (e.g. disuccinimidyl suberate (DSS), disuccinimidyl gluterate (DSG)). Targeting lysine residues is preferable for several reasons: their relatively high overall prevalence (~6% of all residues), their distribution across solvent-accessible protein surfaces, and the specificity of primary amine-targeting chemistries [68, 69]. Other amine residue-targeting chemistries, such as sulfhydryl-targeting [70, 71], carboxyl-targeting [72, 73], and non-specific residue-targeting [74, 75] photo-activatable

functional groups have been explored; however, those reports only contribute to a small percent of total XL-MS publications.

Despite its theoretical simplicity, there are inherent difficulties associated with XL-MS strategies, namely the detection of low abundance cross-linked peptides and their unambiguous identification. The complexity of peptide mixtures often impedes detection of cross-linked peptides due to the significantly higher abundance of non-cross-linked peptides. In addition, heterogeneous populations of cross-linked products (i.e. inter-linked, intra-linked, and dead-end modified peptides) further complicates the analysis. To facilitate the detection of inter-linked peptides, one strategy is to selectively enrich for cross-linked products using enrichable cross-linkers containing either an affinity tag (e.g. biotin tag) [76, 77] or a chemical handle that allows subsequent addition of an affinity tag through chemical conjugation [50, 78]. Another common strategy is to incorporate stable isotopes in cross-linked peptides to generate characteristic isotopic profiles, differentiating them from non-cross-linked peptides [79-81].

The unambiguous identification of inter-linked peptides by peptide sequencing is challenging when conventional cross-linkers are used, due to the difficulty in interpreting tandem mass spectra resulting from the fragmentation of two covalently-linked peptides. Despite recent innovations in bioinformatics tools that have been developed to better dissect fragmentation data of inter-linked peptides [82-84], further improvements are required to make it as applicable as identifying single peptide sequences. To circumvent these problems, various types of cleavable cross-linkers, e.g., MS-, photo-, and chemical-cleavable reagents, have been developed to facilitate MS identification of cross-linked peptides. Among them, MS-cleavable reagents appear to be the most attractive for XL-MS studies [85-87], owing to their unique capability of fragmenting cross-links during collision-induced dissociation (CID) and thus facilitating

independent peptide sequencing for unambiguous identification. To this end, we have developed a new class of MS-cleavable cross-linkers (i.e. sulfoxide-containing MS-cleavable cross-linking reagents) that enable simplified and accurate identification of cross-linked peptides using multistage tandem mass spectrometry (MS^n) [50, 73, 86, 88]. These new types of cross-linkers are robust and reliable, and have been successfully applied to define protein-protein interactions both *in vitro* [51, 65, 86, 89] and *in vivo* [50, 65].

Most cross-linking studies thus far have reported on the static structures of protein complex assemblies. In reality, proteins and protein complexes exist in various conformations, corresponding to different functions or processing states. To further advance XL-MS studies of protein complexes, our goal is the development and application of quantitative cross-linking mass spectrometry (QXL-MS) strategies to elucidate the structural and mechanistic dynamics that govern protein-protein interactions. To this end, we have designed quantitative cross-linking reagents and platforms, employing them to survey the dynamic topologies associated with cullin-RING E3 ligase (CRL) function and regulation [88, 90, 91]. A thorough understanding of protein dynamics, particularly those associated with various human pathologies, has the potential to identify molecular targets for therapeutic intervention [92].

1.3 The Ubiquitin-Proteasome System

The ubiquitin-proteasome system (UPS) represents the major pathway for selective degradation in eukaryotic cells. It is a highly complex and tightly-regulated process central to balancing cellular function and maintaining homeostasis. It is estimated that 80-90% of all cellular proteins are degraded through this pathway, intertwining this system within a broad array of integral biological processes including differentiation, proliferation, gene transcription, protein

quality control, and apoptosis, among others [93, 94]. It has become increasingly clear that defects within this pathway are associated with a multitude of human pathologies, ranging from developmental abnormalities and various types of cancers to autoimmune and neurodegenerative disorders [95-99].

The ubiquitin-proteasome system is comprised of two distinct, successive pathways: selective protein ubiquitination, and the subsequent recognition and degradation by the 26S proteasome. Proteins destined for degradation are first tagged (ubiquitinated) through a covalent linkage to ubiquitin (Ub), a small but highly evolutionarily conserved regulatory protein found in almost all tissues of eukaryotic organisms. This process is facilitated by a cascade of enzymatic reactions featuring E1 ubiquitin-activating enzymes, E2 ubiquitin-conjugating enzymes, and E3 ubiquitin ligases [100, 101]. E1 activating enzymes 'charge' Ub molecules through an ATP-dependent process that results in a high-energy thioester bond between the C-terminal of ubiquitin and the E1 catalytic cysteine residue [102]. The activated ubiquitin is then transferred to a catalytic cysteine on E2 conjugating enzymes via a Ub~E1-E2 intermediate [103, 104]. The ubiquitin-charged E2 then binds to an E3 ubiquitin ligase, which recruits a protein substrate and mediates the transfer of Ub from E2 to a specific lysine residue on the target protein. Each cycle covalently attaches a single Ub; subsequent iterations of this cycle result in the ligation of ubiquitin to other lysine residues on the protein substrate or any of the seven lysine residues (Lys^{6}, Lys^{11}, Lys^{27}, Lys^{29}, Lys^{33}, Lys^{48}, Lys^{63}) of a previously attached Ub. These successive ubiquitination events result in the formation of various poly-ubiquitin species, which in turn encode different signals [105, 106]. For instance, the canonical ubiquitin signal, the Lys^{48}-linked poly-Ub chain, targets substrates to the 26S proteasome for degradation. In contrast, Lys^{63}-linked chains are generally associated with non-proteolytic pathways such as DNA damage repair and

intracellular trafficking, Lys^{11}-linked chains with mitotic regulation and endoplasmic reticulum-associated degradation (ERAD) [107], mono-ubiquitination with intracellular localization and trafficking [108, 109], and Lys^{29}-linked poly-Ub with lysosomal degradation [110], although recent studies have indicated that Lys^{48}- and Lys^{63}-linked poly-Ub chains may also signal lysosomal degradation [111]. In general, Lys^{48}-linked poly-ubiquitin are the predominant poly-Ub post-translational modification found in cells [112], targeting a myriad of regulatory proteins for selective degradation and thereby dictating the timings of their associated biological processes required for cell survival.

Poly-ubiquitinated proteins are delivered to and recognized by the 26S proteasome, a massive, multi-catalytic protease composed of at least 33 distinct subunits. This 2.5 MDa macromolecular protein complex contains two primary subcomplexes: the 20S core particle (CP, approximately 700 kDa) and the 19s regulatory particle (RP, approximately 900 kDa) [113, 114]. Eukaryotic 20S CP comprises seven structural α subunits and seven catalytic β subunits arranged in a conserved 'barrel' of four heptameric rings in the order αββα, for a total of 28 subunits. The inner β rings of this cylindrical stack consist of seven β subunits each, harboring the chymotrypsin-, trypsin-, and caspase-like hydrolytic activities [115, 116] utilized for protein degradation. Conversely, the outer α rings consist of seven α subunits each, serving as both a gating mechanism that blocks unregulated access to the catalytic interior cavity, as well as a docking site for 20S activators. The 19S regulatory particle is one of the major 20S activator complexes in eukaryotes, consisting of at least 19 distinct subunits segregated into two major subassemblies: a 10-subunit base containing a 6-member ATPase ring that directly interfaces with the 20S α ring, and a 9-subunit lid subcomplex [117, 118]. Compared to the rigidly structured 20S, the 19S regulatory particle is heterogenous in both its conformation and functions,

which include the recognition, de-ubiquitination, and unfolding of poly-ubiquitinated substrates, as well as gate opening of the 20S α-ring and subsequent transfer of unfolded substrates into the catalytic core. Due to the conformational complexity of the 19S, the structure of the human 26S proteasome has remained largely recalcitrant to traditional biophysical methods, with cryo-EM studies within the last year reporting high-resolution structures at 3.5 and 3.9 Å [119, 120].

Studies on human malignancies have shown that hyper-activated proteasomal activity sustains cancer cell proliferation through the constitutive up-regulation of pro-survival pathways and down-regulation of cell cycle mediators, resulting in the avoidance of cell cycle arrest and apoptosis [121]. Such proteasomal hyperactivity has been associated with a range of malignancies, including myelomas, lung cancers, and squamous-cell carcinomas [122, 123]. In recent years, the clinical efficacy of proteasome inhibitors such as Bortezomib and Carfilzomib have been well-documented, resulting in their adoption as therapeutic options for hematopoetic tumors such as multiple myeloma (MM) [124]. However, proteasome inhibition for the treatment of solid tumors remains daunting. This is generally due to the higher dosage requirement to treat solid tumors, as the toxicity associated with increasing proteasome inhibition can result in a range of detrimental effects [125-127]. As the ultimate goal of cancer therapy is the design of treatment options that suppresses malignant neoplasms while minimizing the damage to normal cells, therapeutic strategies that specifically target and impede the cancer-relevant pathways of the UPS without its complete inhibition would be better-tolerated by patients and advantageous for a wider range of human malignancies.

1.4 Cullin-Ring E3 Ubiquitin Ligases (CRLs)

The clinical development of drugs targeting upstream components of the ubiquitin-proteasome system that confer specificity to the ubiquitination process has been an avenue of intense research in the last decade [128]. The human genome encodes two E1 ubiquitin-activating enzymes, ~40 E2 ubiquitin-conjugating enzymes, and up to 1,000 different E3 ubiquitin ligases [129]. Each E3 is tasked with facilitating the transfer of Ub from its associated E2 to a single or few select target proteins, thereby conferring the specificity in which proteins are tagged for proteasomal degradation. There are three families of E3 ligases; HECTs (homologous to the E6-AP C-terminus) [130], RINGs (really interesting new genes) [131], and RBRs [132], of which the RING domain ligases are the largest family, comprising ~600 members [131, 133]. Cullin-RING ligases (CRLs) are the largest superfamily of multi-subunit RING-type E3s, modular assemblies that exhibit enormous plasticity in substrate specificity [134]. Each CRL subfamily is characterized by the Cullin scaffolding protein (Cul1, 2, 3, 4a, 4b, 5, or 7) in which RING domain-containing proteins (usually Rbx1/Roc1/Hrt1), adaptor proteins, and their substrate recognition elements assemble. SCF (Skp1-Cul1-F-box) complexes are the archetypal CRL subfamily, assembling along Cullin1 and utilizing over 70 interchangeable F-box proteins that recognize distinct target proteins [135]. In general, the proteins ubiquitinated by SCF complexes are typically involved in cell cycle progression, gene transcription, and signal transduction. Deregulation of these pathways play significant roles in human diseases—such as cancers—where CRLs or their target substrates often function as tumor suppressors or oncogenes. For instance, CRLs that assemble along Cul4A regulate numerous key processes such as DNA damage repair, chromatin remodeling, DNA replication, and cell cycle control through the ubiquitination of key regulatory proteins. Other human diseases in which CRLs have

been associated include diabetes, inflammation, and neurodegenerative disorders [136-138], making this family of enzymes a high-potential target for therapeutic drug development. To this end, a detailed understanding of the structure and function of these individual complexes is necessary to determine the molecular mechanisms that can be targeted for disease intervention. Through the development of quantitative cross-linking mass spectrometry (QXL-MS) approaches, we aim to design and utilize new platforms to address the questions of CRL structure and dynamics that remain recalcitrant to traditional structural methods.

CHAPTER 2: Development of Isotope-coded, MS-cleavable Cross-linkers for Elucidating Protein Structures through Quantitative XL-MS

Reprinted with permission from:

Clinton Yu, Wynne Kandur, Athit Kao, Scott Rychnovsky, and Lan Huang. **Developing New Isotope-Coded Mass Spectrometry-Cleavable Cross-Linkers for Elucidating Protein Structures.** *Analytical Chemistry*, 2014; 86 (4): 2099–2106.

2.1 Summary

The structural characterization of protein complexes is essential for the understanding of their function and regulation. However, it remains challenging due to limitations in existing tools. With recent technological improvements, cross-linking mass spectrometry (XL-MS) has become a powerful strategy to define protein-protein interactions and elucidate structural topologies of protein complexes. To further advance XL-MS studies, we present here the development of new isotope-coded, MS-cleavable, homo-bifunctional cross-linkers: d_0- and d_{10}-labeled dimethyl disuccinimidyl sulfoxide (DMDSSO). Detailed characterization of DMDSSO cross-linked peptides further demonstrates that sulfoxide-containing MS-cleavable cross-linkers offer robust and predictable MS^2 fragmentation of cross-linked peptides, permitting subsequent MS^3 analysis for simplified, unambiguous identification. Concurrent usage of these reagents provides a characteristic doublet pattern of DMDSSO cross-linked peptides, thus aiding in the confidence of cross-link identification by MS^n analysis. More importantly, the unique isotopic

profile permits quantitative analysis of cross-linked peptides, and therefore expands the capability of XL-MS strategies to analyze both static and dynamic protein interactions. Together, our work has established a new XL-MS workflow for future studies towards the understanding of structural dynamics of protein complexes.

2.2 Introduction

Protein complexes represent essential functional entities in cells for carrying out multiple biological processes including translation, replication, cell division and cell cycle control. Protein-protein interactions are integral in modulating the assembly, structure and function of protein complexes. Perturbations of endogenous protein-protein interactions can result in deleterious effects on cellular activities and lead to human disease. In recent years, protein-protein interaction interfaces have become a new and attractive platform for therapeutics [9]. Therefore, characterization of structures and interaction dynamics of protein complexes is critical to understanding their function and regulation, thus unraveling molecular mechanisms underlying human pathologies and providing insight on potential targets for drug development. Traditional structural tools such as nuclear magnetic resonance (NMR) and x-ray crystallography are able to yield detailed, high-resolution information on protein structures. However, these technologies have difficulty in analyzing heterogeneous and dynamic protein complexes. Following decades of method development alongside technological advances in mass spectrometry, cross-linking mass spectrometry (XL-MS) has emerged as a powerful strategy not only for mapping protein interaction networks [49, 60, 139], but also for structural elucidation of protein complexes [41, 43, 63, 89]. The cross-links between proteins can be used to derive topological ordering of protein complexes by computational modeling [89, 140]. In addition,

spatial distances between cross-linked residues can be converted to distance restraints for protein homology modeling [43].

The major difficulties that plague XL-MS studies are the detection of low-abundance cross-linked peptides and their unambiguous identification. The complexity of peptide mixtures often impedes detection of cross-linked peptides, which are typically in relatively low abundance. In addition, various species of cross-linked products (i.e. inter-linked, intra-linked, and dead-end modified peptides) further increases the heterogeneity of the peptide mixture. To increase the likelihood of detecting cross-linked peptides, one strategy is to selectively enrich cross-linked products for MS analysis using enrichable cross-linkers containing either an affinity tag (e.g. biotin tag) [141 2005] or a chemical handle that allows subsequent addition of an affinity tag through chemical conjugation [50]. Another strategy is to incorporate stable isotopes in cross-linked peptides to generate characteristic isotopic profiles, thus separating them from non-cross-linked peptides [43, 63, 79-81, 141, 142]. These isotopes can be introduced through metabolic labeling and replacement within amine residues, or incorporated directly into cross-linking reagents. Additionally, isotopic differentiation can also be achieved by carrying out enzymatic digestion of cross-linked proteins in ^{16}O and ^{18}O water, and then mixing prior to MS analysis [80, 143]. However, enzymatic incorporation of ^{18}O is troublesome as its labeling efficiency relies heavily on peptide sequences. Interestingly, performing protein cross-linking in ^{18}O water can result in the incorporation of one ^{18}O to dead-end modified peptides but not to other types of peptides, thus effectively distinguishing them from intra-linked and inter-linked peptides [141]. In general, the most common practices to produce cross-linked peptides as isotopic pairs for confident identification is to cross-link proteins with a 1:1 mixture of non-labeled and labeled cross-linkers [43, 63, 79, 81, 87, 142].

Unambiguous identification of inter-linked peptides by peptide sequencing is challenging when non-cleavable cross-linkers are used. This is due to the difficulty in interpreting convoluted tandem mass spectra resulted from the fragmentation of two inter-linked peptides. Despite recent innovation in bioinformatics tools that have been developed to better dissect fragmentation data of inter-linked peptides [82-84, 144], further improvements are required to make it as accurate and applicable as the identification of single peptides. To circumvent these problems, various types of cleavable cross-linkers (e.g. MS-, photo-, and chemical-cleavable) have been developed to simplify the identification of cross-linked peptides. Among them, MS-cleavable reagents appear to be most attractive for XL-MS studies [83, 85, 86, 145, 146], due to their ability to cleave within the mass spectrometer, physically separating the peptides that comprise each cross-link and permitting individual peptide sequencing for unambiguous identification. Recently, we have developed a novel MS-cleavable homobifunctional NHS ester, disuccinimidyl sulfoxide (DSSO), in which the MS-cleavable C-S bond cleaves preferentially during MS^2 analysis prior to the breakage of peptide backbone [86]. Within an MS^n workflow utilizing three layers of MS analysis, CID-induced fragmentation of the cross-linker at the MS^2 level separates the bound peptides, which are detected as characteristic fragment ions. These ions are then sequenced in subsequent MS^3, permitting their accurate identification. This novel integrated workflow has proven to be effective for fast and accurate identification of cross-linked peptides using conventional bioinformatics tools, and has been successfully applied to elucidate structures of proteasome complexes [86, 89].

To further advance XL-MS studies of protein complexes, we have developed a pair of new isotope-coded DSSO derivatives, i.e. d_0- and d_{10}-labeled dimethyl-disuccinimidyl sulfoxide (DMDSSO). Incorporation of deuterium labeling into our robust sulfoxide-containing MS-

cleavable cross-linker adds new features that not only enhance the detection and identification of cross-linked peptides, but also provide the capability of quantifying cross-linked peptides. Here we present the detailed characterization of the DMDSSO-based cross-linking strategy using synthetic peptides and model protein cytochrome C. We have compared MS^n analyses of d_0- and d_{10}-DMDSSO cross-linked peptides and performed quantitative assessments of cross-linked peptides with different sample preparation strategies.

2.3 Experimental Procedures

2.3.1 Materials and Reagents

General chemicals were purchased from Fisher Scientific or VWR International, bovine heart cytochrome C (98% purity) from Sigma-Aldrich, and Ac-Myelin peptide (Ac-ASQKRPSQRHG, 92.7% purity) from American Peptide (Sunnyvale, CA).

2.3.2 Synthesis and Characterization of d_0-DMDSSO and d_{10}-DMDSSO

The synthesis of DMDSSO is depicted in Figure 2-1. Briefly, the preparation of d_0-DMDSSO began with the addition of thioacetic acid to methyl methacrylate. Methanol and triethylamine were added to the mixture along with another equivalent of methyl methacrylate to afford the symmetrical diester in one pot. The diester was hydrolyzed with lithium hydroxide in THF/H_2O before coupling with NHS, in the presence of trifluoroacetic anhydride, pyridine, and DMF [147]. Lastly, oxidation of the sulfide to the sulfoxide yielded the desired linker as described [86]. Preparation of d_{10}-DMDSSO was carried out similarly, beginning with commercially available d_8-methyl methacrylate.

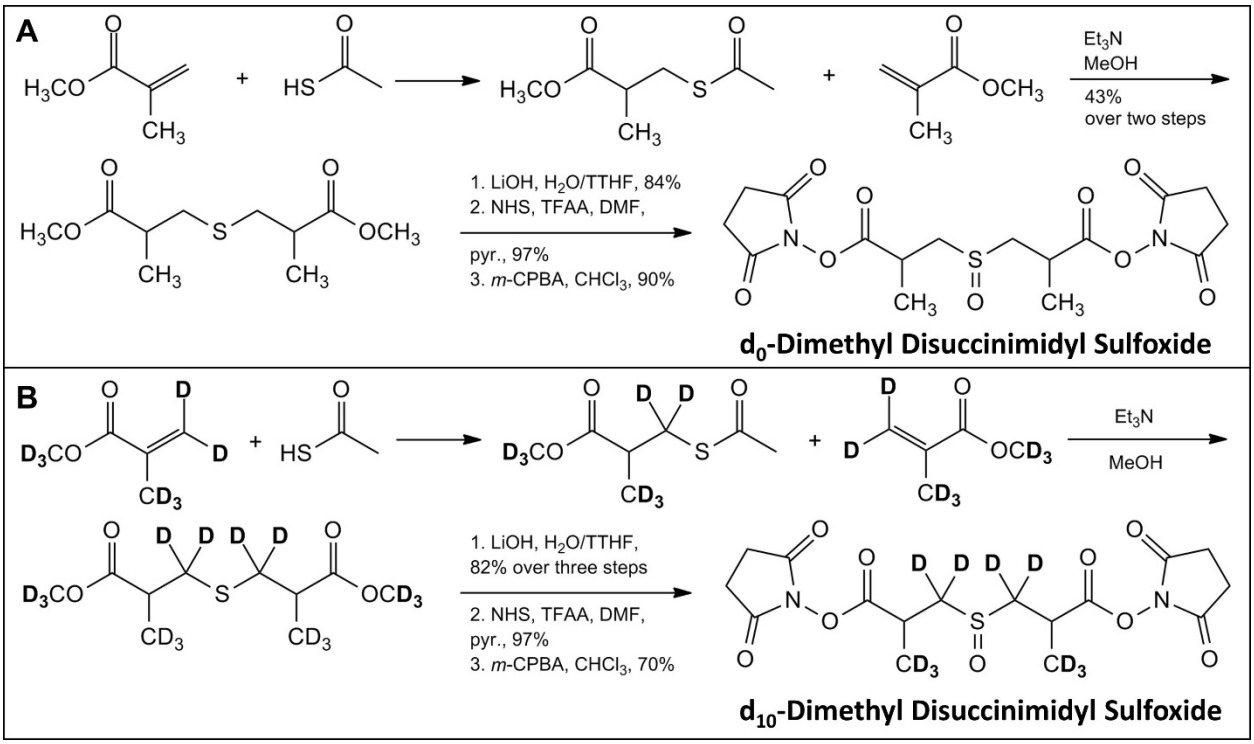

Figure 2-1. Chemical synthesis schemes for d_0- and d_{10}-DMDSSO. Synthesis of **(A)** d_0-DMDSSO and **(B)** d_{10}-DMDSSO.

2.3.3 Cross-linking of Synthetic Peptides with d_0- and d_{10}-DMDSSO.

Synthetic peptide Ac-Myelin was dissolved in DMSO to 1 mM and cross-linked with either d_0- or d_{10}-DMDSSO in a 1:1 molar ratio of peptide to cross-linker in the presence of 1 eq of diisopropylethylamine. The resulting samples were diluted to 5 pmol/µL in 3% ACN/2% formic acid for MS analysis.

2.3.4 Cross-linking of Cytochrome C with d_0- and d_{10}-DMDSSO

40 µL of 200 µM cytochrome C in PBS buffer (pH 7.4) was reacted with d_0- or d_{10}-DMDSSO in a molar ratio of 1:10 (protein: cross-linker) for 2 h at room temperature and quenched with excess ammonium bicarbonate. Samples were then subjected to SDS-PAGE and visualized by Coomassie blue. The dimerized bands were excised, reduced with TCEP for 30

min and alkylated with chloroacetamide for 45 min in dark, and then digested with trypsin at 37° C overnight. Peptide digests were extracted, concentrated and reconstituted in 3% ACN/2% formic acid prior to MS analysis.

2.3.5 Liquid Chromatography-Multistage Tandem Mass Spectrometry (LC-MS^n)

DMDSSO cross-linked peptides were analyzed by LC-MS^n utilizing an LTQ-Orbitrap XL mass spectrometer (Thermo Fisher, San Jose, CA) coupled on-line with an Eksigent NanoLC system (Dublin, CA) as previously described [86]. Each MS^n experiment has a duty cycle of 1.3 s, consisting of one MS scan in FT mode (350-1400 m/z, resolution of 60,000 at m/z 400) followed by two data-dependent MS2 scans in FT mode (resolution of 7500) with normalized collision energy at 15% on the top two MS peaks with charges at 3+ or up, and three MS^3 scans in the LTQ with normalized collision energy at 35% on the top three peaks from each MS^2.

2.3.6 Data Analysis of Cross-linked Peptides

Data processing of LC-MS^n spectra was carried out as described [86]. MS^3 data were subjected to a developmental version of Protein Prospector (v. 5.10.10) for database searching, using Batch-Tag against cytochrome C sequence (SwissProt accession #: P62894) with mass tolerances for parent ions and fragment ions set as ± 20 ppm and 0.6 Da respectively. Trypsin was set as the enzyme with four maximum missed cleavages allowed. Protein N-terminal acetylation, methionine oxidation, N-terminal conversion of glutamine to pyroglutamic acid, asparagine deamidation, and cysteine carbamidomethylation were selected as variable modifications. In addition, six defined modifications on uncleaved lysines and free protein N-termini were selected: alkene (A: C_4H_4O, +68 Da; or A*: $C_4H_{-1}D_5O$, +73 Da), sulfenic acid (S: $C_4H_6O_2S$, +118 Da; or S*: $C_4H_1D_5O_2S$, +123 Da), and unsaturated thiol (T: C_4H_4OS, +100 Da;

or T*: $C_4H_{-1}D_5OS$, +105 Da) modifications, due to remnant moieties for d_0- (i.e. A, S, T) or d_{10}-DMSSO (i.e. A*, S*, T*) cross-linker, respectively. Initial acceptance criteria for peptide identification required a reported expectation value ≤ 0.1.

MS-Bridge was used to confirm the identification of cross-linked peptides by mass mapping against bovine cytochrome C with the parent mass error set as ± 10 ppm [86]. The in-house program Link-Hunter is a revised version of the previously written Link-Finder program, designed to automatically validate and summarize cross-linked peptides based on MS^n data and database searching results as previously described [86, 89].

2.4 Results & Discussion

2.4.1 Design and Synthesis of New Isotope-coded DSSO Derivatives

In order to improve MS identification of cross-linked peptides and allow quantitative determination of structural dynamics of protein complexes, we aimed to generate deuterium-labeled, MS-cleavable cross-linkers. Given our previous success of DSSO-based XL-MS strategies in protein structural characterization [86, 89], we first attempted to produce d_4-DSSO by introducing deuterium at the positions alpha to the carbonyl through deuterium exchange. Although feasible, complete labeling was problematic due to slow exchange. Additionally, labeling with four deuteriums proved to be insufficient for effective separation of highly charged d_0/d_4-DSSO cross-linked peptide pairs (4+ and above) during MS^n analysis. Therefore, d_8-labeled DSSO would be ideal; however, incorporation of eight deuteriums in DSSO appeared to be even less practical due to cost and experimental difficulties. To circumvent this problem, we designed a derivative of DSSO, dimethyl disuccinimidyl sulfoxide (DMDSSO). With the commercial availability of methyl methacrylate and d_8-methyl methacrylate, the synthesis of d_0-

or d_{10}-DMDSSO was economical and straightforward (Figure 2-1). Similar to DSSO, DMDSSO also has an ideal length (average extended length of 9.3 Å) for structural proteomics studies.

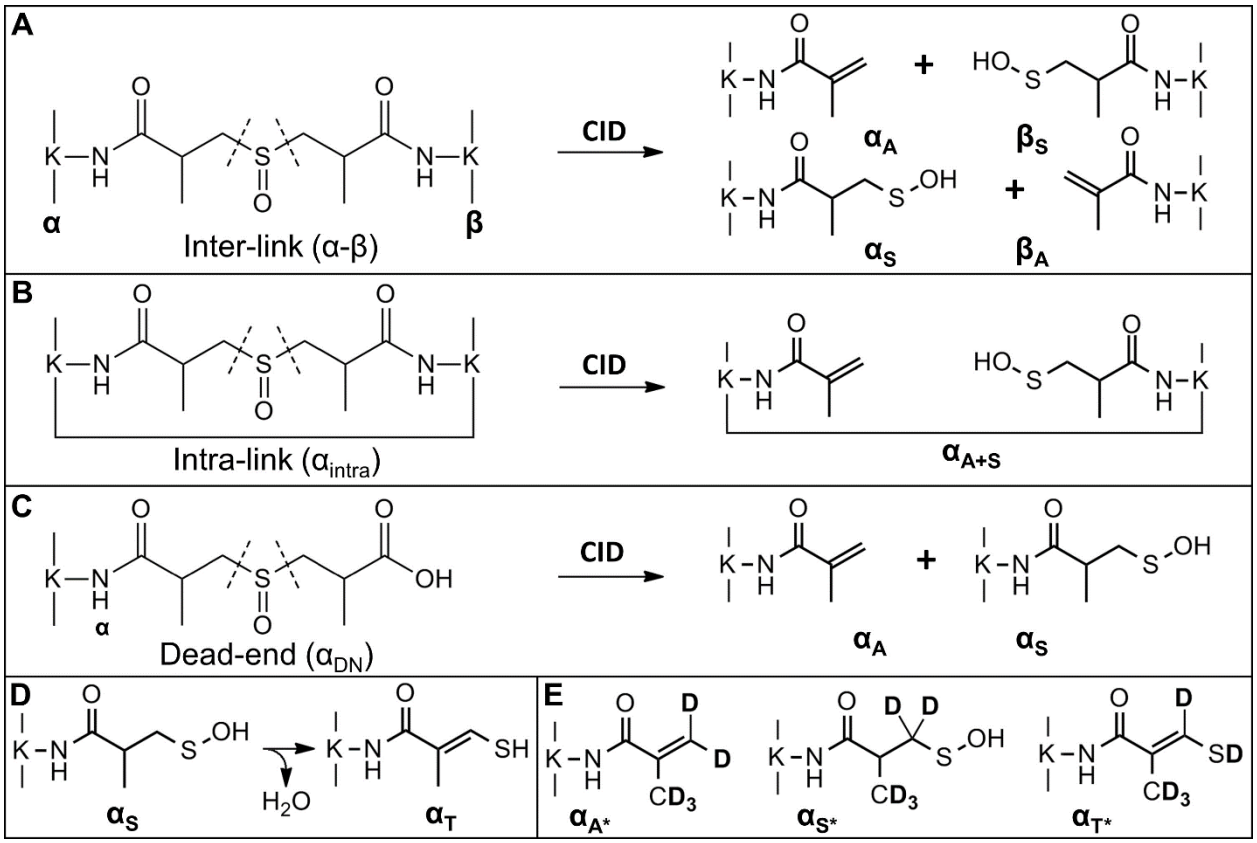

Figure 2-2. Characteristic MS^2 fragmentation patterns for DMDSSO cross-linked peptides. MS^2 fragmentation of **(A)** d_0-DMDSSO inter-linked heterodimer α-β**. (B)** d_0-DMDSSO intra-linked peptide α_{intra}. **(C)** dead-end modified peptide α_{DN}. **(D)** The conversion scheme of α_S to α_T. (E) Illustrations of α_{A*}, α_{S*}, and α_{T*} fragments with lysines modified with d_{10}-DMDSSO remnants.

2.4.2 Expected CID Fragmentation Patterns of d_0- and d_{10}-DMDSSO Cross-linked Peptides

Three types of cross-linked products can result from the digestion of cross-linked proteins: inter-linked, intra-linked and dead-end modified peptides. Previously we have shown that DSSO cross-linked peptides display characteristic fragmentation patterns during MS^2 analysis due to preferential cleavage of CID-cleavable C-S bonds adjacent to the sulfoxide [86]. Aside from two additional methyl groups, DMDSSO has a structure very similar to DSSO, with

two symmetric MS-cleavable C-S bonds. Therefore, we expect that DMDSSO cross-linked peptides will display the same characteristic MS^2 fragmentation patterns as DSSO cross-linked peptides. Since deuterium labeling should not interfere with peptide fragmentation, d_0- and d_{10}-DMDSSO cross-linked peptides would also behave similarly during MS^n analysis. For simplicity, we use d_0-DMDSSO cross-linked peptides to illustrate their predicted fragmentation patterns (Figure 2-2). Prior to peptide backbone fragmentation, MS^2 analysis selectively cleaves either of the two symmetric C-S bonds in the linker region of DMDSSO cross-linked peptides, yielding peptide fragments with predictable modifications (due to the remnants of DMDSSO) on cross-linked lysine residues. For a d_0-DMDSSO inter-linked peptide α-β, cleavage of a C-S bond leads to physical separation of the two inter-linked peptides into a pair of peptide fragments (i.e. α_A/β_S or α_S/β_A), in which α and β peptide fragments are modified by two complementary cross-linker remnant moieties, i.e. alkene (A) and sulfenic acid (S) (Figure 2-2A). Thus, the resulting MS^2 peptide fragments can be subjected to MS^3 sequencing for unambiguous identification of inter-linked peptides [86]. For a d_0-DMDSSO intra-linked peptide α_{intra}, one peptide fragment (i.e. α_{A+S}) is anticipated, carrying an alkene- and a sulfenic acid-modified lysine, respectively (Figure 2-2B). This MS^2 fragment ion α_{A+S} in fact represents two different ion species that have identical peptide sequences and *m/z* values but transposed DMDSSO remnant-modified lysine residues (i.e. α_{A+S} and α_{S+A}). For a d_0-DMDSSO dead-end modified peptide (α_{DN}), two peptide fragments (i.e. α_A and α_S) are expected (Figure 2-2C). It is noted that the sulfenic acid moiety often undergoes dehydration to become a more stable and dominant unsaturated thiol moiety (i.e. T, +100 Da) as previously described (Figure 2-2D) [86]. This conversion does not appear to complicate data analysis, as observed for DSSO cross-linked peptides [86]. In comparison to d_0-DMDSSO cross-linked peptides, MS^2 fragmentation patterns for d_{10}-DMDSSO cross-linked

peptides should be identical, other than the masses of d_{10}-DMDSSO remnants (i.e. A*: alkene; S*: sulfenic acid; or T*: unsaturated thiol) being 5 Da higher due to the presence of 5 deuteriums after cleaving the C-S bond (Figure 2-2E). In addition to distinct MS^2 fragmentation patterns, DMDSSO cross-linked peptides have fixed mass relationships between parent ions and their respective fragment ions, similar to those of DSSO cross-linked peptides [86], thus providing an additional confirmation of the identified cross-linked peptides at the MS^2 level. Together with MS^3 sequencing and MS^1 mass matching, three different types of evidence can be obtained for the identification of DMDSSO cross-linked peptides with significantly improved confidence and accuracy.

2.4.3 Characterization of DMDSSO Cross-linked Model Peptides by MS^n Analysis

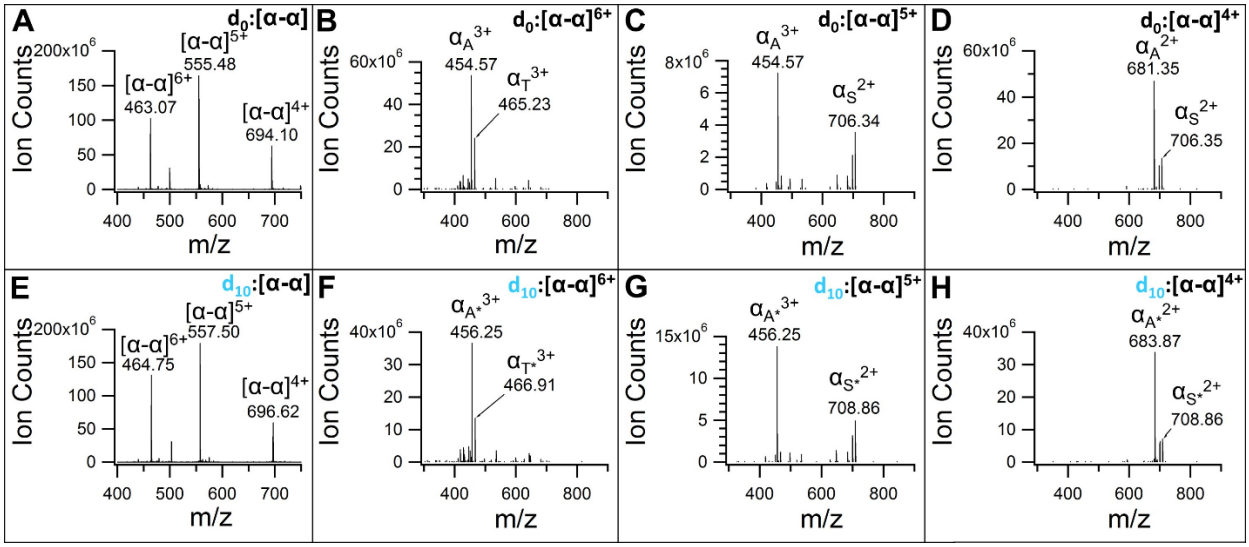

Figure 2-3. MS^n analyses of d_0- and d_{10}-DMDSSO inter-linked Ac-Myelin peptides. (A) MS^1 spectrum of d_0-inter-linked Ac-Myelin. **(B-D)** MS^2 spectra of d_0-inter-linked Ac-Myelin at three different charge states: **(B)** $[\alpha\text{-}\alpha]^{6+}$, **(C)** $[\alpha\text{-}\alpha]^{5+}$, and **(D)** $[\alpha\text{-}\alpha]^{4+}$. **(E)** MS^1 spectrum of d_{10}-inter-linked Ac-Myelin. **(F-H)** MS^2 spectra of d_{10}-inter-linked Ac-Myelin at three different charge states: **(F)** $[\alpha\text{-}\alpha]^{6+}$, **(G)** $[\alpha\text{-}\alpha]^{5+}$, and **(H)** $[\alpha\text{-}\alpha]^{4+}$.

We first performed DMDSSO cross-linking on synthetic peptide Ac-Myelin. Under our experimental conditions, the resulting cross-linked products were primarily inter-linked Ac-

Myelin homodimer (α-α), which were detected as a series of multiply-charged ions for d_0-DMDSSO (m/z 462.9033^{6+}, 555.2822^{5+}, 693.8497^{4+}) and d_{10}-DMDSSO (m/z 464.5796^{6+}, 557.2951^{5+}, 696.3656^{4+}) (Figure 2-3A and 2-3E, respectively). There is a 10 Da mass difference between d_0- and d_{10}- labeled cross-linked peptides due to incorporation of ten deuteriums in d_{10}-DMDSSO. As shown in Figure 2-3B, MS^2 analysis of the sextuply-charged d_0-inter-linked Ac-Myelin (d_0: α-α^{6+}) yielded a pair of dominant fragment ions (α_A/α_T), demonstrating effective separation of the inter-linked homodimer as expected. Similarly, the α_{A*}/α_{T*} ion pair was also detected as the most abundant ions in MS^2 spectrum for d_{10}-inter-linked Ac-Myelin peptide (d_{10}: α-α^{6+}) (Figure 2-3F), indicating no interference from deuterium labeling. MS^2 analyses of the quadruply- and quintuply-charged Ac-Myelin peptides also resulted in one pair of fragment ions (d_0:α_A/α_S; d_{10}: α_{A*}/α_{S*}) (Figure 2-3C-D and 2-3G-H, respectively), in which α_S or α_{S*} appears to be more dominant than α_T or α_{T*} respectively, compared to the fragmentation of sextuply-charged

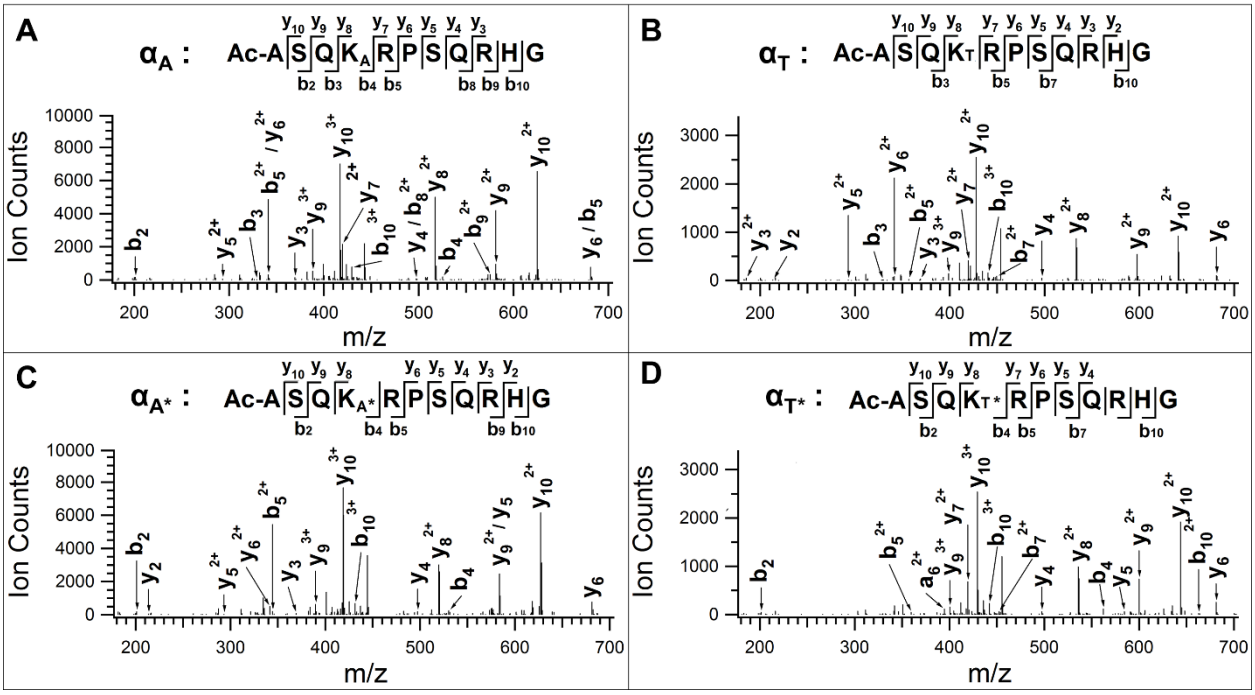

Figure 2-4. MS^3 analyses of d_0- and d_{10}-DMDSSO inter-linked Ac-Myelin peptides. MS^3 spectrum of **(A)** d_0 alkene-modified Ac-Myelin, **(B)** d_0 thiol-modified Ac-Myelin, **(C)** alkene moiety of d_{10}-inter-linked Ac-Myelin, **(D)**, thiol moiety of d_{10}-inter-linked Ac-Myelin.

inter-linked peptides (Figure 2-3B and 2-3F). This observation may be due to the susceptibility of highly-charged species to fragment when the same energy is applied to all precursor ions during CID analysis regardless of their charge. Such fragmentation behavior was also previously observed for DSSO inter-linked Ac-Myelin peptides [86]. MS^3 sequencing of α_A, α_T, α_{A*} and α_{T*} fragment ions confirmed the peptide sequences of d_0- and d_{10}-inter-linked Ac-Myelin peptides unambiguously (Figure 2-4), and none of the DMDSSO remnants appear to complicate peptide sequencing during MS^3. Taken together, these results show that the addition of methyl substituents in the linker region does not change the unique fragmentation of sulfoxide-containing, MS-cleavable, cross-linked peptides, and that preferential cleavage of C-S bonds is independent of peptide charges. Thus, MS^n analysis of DMDSSO cross-linked peptides can be performed the same way as that of DSSO cross-linked peptides [86].

2.4.4 Characterization of DMDSSO Cross-linked Cytochrome C by MS^n Analysis

We next evaluated the applicability of d_0- and d_{10}-DMDSSO for protein cross-linking. Model protein cytochrome C has been extensively used to test various new cross-linking strategies due to the large number of lysine residues relative to its size [86, 142]. In this work, DMDSSO cross-linked cytochrome C was separated by 1-D SDS-PAGE and visualized by Coomassie blue staining. In comparison to DSSO, d_0- and d_{10}-DMDSSO showed comparable efficiency in protein cross-linking (Figure 2-5). The general workflow for analyzing cross-linked cytochrome C is illustrated in Figure 2-5. We first analyzed in-gel digests of d_0- and d_{10}-DMDSSO dimerized cytochrome C separately. Figure 2-6A and 2-6D display respective MS^2 spectra of a selected pair of d_0- and d_{10}-DMDSSO inter-linked cytochrome C peptides (*m/z* 574.6436^{3+}, 577.9993^{3+}), in which 2 pairs of peptide fragment ions (d_0: α_A/β_T and α_T/β_A; d_{10}: α_{A*}/β_{T*} and α_{T*}/β_{A*}) were detected, demonstrating characteristic fragmentation pattern of inter-

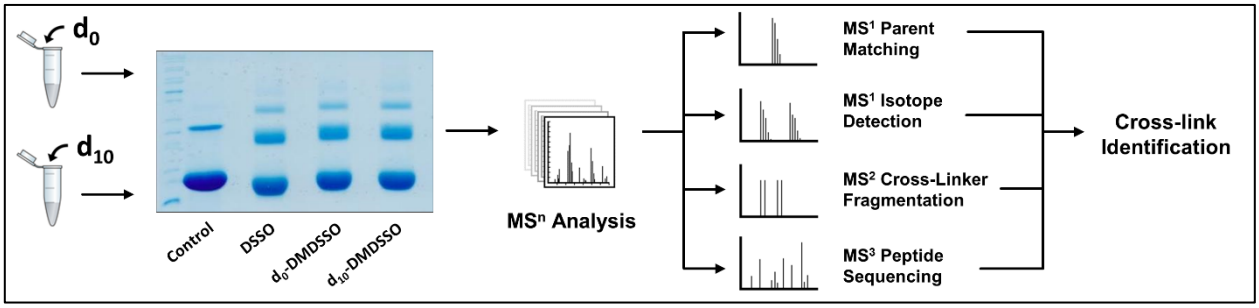

Figure 2-5. General workflow for the analysis and identification of d_0/d_{10} DMDSSO cross-linked cytochrome C peptides.

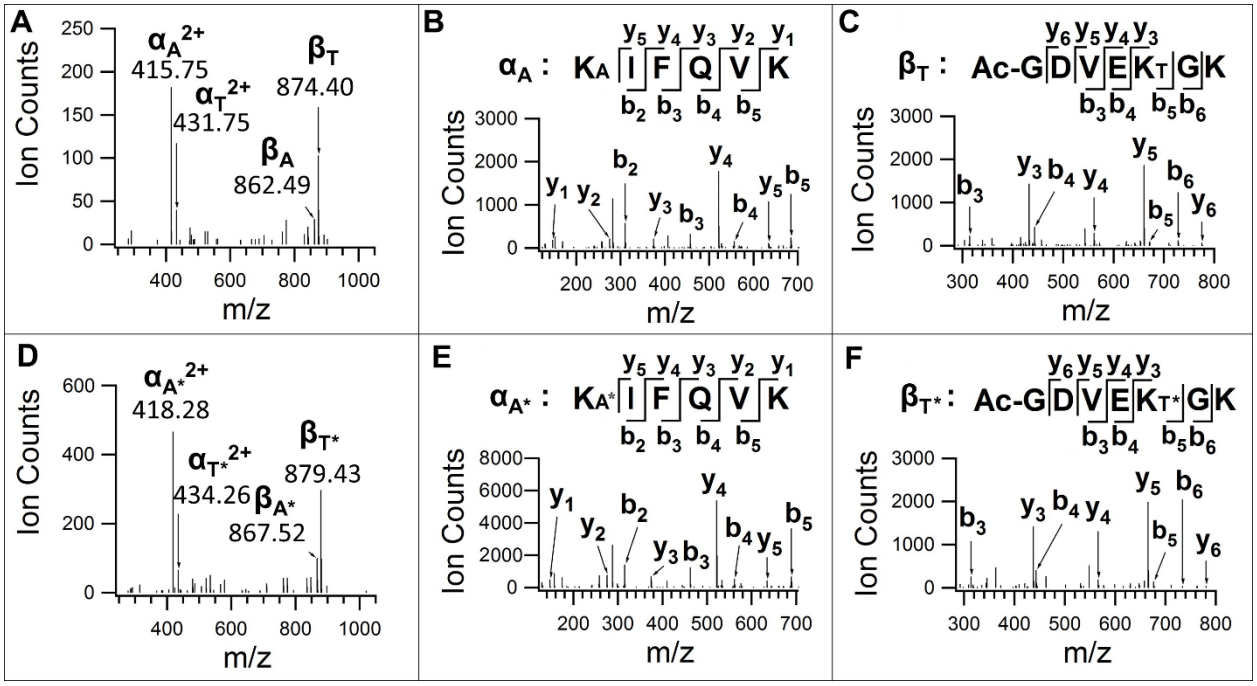

Figure 2-6. MSⁿ analysis of d_0/d_{10}-DMDSSO inter-linked cytochrome C peptides. (A) MS^2 cleavage of a d_0-inter-linked cytochrome C peptide α-β (*m/z* 574.6436^{3+}). MS^3 analyses of MS^2 fragment ions **(B)** α_A (*m/z* 415.76^{2+}) and **(C)** β_T (*m/z* 874.40) yield series of b and y ions that unambiguously identify α_A as K_AIFQVK and β_T as Ac-GDVEK$_T$GK. **(D)** MS^2 spectrum of corresponding d_{10}-inter-linked cytochrome C peptide α-β (*m/z* 577.9993^{3+}). MS^3 spectra of its MS^2 fragment ions **(E)** α_{A^*} (*m/z* 418.28^{2+}) and **(F)** β_{T^*} (*m/z* 879.43) unambiguously identify α_{A^*} as K_{A^*}IFQVK and β_{T^*} as Ac-GDVEK$_{T^*}$GK.

linked heterodimeric peptides. The most dominant fragment pair ions—α_A/β_T for d_0- and α_{A^*}/β_{T^*} for d_{10}-labeled inter-linked peptides—were subsequently subjected to MS^3 analysis (Figure 2-6B-C, E-F). Based on the series of y and b ions detected, the sequences of α_A (*m/z* 415.76^{2+}) and α_{A^*} (*m/z*, 418.28^{2+}) were determined as K_AIFQVK and K_{A^*}IFQVK respectively, in which the N-

terminal lysine is modified with the alkene moiety. Similarly, MS^3 analysis of the corresponding β_T (*m/z* 874.40) and β_{T*} (*m/z* 879.43) ions identified their sequences as Ac-GDVEK$_T$GK and Ac-GDVEK$_{T*}$GK respectively, in which the lysine at the fifth position from the N-terminus is modified with the thiol moiety. Together with mass mapping of the parent ions using MS-Bridge, the inter-linked peptides were unambiguously identified as Ac-^{1}GDVEKGK^7 inter-linked to ^{8}KIFQVK^{13}, in which a cross-link was formed between Lys5 and Lys8 in cytochrome C.

In addition to inter-linked peptides, we also identified DMDSSO intra-linked and dead end-modified cytochrome C peptides, confirming that their MS^2 fragmentation patterns are as expected according to Figure 2-2. For example, MS^2 analysis of a selected d_0-intra-linked cytochrome C peptide (*m/z* 621.3203^{3+}) yielded a single dominant fragment ion (α_{A+T}, *m/z* 615.32^{3+}) (Figure 2-7A). Similarly, its corresponding d_{10}-labeled cross-linked peptide (*m/z* 624.6746^{3+}) also generated the same type of MS^2 fragment ion (α_{A*+T*}, *m/z* 618.67^{3+}) (Figure 2-7B), corroborating well with the predicted fragmentation unique to intra-linked peptides. As for dead-end modified peptides, they are expected to generate two distinct MS^2 fragment ions (Figure 2-2C). Such characteristic fragmentation was observed for DMDSSO dead-end peptides as demonstrated by MS^2 spectra of a selected pair of d_0- (*m/z* 546.6116^{3+}) and d_{10}-dead-end (*m/z*

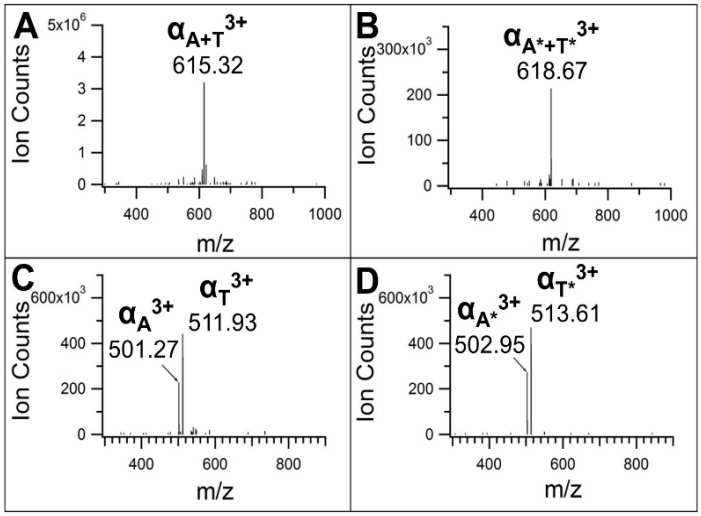

Figure 2-7. MS^2 spectra of d_0/d_{10}-DMDSSO intra-link and dead-end cytochrome C peptides. MS^2 cleavage of a **(A)** d_0-inter-linked peptide α (*m/z* 621.3203^{3+}) and **(B)** d_{10}-inter-linked peptide α (*m/z* 624.6746^{3+}) yielding a single dominant fragment ion α_{A+T} as expected. MS^2 cleavage of a **(C)** d_0-dead-end peptide α (*m/z* 546.6116^{3+}) and **(D)** d_{10}-dead-end peptide α (*m/z* 549.9661^{3+}) yielding characteristic fragment ions α_A/α_T and α_{A*}/α_{T*} as predicted.

549.9661^{3+}) modified cytochrome C peptides, in which a pair of fragment ions α_A/α_T and α_{A*}/α_{T*} were detected in MS^3, respectively (Figure 2-7C-D). Taken together, the results further demonstrate that DMDSSO cross-linked peptides indeed produce specific MS^2 fragmentation patterns that are predictable and reliable, permitting subsequent MS^3 analysis of unique MS^2 fragments for unambiguous identification of cross-linked peptides. These features are consistent with those of DSSO cross-linked peptides [86], further attesting the dependability and versatility of sulfoxide-containing, MS-cleavable cross-linkers in XL-MS studies.

2.4.5 Detection of d_0/d_{10}-DMDSSO Cross-linked Peptide Pairs

To further facilitate the detection and identification of cross-linked peptides, we next mixed the digests of d_0- and d_{10}-DMDSSO cross-linked cytochrome C at 1:1 for LC-MS^n analysis. When analyzed together, d_0- and d_{10}-DMDSSO cross-linked peptides should be detected as isotopic doublets in MS^1 with a defined mass difference ($\Delta(d_{10}\text{-}d_0)$ = n x 10 Da) depending on the number of cross-links (n) in each cross-linked peptide. In contrast, non-cross-linked peptides should be detected only as singlets. This provides additional confirmation to cross-linked peptides identified by MS^n. Not surprisingly, all cross-linked peptides identified display the expected isotopic doublets with 10 Da mass difference, indicative of cross-linked peptides containing one cross-link. This is exemplified by respective peptide pairs detected in MS^1 for the three representative DMDSSO cross-linked cytochrome C peptides described above (Figure 2-8A-C).

In total, 33 unique inter-linked cytochrome C peptides were identified, with 19 being contributed from MS^n analysis of both d_0- and d_{10}-DMDSSO-cross-linked peptides (Table 2-1).

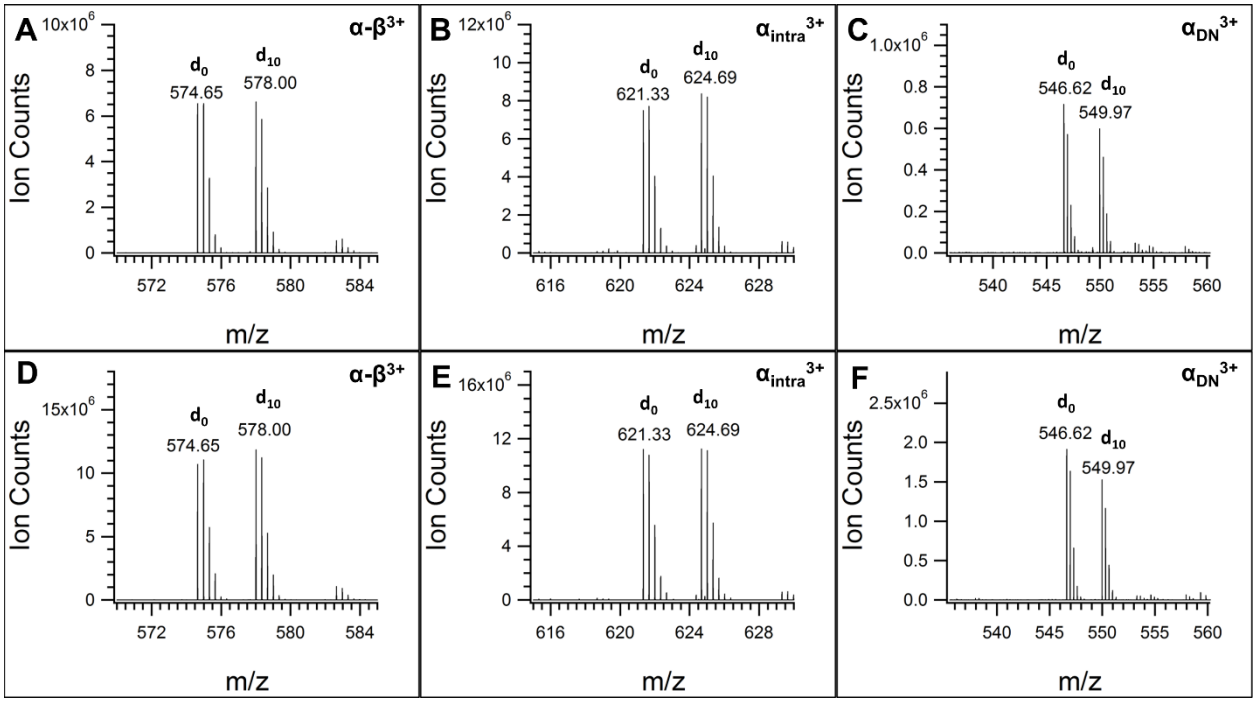

Figure 2-8. MS[1] quantitation of d_0/d_{10}-DMDSSO cross-link species. (A-C) MS^1 spectra of representative inter-link, intra-link, and dead-end peptides from mixed cytochrome C when cross-linked individually with d_0 and d_{10}-DMDSSO. **(D-F)** MS^1 spectra of representative inter-link, intra-link, and dead-end peptides from cytochrome C when cross-linked with 1:1 mixture of d0/d10-DMDSSO.

The remaining 14 inter-links were determined only by MS^n sequencing of either d_0- or d_{10}-DMDSSO-cross-linked peptides. Importantly, the detection of d_0/d_{10} peptide doublets confirms the presence of the missing corresponding cross-linked peptides, even if only one of the d_0 and d_{10} forms is selected and analyzed by MS^n. These results demonstrate that isotope-coded cross-linkers further improve the identification confidence of cross-linked peptides. The 33 identified inter-linked peptides represent 26 unique K-K linkages in cytochrome C, corresponding to C_α-C_α distances that range from 5.3 to 26.2 Å based on the reported monomer crystal structure (PDB:2B4Z). These distances are well within the expected range of our cross-linkers (≤ 26 Å). However, it is noted that several of the identified cross-linked peptides represent inter-protein cross-links and may have larger spatial distances compared to their mapped distance in a monomer structure. For instance, a cytochrome C peptide ^{39}KTGQAPGFSYTDANK^{53} was

found to be cross-linked to another peptide with sequence ^{39}KTGQAPGFSYTDANKNK^{55} through a linkage between Lys39 and Lys53 (Table 2-1). As these two inter-linked peptides share a significant overlap in sequences, they must originate from two separate cytochrome C molecules, indicating an inter-protein inter-link between a cytochrome C dimer.

Previously, we identified 14 inter-linked cytochrome C peptides using DSSO cross-linking [86], eight of which were also determined by d_0/d_{10}-DMDSSO cross-linking in this study. Although each study resulted in several unique cross-linked peptides, it is noted that many of the identified inter-linked lysine residues were in close sequence proximity. For example, while the Lys53 to Lys79 (11.6 Å) linkage was only identified with DSSO cross-linking, Lys55 to Lys73 (11.6 Å) was only detected by DMDSSO cross-linking. Due to the similar calculated distances within these cross-linked lysine residues and the proximities of Lys53 to Lys55 and Lys73 to Lys79, we considered their interaction regions to be similar. Therefore, we clustered 17 lysine residues of cytochrome C into 8 'groups', in which adjacent lysines are within a string of 6 amino acids (Figure 2-9). In comparison to the inter-links identified within these lysine groups, this work has mapped all the cross-linked regions determined by DSSO cross-linking [86]. In addition, 5 additional regional linkages derived from 10 DMDSSO cross-linked peptides were

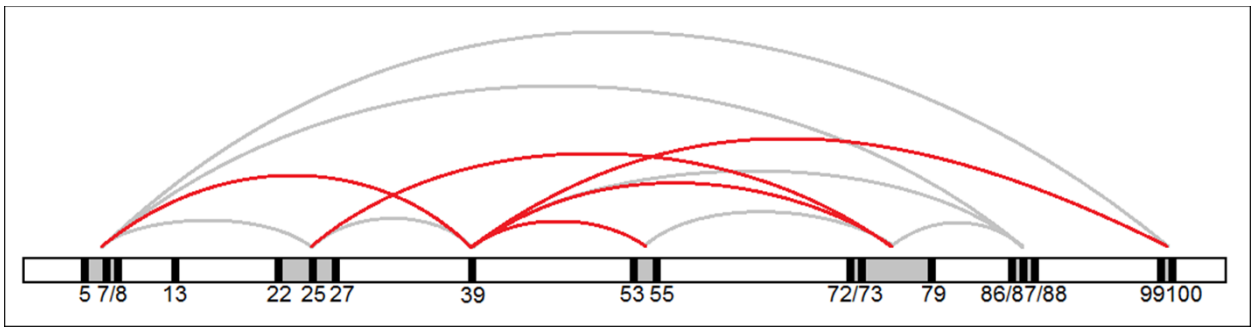

Figure 2-9. Cytochrome C DMDSSO cross-linking map. Cytochrome C lysine residues clustered into 'groups' (gray) based on proximity to one another. Gray lines (7) represent regional inter-links identified in both DSSO cross-linking and DMDSSO cross-linking experiments, while red lines (5) represent newly identified regional inter-links presented in DMDSSO studies.

identified, representing the most extensive cross-linking data on cytochrome C. The increase in results reported in this study are likely attributed to combined improvements in sample preparation and data acquisition, in addition to simultaneous usage of both isotope-coded cross-linkers.

In contrast to previous analyses in which the entire mixture of cross-linked cytochrome C was digested [86], here we only focused on analyzing gel-separated cytochrome C dimer bands. This resulted in a decrease in sample complexity, as monomeric cytochrome C is typically the most abundant species. We also modified the data acquisition method to select only higher charged ions (i.e. 3+ and up) for MS^n analysis. This is because non-cross-linked, dead-end, and intra-linked peptides generally have lower charges compared to inter-linked peptides. This allows the instrument to selectively carry out data-dependent MS^n acquisitions on ions that are more likely to represent inter-linked peptides. Lastly, the concurrent usage of the isotope-labeled cross-linkers also permits confident detection of cross-linked peptides and increases the overall number of inter-linked peptide identifications. Taken together, our current workflow has proven its effectiveness in identifying cross-linked peptides.

2.4.6 Quantitation of d_0-/d_{10}-DMDSSO Cross-linked Peptides

In addition to assisting MS detection and identification of cross-linked peptides, we expect that isotope-coded cross-linkers can be used to study protein structural changes by quantifying relative abundances of non-labeled and labeled cross-linked peptides. To accomplish this, proteins must be cross-linked using non-labeled and labeled cross-linkers separately prior to mixing. The reaction efficiencies of the cross-linking reagents must also be similar. In our experiments, we observed similar cross-linking efficiencies between d_0- and d_{10}-DMDSSO on

cytochrome C (Figure 2-5). Since previous XL-MS studies utilized protein cross-linking using a 1:1 mixture of non-labeled and labeled cross-linkers to generate isotopic pairs, we wanted to confirm that equivalent results could be achieved using a similar sample preparation. Therefore, we first cross-linked cytochrome C with a equimolar mixture of d_0- and d_{10}-DMDSSO, and then analyzed the resulting cross-linked peptide digests by MS^n (Figure 2-8D-F). Similarly, equal mixing of individually cross-linked d_0- and d_{10}-DMDSSO peptide digests also yielded doublets of DMDSSO cross-linked peptides with relative intensity ratios close to 1 (Figure 2-8A-C). Therefore, we concluded that corresponding d_0- and d_{10}-labeled cross-linked peptides display similar relative abundance ratios regardless of whether mixing was done before or after protein cross-linking. These results suggest that our isotopically-labeled cross-linkers are indeed comparable in their cross-linking ability and that the resulting d_0- and d_{10}-labeled cross-linked products behave similarly during sample preparation and MS^n analysis, thus providing additional flexibility for these isotope-labeled reagents in XL-MS studies.

To further explore the capability of d_0- and d_{10}-DMDSSO for quantitative analysis, we aimed to determine whether the signal intensity ratios of ions in each d_0- and d_{10}-DMDSSO doublet reflected their relative concentrations in solution. We first cross-linked cytochrome C with d_0- and d_{10}-DMDSSO separately, carried out their in-gel digestions, and then mixed the resulting peptide digests in five chosen d_0/d_{10} ratios (i.e. 5:1, 2:1, 1:1; 1:2, 1:5) prior to LC-MS^n analysis. To determine their relative abundance ratios, we manually obtained the extracted ion chromatograms (XIC) for five selected d_0- and d_{10}-labeled cross-linked peptide pairs in each sample. As an example, we show the overlays of XICs for a representative d_0- and d_{10}-DMDSSO inter-linked peptide pair in five samples mixed with different ratios (Figure 2-10A-E). The corresponding MS^1 spectra are also displayed. (Figure 2-10F-J). Based on the calculated area

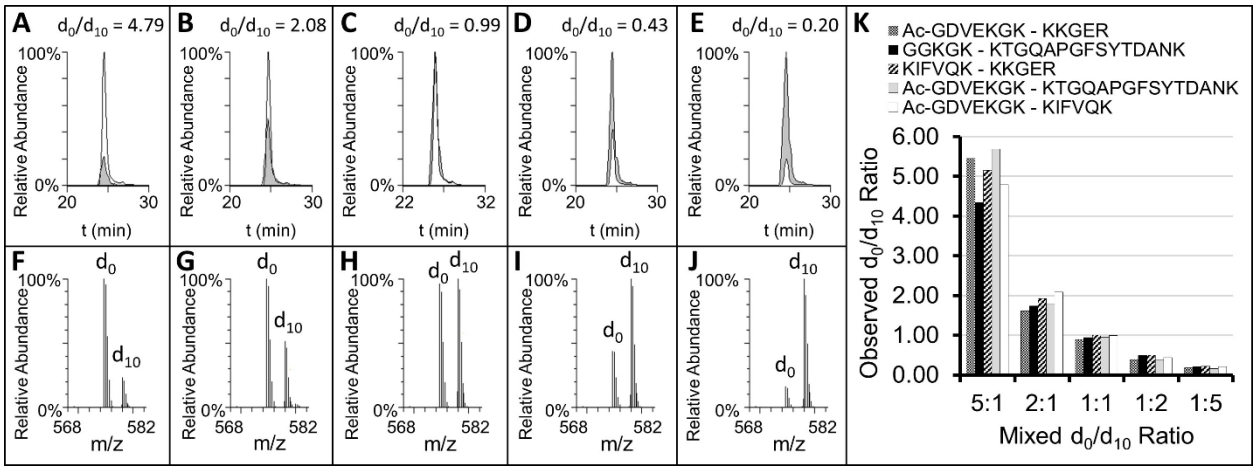

Figure 2-10. Quantitative analysis of d_0/d_{10}-DMDSSO cross-linked cytochrome C peptides. (A-E) Extracted ion chromatogram (XIC) overlays for a selected d_0- and d_{10}-inter-linked peptide pair (*m/z* $574.64^{3+}/578.00^{3+}$) from digests of d_0- and d_{10}-DMDSSO cross-linked peptides mixed at 5:1, 2:1, 1:1, 1:2, and 1:5 ratios. The shaded portions represent the area of the XICs of d_{10}-inter-linked peptides. **(F-J)** Representative MS^1 spectra obtained at peak intensity for each corresponding XIC overlay shown in A-E, respectively. **(K)** Observed ratios of d_0/d_{10} ion signals for five selected inter-linked cytochrome C peptides. Peptide sequences are shown in the inset.

under each XIC curve, the relative abundances (d_0/d_{10}) were determined as 4.79, 2.08, 0.99, 0.43 and 0.20 respectively, which correlate well with the initial sample mixing. In addition, the ratios obtained from peptide peak intensities were similar to those obtained using XIC areas, indicating that both approaches are applicable for calculating the relative abundances of cross-linked peptides. As shown in Figure 2-10K, the average ratios of the five selected cross-linked peptides for each sample corroborate very well with initial sample mixing. Collectively, these results have demonstrated the capability of quantifying cross-linked peptides using isotope-coded DMDSSO reagents.

2.5 Conclusion

We report here the development and characterization of new DSSO derivatives, a pair of isotope-coded, MS-cleavable cross-linkers: d_0- and d_{10}-DMDSSO. DMDSSO cross-linked peptides preserve the same characteristic MS^2 fragmentation patterns distinctive to various

DSSO cross-linked peptide species, facilitating the identification of cross-linked peptides using our previously developed MS^n workflow. In combination with MS^3 sequencing and MS^1 mass mapping and isotopic profiling, the type and identity of cross-linked peptides can be determined readily and unambiguously. In addition, we have shown the flexibility in using d_0- and d_{10}-DMDSSO for quantitative analysis of cross-linked peptides, thus establishing a solid foundation for our future studies towards the understanding of structural dynamics of protein complexes. Lastly, this work further demonstrates the robustness of sulfoxide-containing, MS-cleavable cross-linkers in XL-MS studies and provides a strong basis for us to further develop new sulfoxide-containing derivatives to explore the structural minutia of protein-protein interactions.

Table 2-1. Summary of Cytochrome C Cross-links Identified by d_0- and d_{10}-DMDSSO.

Peptide Sequence	Resi	Mod Resi	Distance (c_α-c_α)	d_0-DMDSSO	d_{10}-DMDSSO
Ac-GDVEKGK KIFVQK	1-7 8-13	5T 8A	5.32	**X**	
Ac-GDVEKGK KTGQAPGFSYTDANK	1-7 39-53	5T 39A	26.19	**X**	**X**
Ac-GDVEKGK KK*	1-7 87-88	5A 87	12.98	**X**	**X**
Ac-GDVEKGK KKGER	1-7 87-91	5T 87A	12.98	**X**	**X**
Ac-GDVEKGK KKGEREDLIAYLK	1-7 87-99	5T 87|88A	13.03	**X**	**X**
Ac-GDVEKGKK KK*	1-8 87-88	5|7A 87T	15.70		**X**
Ac-GDVEKGKK KKGER	1-8 87-91	5|7A 87|88A	15.73	**X**	**X**
Ac-GDVEKGKK KKGEREDLIAYLK	1-8 87-99	5|7T 87|88A	15.73	**X**	**X**

KIFVQK GGKHK*	8-13 23-27	8A 25T	20.41	**X**	**X**
KIFVQK KTGQAPGFSYTDANK	8-13 39-53	8T 39A	25.89	**X**	
KIFVQK KK*	8-13 87-88	8A 87T	14.81	**X**	**X**
KIFVQK KKGER	8-13 87-91	8A 87|88T	15.72	**X**	**X**
KIFVQK KGER*	8-13 88-91	8A 88T	15.72	**X**	**X**
KIFVQK EDLIAYLKK	8-13 92-100	8T 99A	14.39		**X**
KIFVQK GEREDLIAYLKK	8-13 89-100	8A 99T	14.39	**X**	**X**
GGKHK* HKTGPNLHGLFGR	23-27 26-38	25A 27T	6.29	**X**	**X**
GGKHK KTGQAPGFSYTDANK	23-27 39-53	25T 39A	19.25	**X**	**X**
GGKHK GITWGEETLMEYLENPKK	23-27 56-73	25T 72A	24.02	**X**	
KTGQAPGFSYTDANK KTGQAPGFSYTDANKNK	39-53 39-55	39A 53T	8.35	**X**	
KTGQAPGFSYTDANK NKGITWGEETLMEYLENPKK	39-53 54-73	39A 55T	8.49	**X**	
KTGQAPGFSYTDANK GITWGEETLMEYLENPKK*	39-53 56-73	39A 72T	17.37	**X**	
KTGQAPGFSYTDANK KYIPGTK	39-53 73-79	39A 73T	17.75	**X**	
KTGQAPGFSYTDANK MIFAGIKK	39-53 80-87	39A 86T	24.17	**X**	**X**
KTGQAPGFSYTDANK KGER*	39-53 88-91	39A 88T	23.26	**X**	**X**
KTGQAPGFSYTDANK EDLIAYLKK	39-53 92-100	39A 99T	15.09	**X**	**X**
KTGQAPGFSYTDANK GEREDLIAYLKK	39-53 89-100	39A 99T	15.09		**X**

KTGQAPGFSYTDANK KATNE*	39-53 100-104	39T 100A	18.01	**X**	**X**
NKGITWGEETLMEYLENPK KYIPGTK	54-72 73-79	55A 73T	11.62	**X**	**X**
GITWGEETLMEYLENPKK MIFAGIKK	56-73 80-87	72T 86A	13.65		**X**
GITWGEETLMEYLENPKK M(ox)IFAGIKK	56-73 80-87	72A 86T	13.65	**X**	
KYIPGTK M(ox)IFAGIKK	73-79 80-87	73A 86T	13.22		**X**
MIFAGIKK KGER*	80-87 88-91	86T 88A	6.41	**X**	**X**
M(ox)IFAGIKK KGER*	80-87 88-91	86T 88A	6.41		**X**

Peptides not selected for MS^3, but corresponding isotope for parent ion detected.

CHAPTER 3: Gln40 deamidation Blocks Structural Reconfiguration and Activation of SCF Ubiquitin Ligase Complex by Nedd8

Reprinted with permission from:

Clinton Yu, Haibin Mao, Eric J. Novitsky, Xiaobo Tang, Scott D. Rychnovsky, Ning Zheng, & Lan Huang. **Gln40 deamidation Blocks Structural Reconfiguration and Activation of SCF Ubiquitin Ligase Complex by Nedd8.** *Nature Communications*, 2015; 6: 10053.

3.1 Summary

The full enzymatic activity of the cullin-RING ubiquitin ligases (CRLs) requires a ubiquitin-like protein (i.e. Nedd8) modification. By deamidating Gln40 of Nedd8 to glutamate (Q40E), the bacterial cycle inhibiting factor (Cif) family can inhibit CRL E3 activities, thereby interfering with cellular functions. Despite extensive structural studies on CRLs, the molecular mechanism by which Nedd8 Gln40 deamidation affects CRL functions remains unclear. We applied a new quantitative cross-linking mass spectrometry (QXL-MS) approach to characterize three different types of full-length human Cul1-Rbx1 complexes, uncovering major Nedd8-induced structural rearrangements of the CRL1 catalytic core. More importantly, we find that those changes are not induced by Nedd8(Q40E) conjugation, indicating that the subtle change of a single Nedd8 amino acid is sufficient to revert the structure of the CRL catalytic core to its unmodified form. Our results provide new insights into how neddylation regulates the conformation and activity of CRLs.

3.2 Introduction

Cullin-RING ubiquitin ligases (CRLs) represent a superfamily of multi-subunit E3 ubiquitin ligases comprised of a cullin-RING catalytic core and adaptor proteins that mediate the recruitment of protein substrates [134, 136, 148-150]. Eight cullin family proteins (Cul1, Cul2, Cul3, Cul4A/B, Cul5, Cul7, and Cul9) are found in humans, each functioning as a scaffold on which a variety of CRLs are assembled. The SCF/CRL1 (Skp1-Cul1-F-box-protein) complex represents the prototypical CRL E3, which uses Cul1-Rbx1 as the catalytic core [134, 151, 152]. The Cul1 scaffold binds the Skp1 adaptor and the Rbx1 RING subunit at its N-terminal and C-terminal domains, respectively. Skp1 in turn docks F-box proteins, which are substrate receptors that confer substrate specificity to the SCF, while the RING-finger domain of Rbx1 engages ubiquitin-charged E2, mediating the transfer of ubiquitin to the F-box protein-bound substrate. A reconstructed structure model of the SCF based on crystal structures of several overlapping sub-complexes reveals an elongated E3 platform, in which the F-box protein is separated from the Rbx1-bound E2 by a ~50 Å distance [153].

Covalent conjugation of ubiquitin-like protein Nedd8 (i.e. neddylation) to a specific lysine residue (Lys720) of Cul1 has been shown to promote both E2 recruitment and subsequent ubiquitin transfer, thereby stimulating the E3 activity of SCF ligases [134, 149, 154-156]. Although the intact neddylated Cul1-Rbx1 complex remains recalcitrant to crystallization, crystal structures of a truncated C-terminal domain of Cul5 in complex with Rbx1 have shed light on the effects of neddylation on the conformation of the cullin-RING catalytic core [157]. In the unneddylated form, the $Cul5^{CTD}$-Rbx1 complex adopts a “closed” conformation in which the RING-finger domain of Rbx1 is nestled within a hydrophobic pocket of $Cul5^{CTD}$. Upon neddylation, the RING-finger domain of Rbx1 is released from the pocket, deemed the “open”

state, but remains tethered by its N-terminus to Cul5, presumably allowing the extended RING-finger to sample the three-dimensional space around Cul5. This conferred flexibility has been proposed to enable Rbx1 to close the distance between substrate and E2, facilitating the transfer of ubiquitin from E2 to substrate protein [149].

Notably, the cycle inhibiting factors (Cifs) found in many pathogenic Gram-negative bacteria can irreversibly deamidate a specific glutamine residue (Gln40) of Nedd8 and convert it to glutamate [158]. While this Q40E modification has no effect on cullin neddylation, it effectively abolishes the E3 activity of CRLs and stimulates increased cullin deneddylation by the COP9 signalosome [158-161]. These observations raise an intriguing question as to how the subtle change of a single Nedd8 amino acid can negate the effect of neddylation in remodeling the ~100 kDa CRL catalytic core. In the structure of the neddylated $Cul5^{CTD}$-Rbx1 complex, Gln40 of Nedd8 is close to the isopeptide bond between Nedd8 and Cul5 and is partially sandwiched between the two proteins. The amide group in the Gln40 side chain, however, is solvent exposed and does not participate in any hydrogen bond interactions [157]. The molecular mechanism by which Nedd8 Gln40 deamidation alters CRL functions remains elusive.

Recently cross-linking mass spectrometry (XL-MS) has risen as a powerful method to study protein-protein interactions and characterize the structure of large protein complexes [41, 43, 63, 89, 162-167]. In comparison to X-ray crystallography or NMR, XL-MS approaches have much less restriction on sample preparation due to its sensitivity, flexibility, and versatility, and can capture the dynamic states of large, heterogeneous protein structures. By stabilizing transient interactions, chemical cross-linking preserves various structural states of dynamic complexes, yielding a representation that describes the average state of a protein complex and providing a complementary set of structural data different from those obtained from rigid state data analyses.

Recently we have developed a new class of cross-linkers (i.e. sulfoxide-containing, MS-cleavable cross-linking reagents), to enable simplified and unambiguous identification of cross-linked peptides using multistage tandem mass spectrometry (MS^n) [50, 86, 88]. These new types of cross-linkers are robust and reliable, and have been successfully applied to define protein-protein interactions both *in vitro* [50, 86, 89] and *in vivo* [50]. To establish a robust quantitative XL-MS platform to study dynamic protein complexes, we have developed a pair of stable isotope-labeled amine reactive cross-linkers (d_0- and d_{10}-labeled dimethyl-disuccinimidyl sulfoxide (DMDSSO)) that allow simultaneous identification and quantitation of cross-linked peptides [88]. In combination with quantitative analysis, XL-MS can determine dynamic conversion between the average states of protein complexes under different conditions.

Here, we employ this DMDSSO-based quantitative XL-MS strategy to define the structural changes of full-length Cul1-Rbx1 modified by either wild-type Nedd8 or its Q40E mutant, which is the product of Gln40 deamidation. Quantitative similarities and differences in cross-linked peptide abundances can be attributed to changes in protein complex structures under different conditions, as the occurrences of spatially proximal amino acid residues suited for cross-linking are directly dependent on the complexes' three-dimensional conformations. Our results have provided new insights on how Nedd8 modification impacts the topology of Cul1-Rbx1 and the effect of Nedd8 Gln40 deamidation on the structure of the activated CRL core.

3.3 Experimental Procedures

3.3.1 Materials and Reagents

General chemicals were purchased from Fisher Scientific or VWR international. Sequencing grade modified trypsin was purchased from Promega (Fitchburg, WI).

3.3.2 Preparation of Cul1-Rbx1 Protein Complexes

Heterodimeric NEDD8-activating enzyme APPBP1-Uba3 was prepared as described previously [168]. Briefly, APPBP1 was subcloned into a modified pGEX4T1 (Amersham Biosciences) vector containing a GST tag followed by a TEV protease cleavage site, while Uba3 was subcloned into a modified pET15b (Novagen) vector containing a chloramphenicol resistance cassette. Glutathione S-transferase (GST)–APPBP1 and Uba3 were co-expressed in BL21(DE3) (Novagen) and purified by glutathione affinity chromatography. After TEV cleavage, the APPBP1-Uba3 complex was further purified by anion exchange and gel filtration.

Nedd8 and the Nedd8-conjugating enzyme Ubc12 were subcloned into the same pGEX4T1 vector, co-expressed in *Escherichia coli* BL-21(DE3) cells, and purified by glutathione affinity and anion exchange chromatography. In this study, we used a truncated version of Nedd8 ending at glycine 76, representing its mature form.

Two short unstructured segments in the N-terminus of Cul1 (residues 1-12 and 58-81) were removed from full length human Cul1 to form $Cul1^{\Delta N}$ (referred to here as Cul1). Both Cul1 and $Rbx1^{16\text{-}108}$ were fused with an N-terminal His_6 tag followed by a TEV cleavage site and co-expressed in BL-21(DE3). The complex was first purified by a Ni^{2+} sepharose affinity column (GE Healthcare) and further purified by cation exchange and gel filtration chromatography after TEV cleavage. To prepare Nedd8~Cul1-Rbx1, 10 μM purified Cul1-Rbx1 was neddylated with 10 μM GST-Nedd8 in the presence of 0.2 μM APPBP1-Uba3 and 0.5 μM Ubc12 for 1 hour at 4 ^{o}C as previously reported [157]. Nedd8~Cul1-Rbx1 was then separated from free Cul1-Rbx1 by a glutathione affinity column. After TEV cleavage, Nedd8~Cul1-Rbx1 was eluted off the column and further purified by cation exchange and gel filtration chromatography. Nedd8(Q40E)-modified Cul1-Rbx1 was purified similarly to the wild-type.

Full-length human ubiquitin-activating enzyme Ube1 was expressed as a GST fusion protein in High Five insect cells using the Bac-to-Bac baculovirus expression system (Invitrogen). Insect cells were collected 48-72 h post-infection and lysed, followed by glutathione affinity chromatography. Recombinant human Cdc34 was overexpressed and purified from *E. Coli* by a similar approach as the Nedd8 purification. Recombinant untagged ubiquitin (Ub) was expressed in BL21(DE3). After sonication and centrifugation, cleared lysate was adjusted to 3.5% perchloric acid. After precipitated proteins were removed by centrifugation, ubiquitin in the supernatant was further purified by cation-exchange chromatography and dialysis against 20 mM Tris, pH 8.0 thoroughly.

3.3.3 Ubiquitination Assays

For free ubiquitin chain synthesis assay, a mixture containing 100 μM Ub, 0.3 μM UBE1 and 1.0 μM Cdc34 was incubated with 0.4 μM Cul1-Rbx1 variants in a reaction buffer of 50 mM Tris-HCl, 200 mM NaCl, 2 mM ATP, 10 mM $MgCl_2$, pH 8.0. After incubation at 37 ^oC for 4 hours, the reaction mixtures were resolved by a 15% SDS-PAGE gel and transferred onto a nitrocellulose membrane, which was incubated overnight with a mouse monoclonal anti-ubiquitin antibody (Sigma-Aldrich, #U0508) at 1:2500 dilution. The membrane was washed and incubated with HRP-linked ECL^{TM}-anti mouse IgG (GE Healthcare, #NA931V) for 1h. Free ubiquitin chains were visualized by SuperSignal West Pico Chemiluminescent Substrate (Pierce Biotechnology, #34080)).

For the CRY2 ubiquitination assay, a reaction mixture containing 0.2 μM CRY2-FBXL3-SKP1 complex [169], 70 μM Ub, 0.15 μM UBE1 and 1.5 μM Cdc34 was incubated with 0.4 μM Cul1-Rbx1 variants in a reaction buffer of 40 mM Tris-HCl (pH7.5), 2 mM DTT, 5 mM $MgCl_2$ and 2 mM ATP. The reactions were carried out at 37°C and quenched at different time points by

adding SDS-PAGE loading buffer, then analyzed by western blot with a rabbit anti-CRY2 antibody (LifeSpan BioSciences. Inc #LS-C6229) at 1:1,000 dilution and HRP-linked ECL™-anti rabbit IgG (GE Healthcare, #NA934V).

3.3.4 DMDSSO Cross-linking and Digestion of Cul1-Rbx1 Complexes

Purified complexes were diluted to 4 μM in 20 mM HEPES (pH 7.5) and reacted with d_0- or d_{10}-DMDSSO at a molar ratio of 1:25 (protein: cross-linker) for 45 min at room temperature and quenched with excess ammonium bicarbonate. Cross-linked proteins were then separated by SDS-PAGE and visualized by Coomassie blue. Bands corresponding to cross-linked complexes were excised, reduced with TCEP for 30 min at RT and alkylated with chloroacetamide for 30min at RT in dark, and then digested with trypsin at 37°C overnight. Peptide digests were extracted, concentrated and reconstituted in 3% ACN/2% formic acid prior to LC-MS^n analysis. To allow quantitative pair-wise complex comparisons, individually cross-linked proteins were strategically mixed, e.g., d_0-DMDSSO-cross-linked Cul1-Rbx1 with d_{10}-DMDSSO-cross-linked Nedd8~Cul1-Rbx1, at a 1:1 ratio and subjected to subsequent sample preparation together as outlined above.

3.3.5 Liquid Chromatography-Multistage Tandem Mass Spectrometry (LC MS^n)

DMDSSO cross-linked peptides were analyzed by LC-MS^n utilizing an LTQ-Orbitrap XL mass spectrometer (Thermo Fisher, San Jose, CA) coupled on-line with an Easy-nLC 1000 (Thermo Fisher, San Jose, CA) as previously described [86, 88]. Each MS^n experiment consists of one MS scan in FT mode (350-1400 m/z, resolution of 60,000 at m/z 400) followed by two data-dependent MS^2 scans in FT mode (resolution of 7500) with normalized collision energy at

20% on the top two MS peaks with charges at 3+ or up, and three MS^3 scans in the LTQ with normalized collision energy at 35% on the top three peaks from each MS^2.

3.3.6 Data Analysis, Identification and Quantification of Cross-linked Peptides

Monoisotopic masses of parent ions and corresponding fragment ions, parent ion charge states, and ion intensities from MS^2 and MS^3 spectra were extracted using in-house software based on the Raw_Extract script from Xcalibur v2.4 (Thermo Scientific) [50, 86, 88]. MS^3 data was subjected to a developmental version of Protein Prospector (v. 5.10.10) for database searching, using Batch-Tag against a limited database containing recombinant Cul1, Rbx1, Nedd8 and Nedd8(Q40E) sequences with mass tolerances for parent ions and fragment ions set as ± 20 ppm and 0.6 Da respectively. Trypsin was set as the enzyme with five maximum missed cleavages allowed. A maximum of five variable modifications were also allowed, including protein N-terminal acetylation, methionine oxidation, N-terminal conversion of glutamine to pyroglutamic acid, asparagine deamidation, and cysteine carbamidomethylation. In addition, six defined modifications on uncleaved lysines and free protein N-termini were also selected: alkene (A: C_4H_4O, +68 Da; or A*: $C_4H_{-1}D_5O$, +73 Da), sulfenic acid (S: $C_4H_6O_2S$, +118 Da; or S*: $C_4H_1D_5O_2S$, +123 Da), and unsaturated thiol (T: C_4H_4OS, +100 Da; or T*: $C_4H_{-1}D_5OS$, +105 Da) modifications, due to remnant moieties of d_0- (i.e. A, S, T) and d_{10}-DMDSSO (i.e. A*, S*, T*). It is noted that the sulfenic acid moiety often undergoes dehydration to become a more stable and dominant unsaturated thiol moiety (i.e. T, +100 Da or T*, +105 Da) as previously described [50, 86, 88]. Initial acceptance criteria for peptide identification required a reported expectation value ≤ 0.1. Integration of MS^n data was carried out using the in-house program xl-Discoverer, a revised version of the previously written Link-Finder program, to validate and summarize cross-linked peptides [86, 89].

Only inter-linked DMDSSO cross-linked peptides were subjected to subsequent manual quantitation, as they provide the most useful information on protein structures. Using Skyline (v. 2.5.06157) (https://skyline.gs.washington.edu), we determined the spectral abundances of all d_0- and d_{10}-DMDSSO cross-linked peptides in each pair-wise comparison and calculated the relative abundances of d_0/d_{10} cross-linked peptides. Abundance ratios for cross-linked peptides were then used to determine the relative occurrences of the corresponding K-K linkages across all purified complexes. All linkages were then mapped onto the Cul1-Rbx1 crystal structure (PDB: 1LDJ), as well as the derived homology model of Nedd8~Cul1-Rbx1 [170], in order to compare experimentally-derived occurrences of K-K linkages to the C_α-C_α distances as determined by structural models.

3.4 Results & Discussion

3.4.1 Reconstitution of SCF E3 Activity with Intact Proteins

To enhance the solubility and stability of Cul1, we removed two short segments (details in Methods) of Cul1 which were not visible in the crystal structure of Cul1-Rbx1 complex (PDB: 1LDJ) [170], drastically improving protein behavior. This truncated Cul1 and $Rbx1^{16\text{-}108}$ were co-expressed and purified from *E. coli*. The purified Cul1-Rbx1 was conjugated to wild-type Nedd8 to yield neddylated Cul1-Rbx1 complex (Nedd8~Cul1-Rbx1). The Q40E mutant Nedd8, in which Gln40 was replaced with Glu40 to mimic deamidated Nedd8, can also be efficiently conjugated to Cul1-Rbx1 to form Nedd8(Q40E)~Cul1-Rbx1. Both neddylated Cul1-Rbx1 samples were affinity purified by Nedd8 after neddylation to remove unmodified species.

To understand ubiquitin ligase activities of different forms of Cul1-Rbx1, we have employed two *in vitro* ubiquitination assays: free ubiquitin chain assembly and ubiquitination of

cryptochrome 2 (CRY2). CRY2, a key regulator of circadian rhythm, is a well-characterized substrate of the SCF^{FBXL3} ubiquitin ligase [169, 171-173]. In both assays, we used Cdc34, the canonical E2 of Cul1. Consistent with previous reports, Cul1-Rbx1 can promote substrate-independent free ubiquitin chain assembly, while Nedd8~Cul1-Rbx1 significantly enhanced the reaction kinetics (Figure 3-1A) [174]. In contrast, Nedd8(Q40E)~Cul1-Rbx1 only exhibited comparable activity to unneddylated Cul1-Rbx1, significantly weaker than that of Nedd8~Cul1-

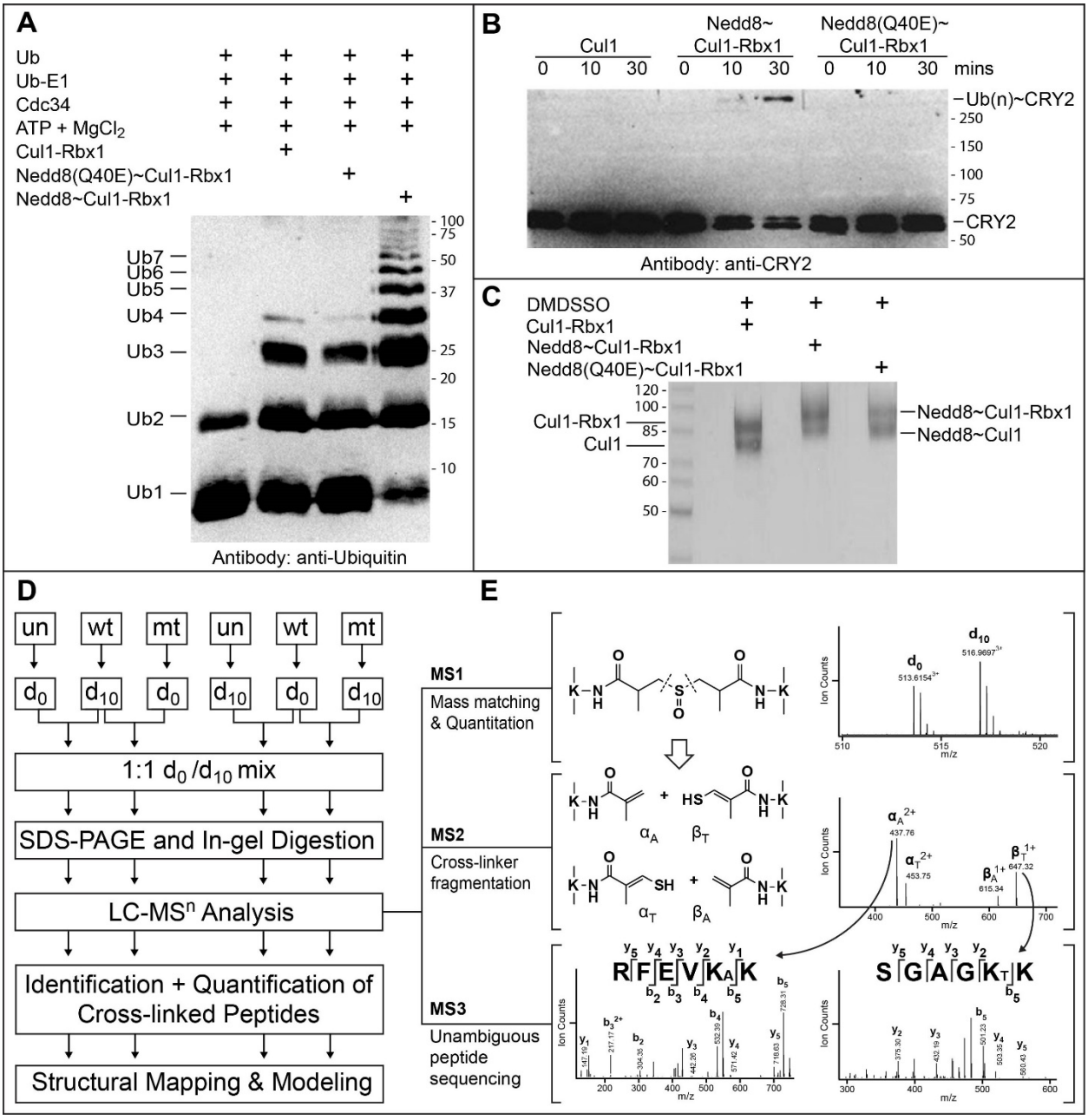

Figure 3-1. Biochemical assays for ubiquitin-ligase activity and general quantitative XL-MS experimental workflow. (A) Comparisons of ubiquitin-ligase activities of different Cul1-Rbx1 variants on free ubiquitin chain assembly. Synthesized unanchored polyubiquitin chains were detected by anti-ubiquitin western blot. Highly efficient polyubiquitin synthesis was only detected in the presence of Nedd8-Cul1-Rbx1 (lane 4). For visual clarity, ubiquitin polymers are simply abbreviated as Ub(n) (e.g. Ub2 as ubiquitin dimer, Ub3 as trimer, etc.). **(B)** Comparison of ligase activities of Cul1-Rbx1 variants on CRY2 ubiquitination. Ubiquitination reactions were quenched at indicated time points. Ubiquitinated CRY2 was detected using an anti-CRY2 antibody. Successful ubiquitination of CRY2 occurs only in the presence of Nedd8-Cul1-Rbx1 (lane 6). **(C)** SDS-PAGE analysis of cross-linked Cul1-Rbx1, Nedd8~Cul1-Rbx1, and Nedd8(Q40E)~Cul1-Rbx1 complexes. **(D)** d_0/d_{10}-DMDSSO based quantitative XL-MS workflow for identifying and quantifying cross-linked peptides of Cul1-Rbx1 complexes. The three types of Cul1-Rbx1 complexes (i.e. un – unneddylated; wt – wild-type neddylated; mt – mutant Q40E-neddylated) were first cross-linked by DMDSSO separately, followed by pair-wise mixing prior to SDS-PAGE. Four types of mixing were made to obtain sufficient pair-wise comparison among the three samples. Gel bands representing cross-linked protein complexes were subsequently excised and in-gel digested prior to LC-MS^n analysis for identification and quantification**. (E)** Representative MS^n analysis of DMDSSO inter-linked peptides. MS^1 spectrum shows the detection of a pair of d_0-DMDSSO and d_{10}-DMDSSO cross-linked peptides (*m/z* 513.6154^{3+} and *m/z* 516.9697^{3+}) whose relative abundance ratio is used for quantitation. MS^2 analysis of the d_0-DMDSSO inter-linked peptides α-β (*m/z* 513.6154^{3+}) yielded two peptide fragment pairs: α_A/β_T (*m/z* $437.76^{2+}/647.32^{1+}$) and α_T/β_A (*m/z* $453.75^{2+}/615.34^{1+}$), confirming its cross-link type as an interlink. Subsequent MS^3 analyses of the α_A (m/z 437.76^{2+}) and β_T (647.32^{1+}) ions produced series of y and b ions which enabled unambiguous identification of α_A as RFEVK_AK of Rbx1 and β_T as SGAGK_TK of Rbx1. Integration of the MS^n (i.e. MS^1, MS^2 and MS^3) data confirmed the d_0-DMDSSO cross-linked peptide as an intra-subunit interlink between Lys19 and Lys25 of Rbx1. K_A: alkene modified lysine; K_T: unsaturated thiol modified lysine.

Rbx1. This is consistent with the discovery that deamidation of Q40 in Nedd8 abolishes the ligase activity of neddylated Cul1-Rbx1[158, 159].

We further confirmed this observation with an *in vitro* ubiquitination assay of CRY2. As shown in Figure 3-1B, polyubiquitin chains were formed on CRY2 in the presence of Nedd8~Cul1-Rbx1. In contrast, neither unneddylated nor Nedd8(Q40E)-modified Cul1-Rbx1 were able to catalyze ubiquitination of CRY2. This further confirms that Nedd8~Cul1-Rbx1 is the only active form and that deamidation of Q40 in Nedd8 can in fact abrogate its activity. Compared to the free ubiquitin chain assembly assay, the polyubiquitin chain synthesis on CRY2 was highly processive, as the ubiquitinated CRY2 band was observed at the top of the gel as

shown by western blot analysis. Taken together, our results have demonstrated neddylation is essential for the activation of the Cul1-Rbx1 complex in protein ubiquitination. Importantly, distinct functional disparity between Nedd8~Cul1-Rbx1 and Nedd8(Q40E)~Cul1-Rbx1 has been further validated, confirming that the CRLs requires functional Nedd8 for protein ubiquitination.

3.4.2 Quantitative XL-MS strategy

To uncover molecular details underlying the functional differences between different forms of Cul1-Rbx1 complexes, we have employed a quantitative XL-MS strategy based on a newly developed pair of stable-isotope coded MS-cleavable cross-linkers, d_0-DMDSSO and d_{10}-

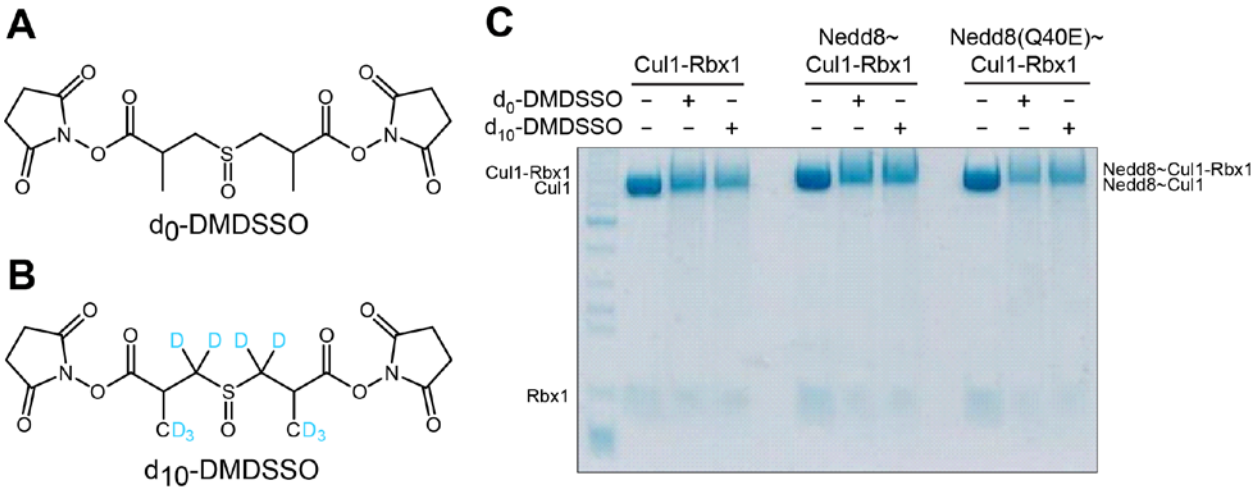

Figure 3-2. d_0- and d_{10}-DMDSSO structure and cross-linking efficiency. Molecular structures of **(A)** d_0-DMDSSO and **(B)** d_{10}-DMDSSO. **(C)** SDS-PAGE separation of unneddylated, wild-type neddylated, and mutant Q40E neddylated Cul1-Rbx1 complexes cross-linked by d_0- and d_{10}-DMDSSO.

DMDSSO [88] (Figure 3-2A, 3-2B), to examine the structural similarities and dissimilarities between these complexes. Concurrent usage of these two cross-linking reagents enables quantitative comparisons between the three-dimensional structures of protein complexes under various states. To establish the quantitative XL-MS workflow for comprehensive structural comparisons among unneddylated (un), wild-type neddylated (wt) and Q40E mutant neddylated

(mt) Cul1-Rbx1 complexes, cross-linking conditions were first optimized through *in vitro* cross-linking of the three protein complexes using various concentrations of either d_0-DMDSSO or d_{10}-DMDSSO and several reaction durations. Cross-linking efficiency was then evaluated by separating the resulting cross-linked products using 1-D SDS-PAGE. As shown in Figure 3-1C, the resulting cross-linked products correspond well to respective molecular weights of these three complexes with approximately 50% cross-linking efficiency. In addition, we have determined that d_0- and d_{10}-DMDSSO cross-linked Cul1-Rbx1 complexes with similar efficiency as illustrated in Figure 3-2C, also reflected in previous testing on standard proteins [88]. These results demonstrate that d_0- and d_{10}-labeled DMDSSO are well suited for quantitative XL-MS analysis of these protein complexes.

To enable sufficient comparisons among the three different types of protein complexes with the minimal number of samples for analysis, we strategically selected Nedd8~Cul1-Rbx1 as the cross-sample reference in each pair-wise comparison experiment. As illustrated in Figure 3-1D, d_{10}-DMDSSO cross-linked Nedd8~Cul1-Rbx1 was mixed with d_0-DMDSSO cross-linked Cul1-Rbx1 or d_0-DMDSSO cross-linked Nedd8(Q40E)~Cul1-Rbx1, followed by SDS-PAGE separation. The regions corresponding to expected cross-linked complexes were in-gel digested and the resulting peptides were subjected to LC-MS^n analysis. DMDSSO cross-linked peptides were identified unambiguously based on MS^n data (i.e. MS^1, MS^2, and MS^3, as previously described) [50, 86, 88]. Representative MS^n analyses of d_0-DMDSSO and d_{10}-DMDSSO inter-linked peptides α-β (*m*/*z* 513.6154^{3+} and *m*/*z* 516.9697^{3+}, respectively) are shown (Figure 3-1E and Figure 3-3). As depicted in Figure 3-1E, MS^2 analysis of the d_0-DMDSSO inter-linked peptide α-β yielded two expected fragment pairs α_A/β_T (*m/z* $437.76^{2+}/647.32^{1+}$) and α_T/β_A (*m/z* $453.75^{2+}/615.34^{1+}$), which are characteristic of DMDSSO inter-linked peptides [88], confirming

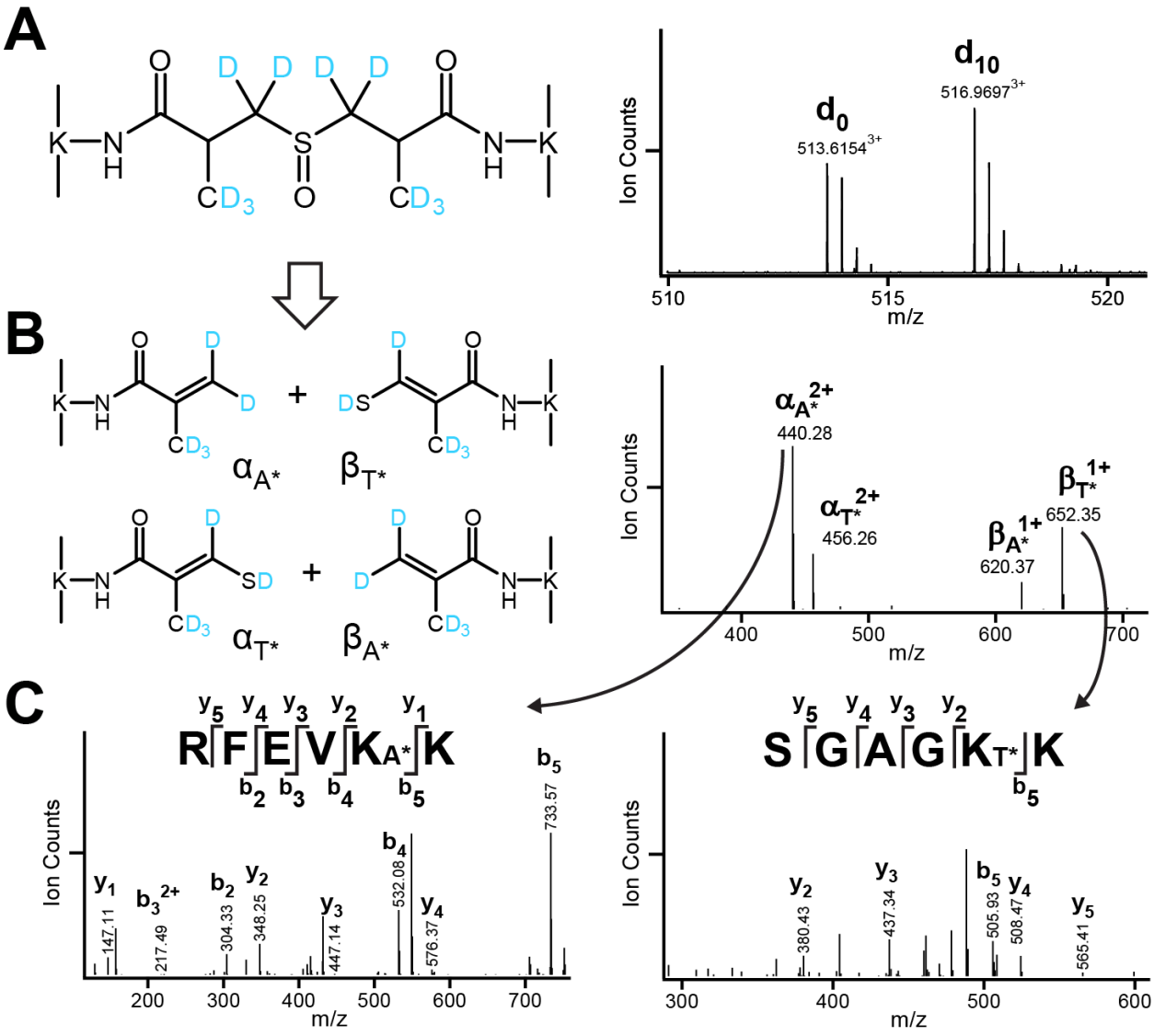

Figure 3-3. MS^n analysis of d$_{10}$-DMDSSO inter-linked peptides. (A) MS^1 spectrum shows the detection of a pair of DMDSSO cross-linked peptides (*m/z* 513.6154^{3+} and *m/z* 516.9697^{3+}). (**B**) MS^2 analysis of the d$_{10}$-DMDSSO inter-linked peptides α-β (m/z 516.9697^{3+}) yielded two peptide fragment pairs: α_{A*}/β_{T*} (m/z 440.28^{2+}/652.35^{1+}) and α_{T*}/β_{A*} (m/z 456.26^{2+}/620.37^{1+}), confirming its cross-link type as an interlink. Subsequent MS^3 analyses of the α_{A*} (m/z 440.28^{2+}) and β_{T*} (652.35^{1+}) ions produced series of y and b ions which enabled unambiguous identification of α_{A*} as RFEVK$_{A*}$K of Rbx1 and β_{T*} as SGAGK$_{T*}$K of Rbx1. Integration of the data confirmed the d$_{10}$-DMDSSO cross-linked peptide as an intra-subunit interlink between K19 and K25 of Rbx1. K$_{A*}$: d$_{10}$-DMDSSO alkene modified lysine; K$_{T*}$: d$_{10}$-DMDSSO unsaturated thiol modified lysine.

the type of cross-link observed here. Subsequent MS^3 analysis of the α_A fragment (*m/z* 437.76^{2+}) produced a series of y and b ions that enabled its unambiguous identification as ^{21}RFEVK$_A$K^{26} of Rbx1 with Lys25 modified with a DMDSSO alkene remnant. Similarly, MS^3 analysis of the β_T

fragment (*m*/*z* 647.32^{1+}) identified its sequence unambiguously as ^{15}SGAGK$_T$K^{20} of Rbx1 with Lys19 modified with an unsaturated thiol remnant. Together with MS^1 mass matching, we confidently identified this d_0-DMDSSO cross-linked peptide as an intra-protein inter-link between Lys19 and Lys25 of Rbx1. MS^n analysis of the corresponding peptide cross-linked with d_{10}-DMDSSO (*m*/*z* 516.9697^{3+}) further confirmed and identified the intra-subunit linkage within Rbx1 (Figure 3-3). Based on the identical fragmentation patterns of d_0- and d_{10}-DMDSSO cross-linked peptides, our results demonstrate that d_0- and d_{10}-DMDSSO contain the same functionality and characteristics required for the unambiguous identification of their respective cross-linked peptides by MS^n analysis. Therefore, identification of either d_0- or d_{10}-DMDSSO cross-linked peptide in each pairwise experiment would allow us to quantify differences in their relative abundances.

To quantify the identified d_0- and d_{10}-DMDSSO cross-linked peptides, we determined their relative abundance ratios for each pair based on their MS^1 spectral intensities. The same pair-wise comparison experiments were repeated using reversed cross-linker treatments (i.e., d_0-DMDSSO cross-linked Nedd8~Cul1-Rbx1 was mixed with d_{10}-DMDSSO cross-linked Cul1-Rbx1 or d_{10}-DMDSSO cross-linked Nedd8(Q40E)~Cul1-Rbx1) in order to rule out cross-linking bias due to reagent deuteration (Figure 3-1D).

3.4.3 Mapping XL-MS Data to Cul1-Rbx1 Complexes

The current structural model of unneddylated Cul1-Rbx1 is described in Figure 3-4A, based on a previously reported crystal structure of full-length human Cul1-Rbx1 (PDB 1LDJ) [170]. In this structure, the N-terminal domain (NTD) of Cul1 consists of three helical repeats (Repeat 1, 2 and 3), each comprising five α-helices. These three repeats pack consecutively to form a long stalk-like shape. The Cul1 C-terminal domain (CTD) is composed of a four-helix

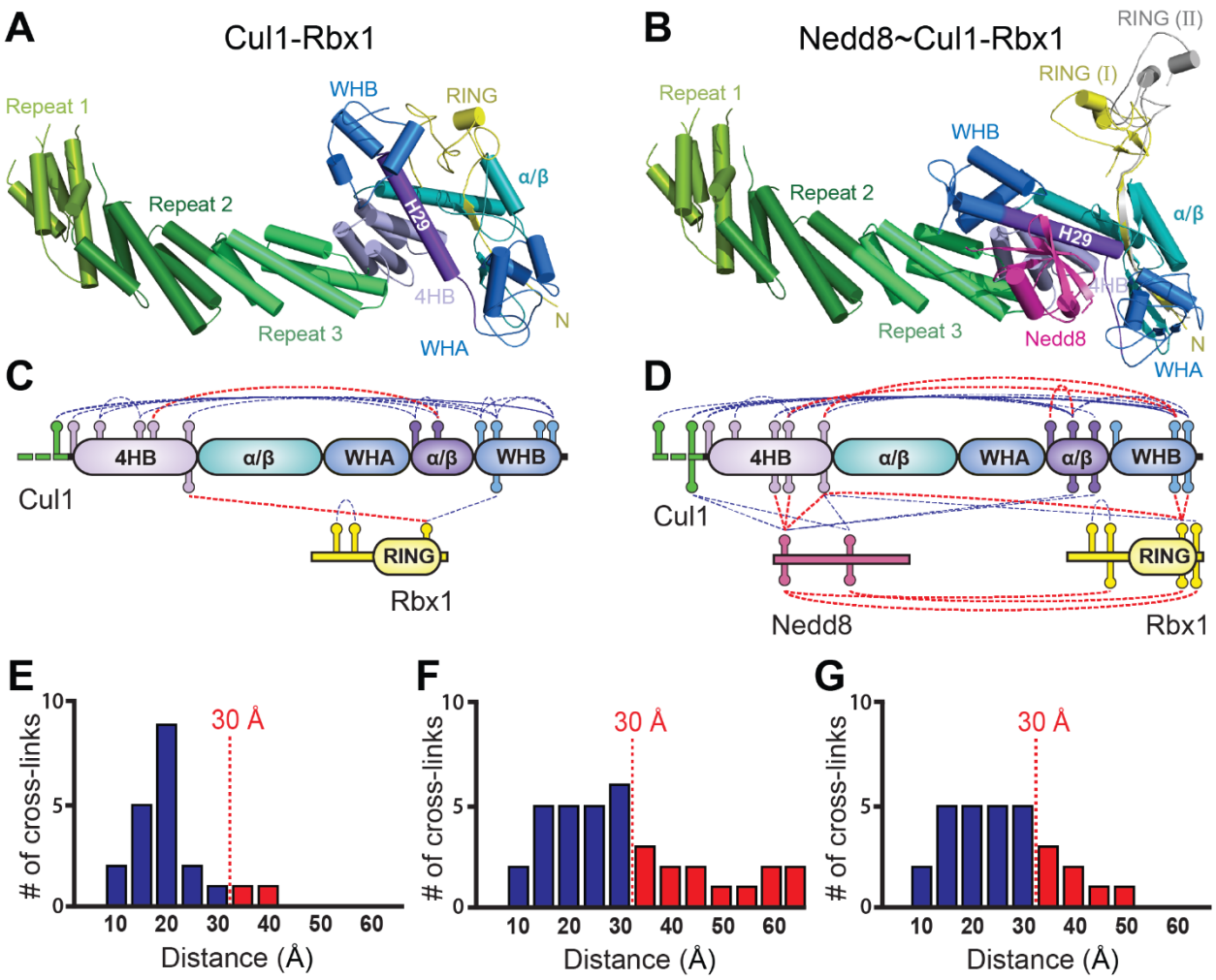

Figure 3-4. Mapping cross-link data onto current structural models of Cul1-Rbx1 complexes. (A) Known structure of unneddylated Cul1-Rbx1 complex. **(B)** The overlay of the two homology models of neddylated Cul1-Rbx1 derived from Nedd8~Cul5^{CTD}-Rbx1 structure, depicting two conformations of the Rbx1 RING domain with I in yellow and II in grey. Based on the identified inter-linked peptides, the cross-link maps were generated for **(C)** Cul1-Rbx1 and **(D)** Nedd8~Cul1-Rbx1 complexes. **Note:** Linkages between residues with spatial distances below 30 Å are shown in blue dotted lines; those above 30 Å in red dotted lines, correlating with color-coded bar graphs in **(E-G)**. **(E)** The distribution plot of identified linkages vs. their spatial distances between inter-linked lysines in Cul1-Rbx1 structure. **(F)** The distribution plot of identified linkages vs. their spatial distances between inter-linked lysines in Nedd8~Cul1-Rbx1 structure models. **(G)** The distribution plot of identified linkages involving only Cul1 and Nedd8 vs. their spatial distances between inter-linked lysines in Nedd8~Cul1-Rbx1 structure models.

bundle (4HB), an α/β domain, and two copies of the winged-helix motif (WHA and WHB). The 4HB connects the NTD to CTD and organizes other subdomains in the CTD. It packs with the α/β domain and the long H29 helix, which connects WHA and WHB. The α/β domain and

the N-terminal β strand of Rbx1 form an intermolecular five-stranded β-sheet. One face of the WHB interacts with the long H29 helix and the 4HB, and the other contacts the RING domain of Rbx1. This compact architecture has been proposed to represent the "closed" conformation of the Cul1-Rbx1 complex (Figure 3-4A) [157].

Although there is no high-resolution structure currently available for the Nedd8~Cul1-Rbx1 complex, the crystal structure of Nedd8~Cul5^{CTD}-Rbx1 was previously resolved [157]. By threading the Cul1^{CTD} sequence into the neddylated Cul5 structure, we have derived a homology model of Nedd8~Cul1-Rbx1 (Figure 3-4B). Similar to the structure of Nedd8~Cul5^{CTD}-Rbx1[157], this model shows that neddylation has minor effects on the structures of individual subdomains, but induces dramatic rearrangements in their relative positions. The H29 helix rotates about 45^{o}, which changes the WHB position relative to the 4HB and α/β domain. The repositioning of WHB abolishes the interaction between WHB and the Rbx1 RING domain and frees the latter from the Cul1 scaffold. Nedd8 contacts the WHB to stabilize this "open" state of the Cul1-Rbx1 complex. Two orientations for the RING, resulting from crystal packing, are observed in the crystal structure of Nedd8~Cul5^{CTD}-Rbx1, indicating that the relative position of the RING domain and cullin scaffold are very promiscuous in solution. Therefore, we generated two structural models of Nedd8~Cul1-Rbx1 to describe the two different RING conformations (I and II) in the complex, and their overlays are illustrated in Figure 3-4B. As shown, RING (I) (in yellow) is closer to the Cul1 scaffold, whereas RING II (in grey) is more distal. It is noted that the orientations of the Cul1 scaffold and Nedd8 remain the same in both RING conformations (Figure 3-4B).

To further characterize the structural dynamics of Cul1-Rbx1 complexes, we focused on the identification and quantification of inter-linked peptides as they are most informative in

describing residue proximity and interaction contacts in 3-D structures. With our XL-MS strategy, we identified a total of 68 unique inter-linked d_0/d_{10} peptide pairs from eight replicate sets of comparison experiments (Table 3-1), representing 27 intra-protein and 17 inter-protein linkages. To correlate our XL-MS data with the current structural models of Cul1-Rbx1 complexes, we first generated cross-link maps of Cul1-Rbx1 and Nedd8~Cul1-Rbx1 based on the inter-links identified from each sample (Figure 3-4C-D). For simplicity, only the structural model of Nedd8~Cul-Rbx1 with RING (I) conformation was represented for cross-link mapping (Figure 3-4D), as the two RING conformations provide the same profiles. Interestingly, 23 of 25 intra-protein Cul1 K-K linkages are localized in $Cul1^{CTD}$ regions that interact with Rbx1 and Nedd8. In addition, 5 and 10 linkages represent inter-protein interactions of Cul1 with Rbx1 and Nedd8, respectively. Collectively, extensive interactions among the three proteins were detected, permitting comparative analysis between the various forms of Cul1-Rbx1 complexes. Next, we mapped the identified cross-linked residues onto the structural models of Cul1-Rbx1 and Nedd8~Cul1-Rbx1 in order to calculate the distances between α carbons (C_α-C_α distances) of cross-linked lysine residues using the molecular visualization software PyMOL. Considering the average lengths of DMDSSO (9.3 Å) and lysine side chains as well as backbone dynamics, the theoretical upper limit for the C_α-C_α distance between DMDSSO cross-linked lysine residues is roughly ~30 Å, suggesting that lysines within 30 Å are able to be cross-linked by DMDSSO. To examine the distance constraints of identified cross-links, we plotted the C_α-C_α distance distribution of the Cul1-Rbx1 cross-link data set (Figure 3-4E). 90% of cross-links satisfy the distance cutoff of 30 Å, indicating a good correlation with the current known structure of Cul1-Rbx1. However, when plotting Nedd8~Cul1-Rbx1 cross-link data to either of our homology-derived models, only 64% of cross-links (23/36) are within the desired distance constraint

(Figure 3-4F). In fact, the cross-links outside the cutoff predominantly represent interactions among Nedd8, Rbx1, and the C-terminal domain of Cul1. As Rbx1 is suspected to be mobile in previous publications [157], we excluded 6 Rbx1-associated cross-links, thus yielding 30 remaining cross-links describing interactions within and between Nedd8 and Cul1 proteins. In total, roughly 73% of linkages (22/30) fall within our expected distance constraints (Figure 3-4G), with the 8 outliers all representing cross-links that involve either Nedd8 or the winged-helix domains of $Cul1^{CTD}$. This discrepancy could be explained by either the inaccuracy of the Nedd8~Cul1-Rbx1 structural model in those regions or a highly dynamic topology associated with the "open" conformation.

3.4.5 Quantitation of DMDSSO Cross-linked Peptides

Generally, the likelihood of forming a cross-link between two given lysine residues is dependent on multiple factors. One of the important aspects is the three-dimensional spatial distance between cross-linkable lysines. In addition, the relative orientations of proteins and their local environments in different conformations can influence the relative reactivity of lysine residues. For instance, lysine residues localized in buried or protected regions would have decreased solvent and cross-linker accessibility compared to flexible, unprotected regions. Moreover, certain conformations could potentially influence the electronic environments of lysine residues by positioning them to form salt-bridge interactions with nearby acidic residues, decreasing their relative reactivity. Therefore, a combination of multiple factors could ultimately be responsible for the differences in observed spectral abundances of cross-linked peptides. Nonetheless, comparative analysis using quantitative XL-MS strategies can unravel conformational changes of protein complexes under different conditions [164, 175]. Of the total 68 unique inter-links identified in this work, 41 were identified at least in three biological

replicates—our minimum requirement for reproducibility—representing 26 unique and high confidence Lys-Lys linkages that were used for quantitative structural comparisons. Among them are two linkages involving Lys720 of Cul1, which is the neddylation site and thereby covalently modified in neddylated Cul1-Rbx1 complexes, but free in unmodified Cul1-Rbx1 complex. As a result, the two identified inter-linked peptides associated with Lys720 of Cul1 were only detected in Cul1-Rbx1 complex, and were excluded from further analyses. The final list of 24 unique and quantifiable linkages used for assessing structural changes of Cul1-Rbx1 complexes is summarized in Table 3-1. As shown, 13 were intra-protein (12 Cul1-Cul1 and 1 Rbx1-Rbx1) and 11 were inter-protein (3 Cul1-Rbx1, 7 Cul1-Nedd8, and 1 Rbx1-Nedd8) inter-links. Among them, 15 linkages exhibited significant changes (≥ 4-fold) in their relative abundances—suggesting neddylation-dependent conformational differences—while the remaining 9 displayed marginal changes (< 2-fold), indicating more stable interaction regions.

Table 3-1. Summary of CRL Cross-links Identified by d_0- and d_{10}-DMDSSO.

LINKAGES IDENTIFIED					MAPPED DISTANCES		QUANTITATIVE RATIO*		
CUL1	**CUL1**	**RBX1**	**RBX1**	**NEDD8**	**CR (Å)**	**wN8~CR (Å)**	**CR**	**wN8~CR**	**mN8~CR**
337	**750**				37.1	26.5	0.05	1.00	0.20
410	**720**				38.1	21.7	1.00	0.01	0.01
410	**743**				17.4	22.5	0.85	0.67	1.00
410	**750**				24.9	21.0	0.14	1.00	0.36
417	**689**				18.8	24.8	1.00	0.60	0.91
431	**472**				9.7	9.3	1.00	0.24	0.50
464	**693**				15.8	11.9	0.36	1.00	0.41
464	**743**				15.7	26.3	0.05	1.00	0.22
468	**693**				13.7	12.2	1.00	0.49	0.85
472	**689**				16.3	10.7	1.00	0.87	0.90
472	**693**				15.7	16.4	0.94	0.87	1.00
693	**743**				24.8	26.6	0.03	1.00	0.17
701	**708**				11.1	10.5	0.69	1.00	0.92

493		**89**			30.2	40.8	1.00	0.67	0.77
720		**89**			11.7	72.8	1.00	0.00	0.00
743		**89**			26.8	59.2	0.06	1.00	0.10
750		**89**			22.6	54.5	0.11	1.00	0.05
		19	**25**		18.1	---	1.00	0.62	0.71
410				**6**	---	17.0	0.01	1.00	0.22
464				**6**	---	30.6	0.01	1.00	0.12
468				**6**	---	35.3	0.05	1.00	0.23
493				**6**	---	41.0	0.04	0.07	1.00
493				**48**	---	29.9	0.01	0.11	1.00
693				**6**	---	28.7	0.00	1.00	0.11
701				**6**	---	19.6	0.01	1.00	0.13
		89		**48**	---	65.0	0.02	0.96	1.00

* Spectral abundances normalized to the highest value for each linkage

3.4.6 Comparison of Cul1-Rbx1 and Nedd8~Cul1-Rbx1 complexes

Existing structural models have suggested that unneddylated Cul1-Rbx1 adopts a "closed" conformation, while neddylated Cul1-Rbx1 exists in an "open" state, as represented in Figure 3-5A and 3-5B. To determine the structural effects of neddylation in the context of the full-length proteins, we examined intra-protein inter-links identified within Cul1 and Rbx1 respectively. For the twelve intra-protein inter-links identified within Cul1, six of them (i.e. $Cul1^{K410\text{-}K743}$, $Cul1^{K417\text{-}K689}$, $Cul1^{K468\text{-}K693}$, $Cul1^{K472\text{-}K689}$, $Cul1^{K472\text{-}K693}$, and $Cul1^{K701\text{-}K708}$) exhibited below 2-fold difference in abundance ratio comparing between Cul1-Rbx1 and Nedd8-Cul1-Rbx1 complexes, suggesting that there were no substantial structural reorientations between the regions described by the cross-linked lysine residues upon neddylation (Table 3-1). In consistence with the cross-linking data, all of their C_α-C_α distances are within 30 Å in the current Cul1-Rbx1 and Nedd8-Cul1-Rbx1 models. For example, the relative spectral abundance ratio of the $Cul1^{K472\text{-}K693}$ linkage in unneddylated and neddylated Cul1-Rbx1 is ~1, and their respective

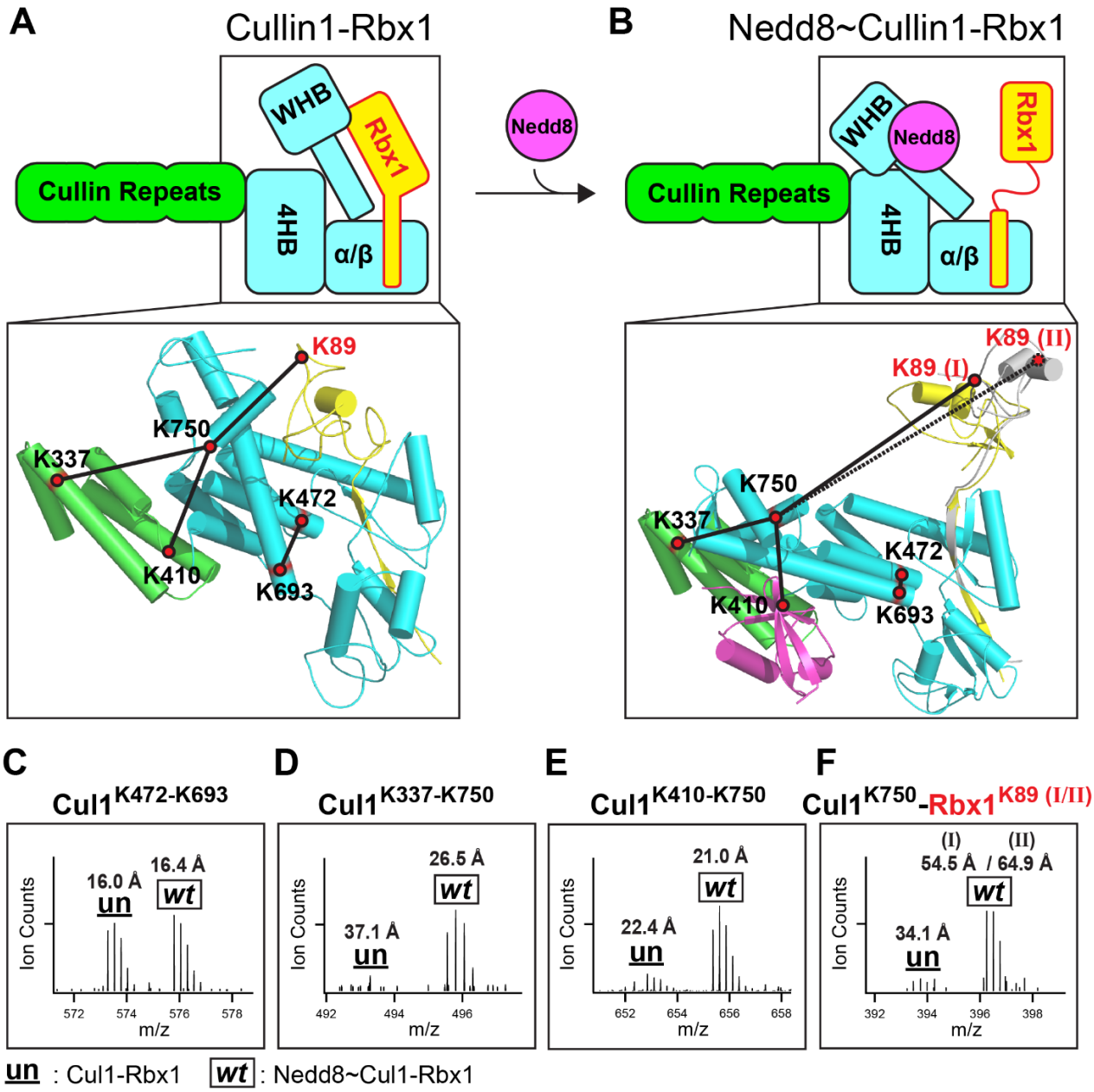

Figure 3-5. Quantitative analysis of K-K linkages to determine neddylation-dependent structural changes in the Cul1-Rbx1 complex. Structural representation of **(A)** unneddylated Cul1-Rbx1 in the "closed" state and **(B)** neddylated Cul1-Rbx1 in the "open" conformation, in which K89 (I) and K89 (II) represent K89 position in Rbx1 RING(I) (in yellow) or (II) (in grey) conformations, respectively. The insets display the mapping of four selected inter-links onto the structures of Cul1-Rbx1 complexes, whose MS^1 spectra are displayed as follows: **(C)** $Cul1^{K472}$-$Cul1^{K693}$, **(D)** $Cul1^{K337}$-$Cul1^{K750}$; **(E)** $Cul1^{K410}$-$Cul1^{K750}$ (**F**) $Cul1^{K750}$-$Rbx1^{K89(I/II)}$. The spectral ratio of d_0/d_{10}-DMDSSO cross-linked peptides measured in MS^1 were used to determine their relative abundance ratios between unneddylated and neddylated Cul1-Rbx1 complexes for quantitative analysis (Table 3-1).

C_α-C_α distances are 16.0 Å and 16.4 Å (Figure 3-5C). Although the 4HB and α/β domains

containing these two residues become closer (Fig. 3-5A, B), the overall 3-D spatial distance of these two residues has minimal change, thus leading to comparable cross-linking efficiency.

In contrast, the remaining six intra-protein inter-links of Cul1 had at least 4-fold difference in their relative abundance ratios, in which five inter-links (i.e. $Cul1^{K337\text{-}K750}$, $Cul1^{K410\text{-}K750}$, $Cul1^{K464\text{-}K693}$, $Cul1^{K464\text{-}K743}$, and $Cul1^{K693\text{-}K743}$) were detected predominantly in Nedd8~Cul1-Rbx1 complex and one (i.e. $Cul1^{K431\text{-}K472}$) significantly more abundant in unneddylated Cul1-Rbx1 (Table 3-1 and Figure 3-5). These differences indicate that the two complexes feature substantial structural differences in regions containing the cross-linked lysines. In this study, two lysine residues that are proximal (< 30 Å) would have a higher chance of being captured by DMDSSO, which in turn increases the spectral abundance compared to one between lysine residues that are spatially distant (> 30 Å). Figure 3-5D displays the MS spectrum of the $Cul1^{K337\text{-}K750}$ inter-link, and quantitative analysis revealed that this interaction occurs much more favorably in Nedd8~Cul1-Rbx1 than Cul1-Rbx1, on average of 20:1. The C_α-C_α distances between Lys337 and Lys750 of Cul1 were calculated to be 36.3 Å and 26.5 Å based on the Cul1-Rbx1 structure and our Nedd8~Cul1-Rbx1 model, respectively. These calculated C_α-C_α distances fall outside of and within the distance that can be cross-linked by DMDSSO, which correlate to the increased spectral abundance of this inter-link in Nedd8~Cul1-Rbx1 compared to Cul1-Rbx1.

Similarly, the intra-protein inter-link $Cul1^{K410\text{-}K750}$ was calculated to be on average 7-fold more abundant in wild-type neddylated than unneddylated forms (Table 3-1 and Fig. 3-5E). However, distinct from the $Cul1^{K337\text{-}K750}$ inter-link, the C_α-C_α distances of Lys410 and Lys750 in the current models were determined to be 22.4 Å and 21.0 Å, respectively. Because of the similarity in their calculated proximities, the differential spectral abundance suggests that this cross-link is in some way obstructed in unneddylated Cul1. In addition to distance, cross-linked

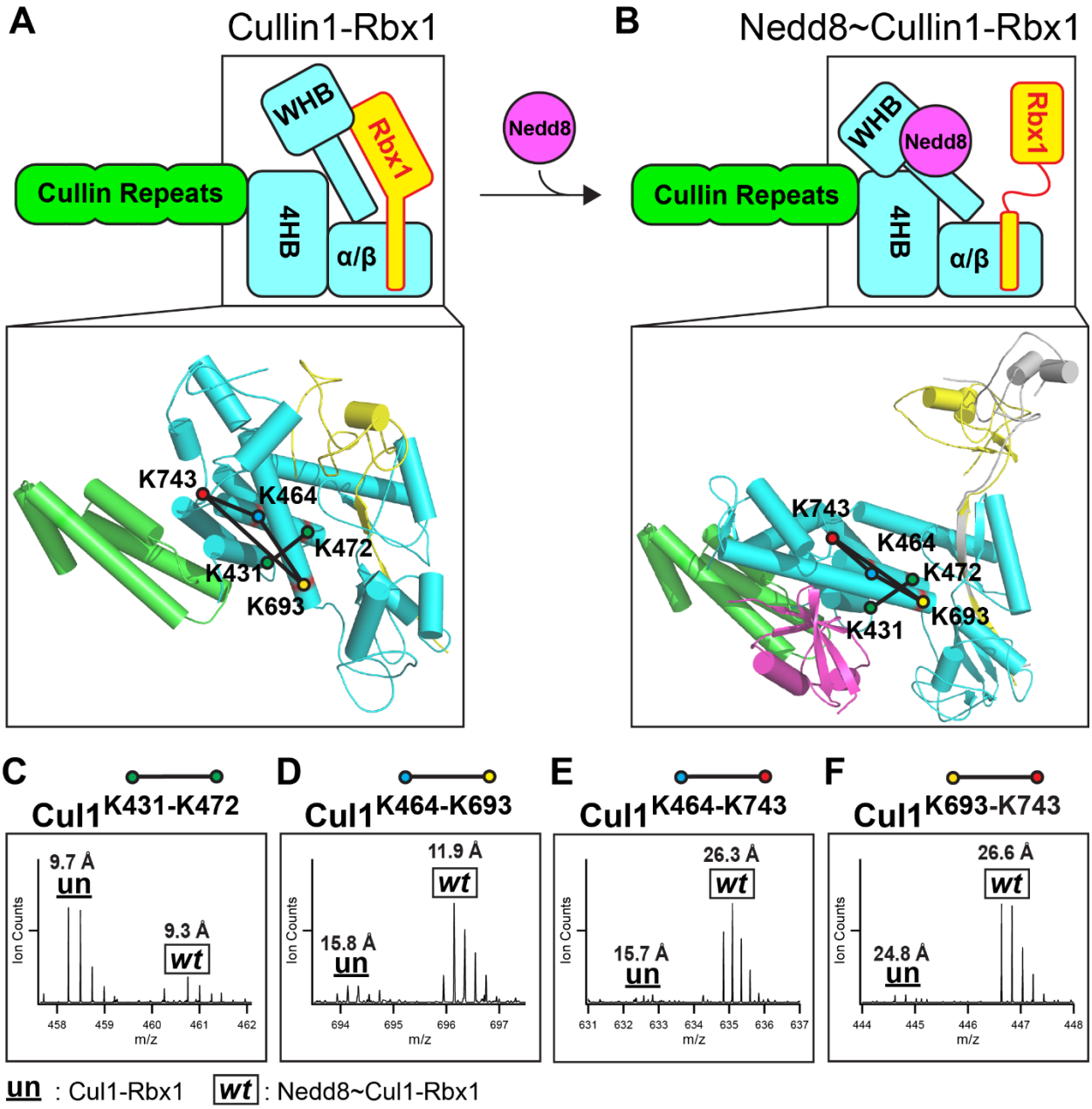

Figure 3-6. Quantitative analysis of intra-subunit Cul1 linkages to determine neddylation-dependent structural changes in the Cul1-Rbx1 complex. Structural representation of (**a**) unneddylated Cul1-Rbx1 in the "closed" state, (**b**) neddylated Cul1-Rbx1 in the "open" conformation. The insets display the mapping of four selected inter-links onto the structures of Cul1-Rbx1 complexes, whose MS^1 spectra are displayed as follows: (**c**) $Cul1^{K43}1$-$Cul1^{K472}$, (**d**) $Cul1^{K464}$-$Cul1^{K693}$, (**e**) $Cul1^{K464}$-$Cul1^{K743}$, and (**f**) $Cul1^{K693}$-$Cul1^{K743}$. These d_0/d_{10}-DMDSSO cross-linked peptide pairs measured in MS^1 were used to determine their relative abundance ratios between unneddylated and neddylated Cul1-Rbx1 complexes for quantitative analysis (Table 3-1).

peptide spectral abundance can be influenced by the relative orientation of the lysine pair and their environment. Lys410 and Lys750 in unneddylated Cul1 point away from each other and are

separated spatially by other Cul1 residues, which can presumably impede the cross-linking reaction. Similarly, four other Cul1 intra-protein inter-links (i.e. $Cul1^{K464\text{-}K693}$, $Cul1^{K464\text{-}K743}$, $Cul1^{K693\text{-}K743}$ and $Cul1^{K431\text{-}K472}$) have no apparent correlation between their relative spectral abundance ratios and respective C_α-C_α distance (Figure 3-6). However, most of them can be rationalized based on the structural environment of the lysine residues in the context of the current structure models. The $Cul1^{K693\text{-}K743}$ interlink represents the only noticeable outlier, which is more than 30 folds more abundant in Nedd8~Cul1-Rbx1 than Cul1-Rbx1, albeit corresponding to similar C_α-C_α distance in the both models. Lys693 and Lys743 are located on the H29 helix and the WHB domain, which together act as a single rigid body. Their preferred cross-links in the neddylated Cul1-Rbx1 cannot be explained without significant changes of the current model of Nedd8~Cul1-Rbx1. Overall, our results suggest that certain regions in the Cul1 scaffold, including the structural elements where those lysines are located, likely undergo profound structural reorientations in response to neddylation.

To further dissect the impact of neddylation, we examined the three unique Cul1-Rbx1 inter-protein K-K linkages identified (Table 3-1, Figure 3-4). Two cross-links, $Cul1^{K743}$-$Rbx1^{K89}$ and $Cul1^{K750}$-$Rbx1^{K89}$, were quantitatively determined to have spectral abundances on average 10-fold higher in neddylated Cul1-Rbx1 compared to their unneddylated counterparts. Mapping of Cul^{K743}-$Rbx1^{K89}$ and Cul^{K750}-$Rbx1^{K89}$ to the Cul1-Rbx1 structure determines their C_α-C_α distances to be 31.9 Å and 34.1 Å, respectively, just outside the range covered by DMDSSO and likely accounting for their low cross-linking abundances. On the other hand, when mapped to our homology-derived models of neddylated Cul1-Rbx1 with either RING (I) or RING (II) conformations, those same inter-links yielded C_α-C_α distances of 59.2 Å (I)/66.0 Å (II) and 57.5 Å (I)/64.9 Å (II) respectively (Table 3-1 and Fig. 3-5F), even more unlikely to be cross-linked by

DMDSSO. Instead, these unusual cross-links must be explained by either the structural flexibility of the "open state" conformation exhibited by Nedd8~Cul1-Rbx1 or a geometry different from the current model. In the crystal structure of Nedd8~Cul5^{CTD}-Rbx1, neddylation causes the globular RING domain of Rbx1 to eject from the WHB while remaining tethered to the Cul5^{CTD} by its N-terminal sequence. Although the lattice structure suggests that the RING domain is positioned in an awkward location distant from Cul1, it is likely that these structures represent two positions of a considerable range of motion rendered by the open state. As a result, Rbx1 is free to sample the 3-dimensional space above Cul5^{CTD}. Our observations on the three Cul1-Rbx1 inter-protein inter-links indicate that such a dynamic topology is plausible and can account for the formation of linkages with lysine residues that are too distant to be cross-linked in the unneddylated complex.

Mapping of the identified K-K linkages between Cul1 and Nedd8 to the homology-derived Nedd8~Cul1-Rbx1 model showed that three out of seven cross-linking events were calculated to bridge C_α-C_α distances greater than 30 Å, with two more above 28.5 Å (Table 3-1). This suggests that the position of Nedd8 relative to 4-HB and α/β subdomains of Cul1, which comprise the majority of the Cul1-Nedd8 inter-links, may not be accurate in the current model. On one hand, the crystal structure of the Nedd8~Cul5^{CTD}-Rbx1 complex, which our Nedd8~Cul1-Rbx1 model was based on, might represent snapshots of an otherwise dynamic scaffold in addition to the flexibly linked Rbx1 RING domain. On the other hand, it remains possible that neddylation may cause different conformational changes on different cullins. Therefore, a more accurate structure model of the Nedd8~Cul1-Rbx1 complex is needed to explain all comparative cross-links between the free and modified Cul1-Rbx1 assembly.

3.4.7 Comparison of Nedd8~ and Nedd8(Q40E)~Cul1-Rbx1 complexes

To investigate the structural mechanism underlying the loss-of-function resulting from deamidation of Nedd8, we conducted pair-wise structural comparisons between Nedd8~Cul1-Rbx1 (wt) and Nedd8(Q40E)~Cul1-Rbx1 (mt) complexes using the same DMDSSO-based quantitative XL-MS strategy as described above. Similar to the previous results obtained from the comparison between unneddylated and wild-type neddylated Cul1-Rbx1 complexes, the six Cul1 inter-links (i.e. $Cul1^{K410\text{-}K743}$, $Cul1^{K417\text{-}K689}$, $Cul1^{K468\text{-}K693}$, $Cul1^{K472\text{-}K689}$, $Cul1^{K472\text{-}K693}$, $Cul1^{K701\text{-}K708}$) and one Rbx1 inter-link (i.e. $Rbx1^{K19\text{-}K25}$) displayed non-significant changes (< 2-fold) when comparing their spectral abundances in wt-neddylated and mt-neddylated~Cul1-Rbx1 complexes (Table 3-1). Interestingly, the five inter-links within Cul1 (i.e. $Cul1^{K337\text{-}K750}$, $Cul1^{K410\text{-}K750}$, $Cul1^{K464\text{-}K693}$, $Cul1^{K464\text{-}K743}$, and $Cul1^{K693\text{-}K743}$) which were significantly more abundant in Nedd8~Cul1-Rbx1 than unneddylated Cul1-Rbx1 were also difficult to detect in Nedd8(Q40E)~Cul1-Rbx1 (Fig. 3-7A-E). Furthermore, the $Cul1^{K431\text{-}K472}$ inter-link, which was found to be much more abundant in unneddylated Cul1-Rbx1 than Nedd8~Cul1-Rbx1, was also detected more readily in Nedd8(Q40E)~Cul1-Rbx1 (Fig. 3-7F). Overall, the relative abundance ratios of these core CRL inter-links are similar when comparing Nedd8~Cul1-Rbx1 to both Cul1-Rbx1 and Nedd8(Q40E)~Cul1-Rbx1, suggesting that covalent attachment of Nedd8(Q40E) to Cul1 did not result in the same conformational changes in Cul1 as wild-type Nedd8 modification. This observation is also supported by the identification of inter-linked peptides between Cul1 and Rbx1. The $Cul1^{K743}$-$Rbx1^{K89}$ and $Cul1^{K750}$-$Rbx1^{K89}$ inter-protein inter-links which were detected predominantly in Nedd8~Cul1-Rbx1 but not in Cul1-Rbx1 were also difficult to detect in Nedd8(Q40E)~Cul1-Rbx1 (Fig. 3-7G-H). Collectively, the quantitative MS profiles of identified and quantitated Nedd8(Q40E)~Cul1-Rbx1 linkages are much more similar

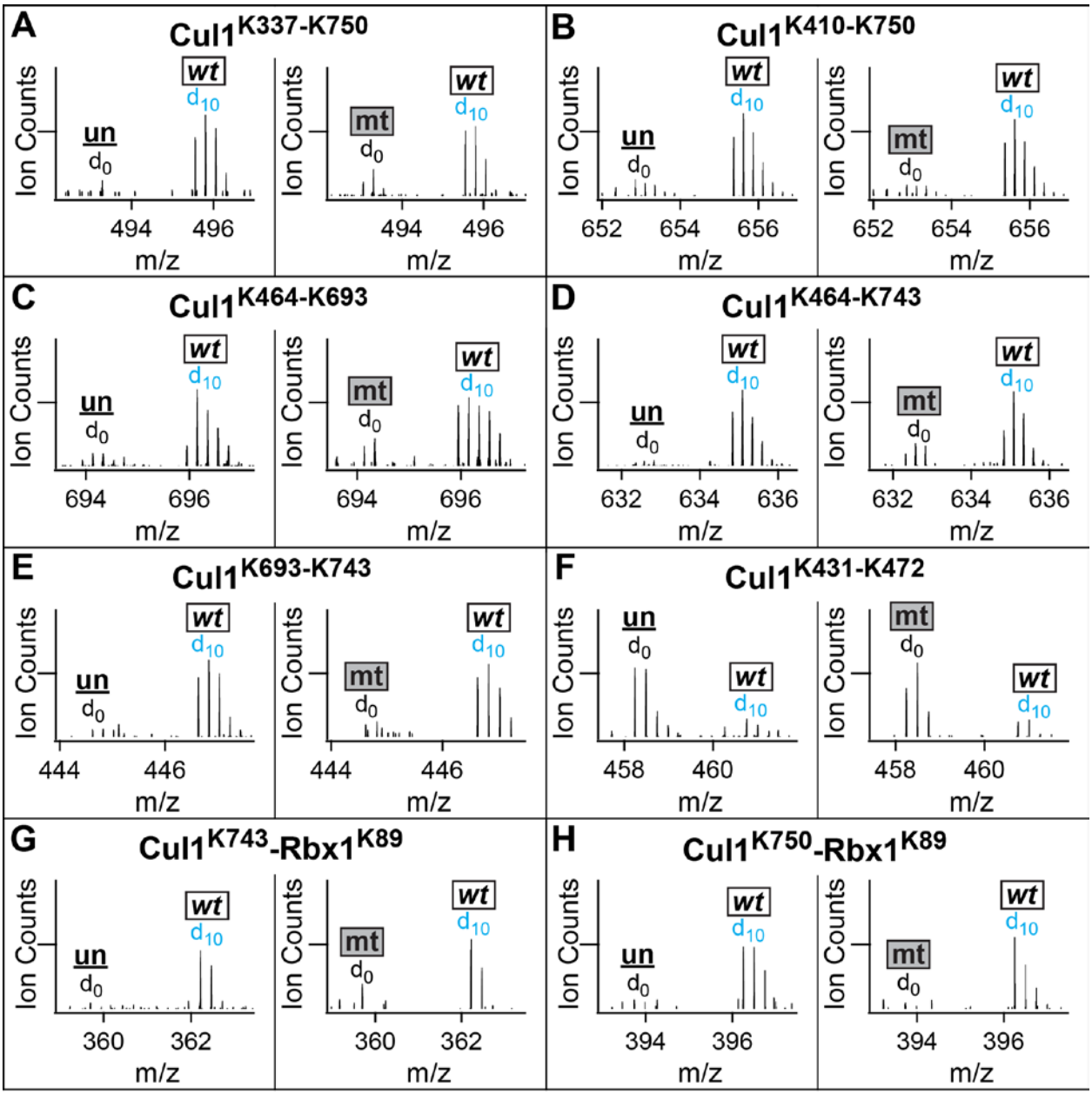

Figure 3-7. Describing the structural dynamics of various Cul1-Rbx1 complexes using QXL-MS. Eight selected K-K linkages are presented to describe conformational changes in the three types of Cul1-Rbx1 complexes. Two sets of pair-wise comparison results (i.e. un (d_0) vs. wt (d_{10}) and mt (d_0) vs. wt (d_{10})) are displayed for each selected cross-link, in which both the un and mt forms were cross-linked by d_0-DMDSSO and the wt form was cross-linked by d_{10}-DMDSSO. MS^1 spectra of (**A**) $Cul1^{K337-K750}$, **(B)** $Cul1^{K410-K750}$, **(C)** $Cul1^{K464-K693}$, **(D)** $Cul1^{K464-K743}$, **(E)** $Cul1^{K693-K743}$, **(F)** $Cul1^{K431-K472}$, **(G)** $Cul1^{K743}$-$Rbx1^{K89}$, and **(H)** $Cul1^{K750}$-$Rbx1^{K89}$. Relative spectral abundance of cross-links (d_0:d_{10}) measured during MS analysis describes the cross-linkability of lysine residues in 3-D structure.

to those of unneddylated Cul1-Rbx1.

The structural dissimilarities in the two types of neddylated Cul1-Rbx1 complexes were further confirmed by comparisons of Cul1-Nedd8 linkages. We have identified seven unique inter-protein K-K linkages between Cul1 and Nedd8 as summarized in Table 3-1. Interestingly, all of the Cul1-Nedd8 inter-subunit inter-links had relative abundance ratios indicating significant differences (≥ 4-fold) between the structures of Nedd8~Cul1-Rbx1 and Nedd8(Q40E)~Cul1-Rbx1 (Fig. 3-8). Among them, five cross-links (Nedd8^{K6}-Cul1^{K410}, Nedd8^{K6}-Cul1^{K464}, Nedd8^{K6}-Cul1^{K468}, Nedd8^{K48}-Cul1^{K693}, and Nedd8^{K6}-Cul1^{K701}) were only

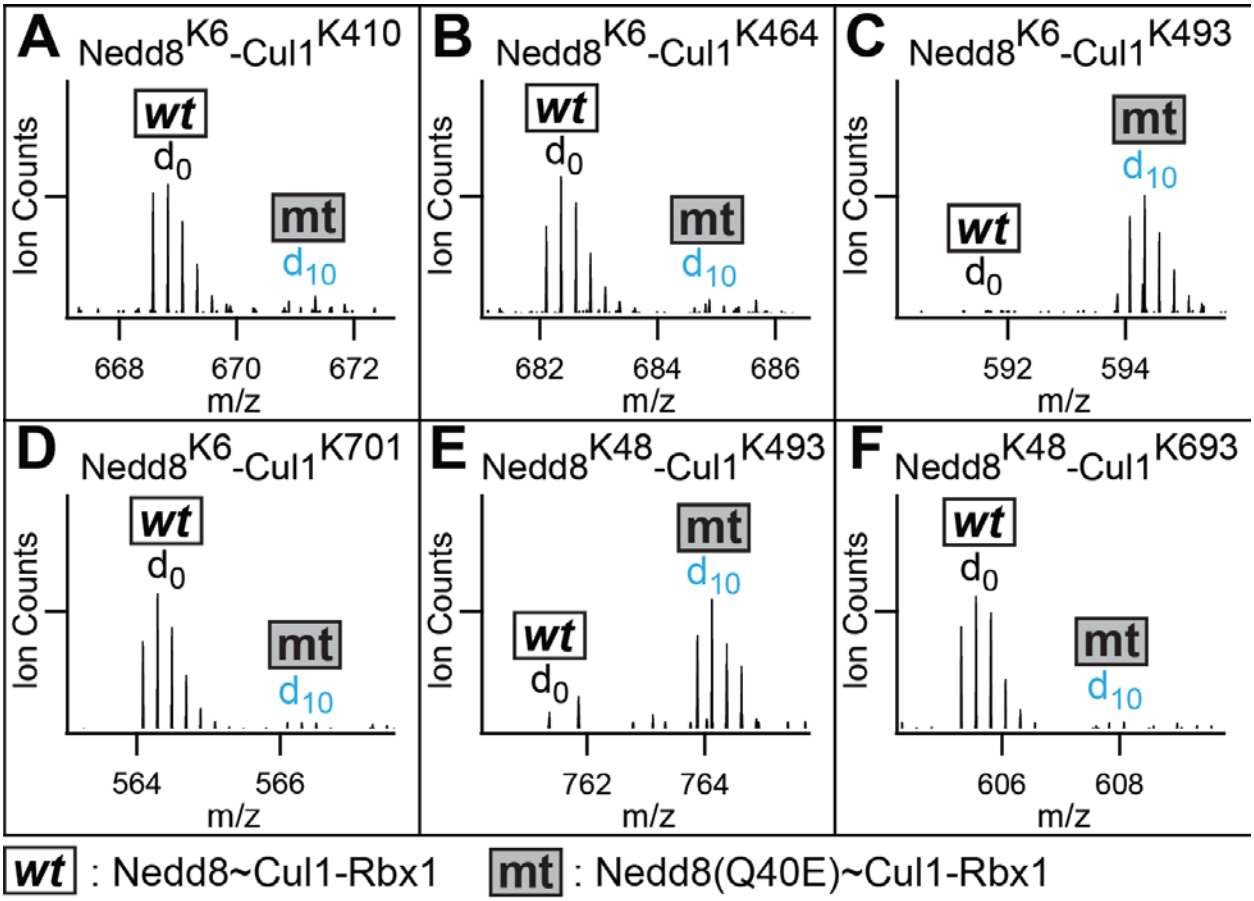

Figure 3-8. Elucidation of structural dissimilarities between wt- and mt-neddylated Cul1-Rbx1 complexes by quantitative analysis of Cul1-Nedd8 inter-links. MS1 spectra of **(A)** Nedd8^{K6}-Cul1^{K410}, **(B)** Nedd8^{K6}-Cul1^{K464}, **(C)** Nedd8^{K6}-Cul1^{K493}, **(D)** Nedd8^{K6}-Cul1^{K701}, **(E)** Nedd8^{K48}-Cul1^{K493} and **(F)** Nedd8^{K48}-Cul1^{K693}. In this example, the mt form was d_0-DMDSSO cross-linked and the wt form was d_{10}-DMDSSO cross-linked.

detected in Nedd8~Cul1-Rbx1, while the remaining cross-links (Nedd8^{K6}-Cul1^{K493} and Nedd8^{K48}-Cul1^{K493}) were only measured in Nedd8(Q40E)~Cul1-Rbx1. In particular, Lys6 of Nedd8 and Lys493 of Cul1 are localized to opposite sides of the Cul1 scaffold in the Nedd8~Cul1-Rbx1 model, resulting in a C_α-C_α distance greater than 30 Å. Therefore, this Nedd8^{K6}-Cul1^{K493} cross-link preferably detected in Nedd8(Q40E)~Cul1-Rbx1 further suggests that the Q40E mutation imparts a large degree of influence on the position of Nedd8 in relation to the Cul1 scaffold. Taken together, our results have demonstrated that Nedd8(Q40E) cannot induce the same structural effect on Cul1-Rbx1 as wild-type Nedd8, and the overall conformation of Nedd8(Q40E)~Cul1-Rbx1 is much more similar to that of unneddylated Cul1-Rbx1.

3.5 Conclusion

We have developed an effective quantitative XL-MS (QXL-MS) workflow based on our previously developed pair of isotope-labeled (i.e. d_0 and d_{10}) MS-cleavable DMDSSO [88] to characterize the structural differences and similarities of three Cul1-Rbx1 complexes. This approach allows us to quantitatively assess neddylation-dependent conformational changes within the Cul1-Rbx1 complex and gain insights into the molecular basis underlying its activation mechanism. In this work, we have demonstrated that DMDSSO reagents are well-suited to quantitatively compare protein complexes as they cross-link proteins with similar efficiency. The relative spectral intensity ratios of d_0- and d_{10}-DMDSSO cross-linked peptides are indicative of their respective abundances in compared samples. Thus, these isotope-coded cross-linkers can be used to study differential protein structures by characterizing their intra-

protein and inter-protein inter-linked peptides to describe changes in interactions associated with conformational changes.

With this QXL-MS approach, we have reproducibly quantified 24 unique intra-protein and inter-protein lysine-lysine linkages within the three different forms of Cul1-Rbx1 complexes (i.e. Cul1-Rbx1, Nedd8~Cul1-Rbx1, Nedd8(Q40E)~Cul1-Rbx1). Although a substantial amount of cross-link data correlates well with existing models, several cross-links have spatial distances outside the desired range and cannot be rationalized based on current structure models. While our results generally support the homology model of Nedd8~Cul1-Rbx1 derived from the Nedd8~Cul5^{CTD}-Rbx1 crystal structure [157], a more accurate description of neddylation-induced conformational changes of the Cul1 scaffold calls for the necessity of a better-defined model.

Independent of such a model, multiple pair-wise comparisons have revealed that the molecular structure of Nedd8(Q40E)-modified Cul1-Rbx1 is very similar to that of its unmodified form and significantly different from wild-type Nedd8-modified Cul1-Rbx1, indicating that Gln40 in Nedd8 is critical for the structural stability of neddylated Cul1-Rbx1. In the structure of Nedd8-Cul5^{CTD}-Rbx1, Gln40 is proximal to the isopeptide bond between Nedd8 and Cul5 [157] and may interact with the cullin scaffold to stabilize its active conformation. The conversion of Gln40 to Glu40 may also influence the local environment due to its acidic side chain. However the effect, the structure of unmodified CRL catalytic core adopts a rigid, thermodynamically stable “closed” structure, lacking ligase activity for polyubiquitination of substrates. Following neddylation, the CRL topology shifts to a flexible, “open” conformation with the extending RING-finger domain [157, 176]. The neddylated CRL remains in its active state until Nedd8 is removed (deneddylated) by the COP9 signalosome. We propose that Gln40

in Nedd8 can interact with amino acid residues in cullin through weak interactions, such as hydrogen bonds and electrostatic interactions, which are responsible for stabilization of the "open" state. Deamidation of Gln40 abolishes or weakens these interactions such that the CRL switches back to its thermodynamically more stable "closed" state. Based on our cross-linking data, we have proposed schematic models representing neddylation-dependent conformational changes in the Cul1-Rbx1 complex by wild-type or mutant Nedd8 (Fig. 3-9). As illustrated, wild type-neddylation leads to the "open" conformation of the CRL core in which Rbx1 is free to rotate as previously shown by crystallography [157]. In contrast, mutant-neddylation of Cul1 prevents switching from the inactive to active state by maintaining the "closed" structure of CRL with Rbx1 embedded. To verify this hypothesis, an experimental structure of neddylated full-length CRL will be required.

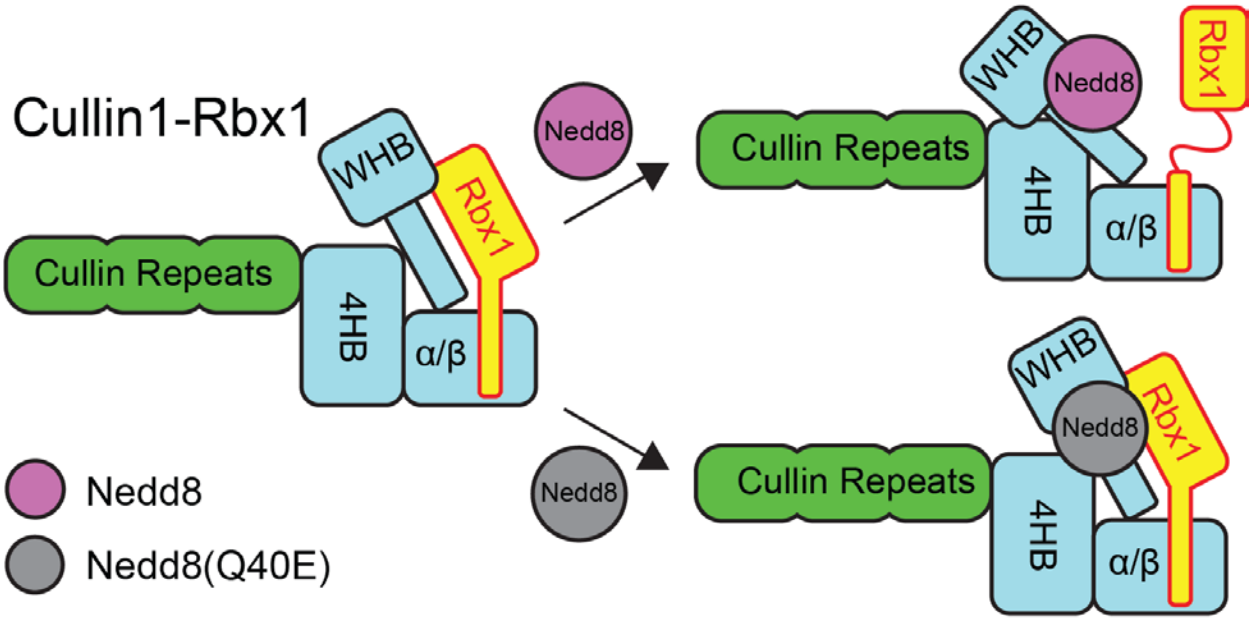

Figure 3-9. Proposed model for Nedd8-dependent conformational changes of the Cul1-Rbx1 complex.

In summary, we have successfully applied our recently developed MS-cleavable, stable isotope-labeled cross-linkers d_0-DMDSSO and d_{10}-DMDSSO to quantitatively study structural differences in Cul1-Rbx1 complexes in response to neddylation. Such structural characterization has previously been hindered using conventional structural tools because of their large sizes (over 100 kDa) and dynamic conformations. Our QXL-MS approach enables us to quantitatively compare multiple lysine inter-links in three types of full-length Cul1-Rbx1 complexes. Comparing these cross-linkage profiles, we found that neddylation can induce large structural rearrangements of the Cul1-Rbx1 complex, which are partially consistent with structural models obtained with truncated and neddylated Cul5-Rbx1 complex. Our results also indicate Nedd8(Q40E)-conjugated Cul1-Rbx1 has a similar structure to that of free Cul1-Rbx1, answering the puzzle of how a subtle change of a single Nedd8 amino acid, Gln^{40}, can abolish the activity of the much larger CRL complex both *in vivo* and *in vitro*. Given the speed and accuracy of the approach, we expect that our QXL-MS strategy will enable us to perform future studies in characterizing E2-E3 interactions and further dissect the action mechanism of CRLs during protein ubiquitination. In addition, our work has paved the way for adapting QXL-MS methods for elucidating dynamic structures of proteins and protein complexes in the future.

CHAPTER 4: Developing a Multiplexed Quantitative Cross-linking Mass Spectrometry Platform for Comparative Structural Analysis of Protein Complexes

Reprinted with permission from:

Clinton Yu, Alexander Huszagh, Rosa Viner, Eric J. Novitsky, Scott D. Rychnovsky, Lan Huang. **Developing a Multiplexed Quantitative Cross-linking Mass Spectrometry Platform for Comparative Structural Analysis of Protein Complexes.** *Analytical Chemistry, 2016, 88 (20), pp 10301–10308*.

4.1 Summary

Cross-linking mass spectrometry (XL-MS) represents a recently popularized hybrid methodology for defining protein-protein interactions (PPIs) and analyzing structures of large protein assemblies. In particular, XL-MS strategies have been demonstrated to be effective in elucidating molecular details of PPIs at the peptide resolution, providing a complementary set of structural data that can be utilized to refine existing complex structures or direct *de novo* modeling of unknown protein structures. To study structural and interaction dynamics of protein complexes, quantitative cross-linking mass spectrometry (QXL-MS) strategies based on isotope-labeled cross-linkers have been developed. Although successful, these approaches are mostly limited to pair-wise comparisons. In order to establish a robust workflow enabling comparative analysis of multiple cross-linked samples simultaneously, we have developed a multiplexed QXL-MS strategy, namely QMIX (Quantitation of Multiplexed, Isobaric-labeled cross (X)-

linked peptides) by integrating MS-cleavable cross-linkers with isobaric labeling reagents. This study has established a new analytical platform for quantitative analysis of cross-linked peptides, which can be directly applied for multiplexed comparisons of the conformational dynamics of protein complexes and protein-protein interactions at the proteome scale in future studies.

4.2 Introduction

Protein-protein interactions (PPIs) are fundamental to the assembly, structure, and function of protein complexes. Disturbances in endogenous PPIs can negatively impact cellular activities, leading to various types of human disease. Characterization of the architectures of protein complexes and their protein interaction interfaces is critical towards unraveling the molecular mechanisms underlying human pathologies and providing insight on potential targets for drug therapies, exemplifying a new paradigm in disease treatment development [9].

Due to its versatility, sensitivity, accuracy and speed, cross-linking mass spectrometry (XL-MS) has emerged as a powerful approach for mapping protein interaction networks [49, 50, 66, 77] and characterizing large protein complex structures [43, 89, 163, 166, 167]. The cross-linked peptides identified within and between proteins represent “peptide resolution” distance constraints that have been successfully used to derive and/or refine the structures of protein complexes [43, 89, 163, 166, 167]. One of the inherent challenges in XL-MS studies is the unambiguous identification of cross-linked peptides. To facilitate this process, we previously developed a new class of MS-cleavable cross-linkers, i.e. sulfoxide-containing MS-cleavable cross-linking reagents, that enable simplified and accurate identification of cross-linked peptides using multistage tandem mass spectrometry (MS^n) [50, 73, 86, 88]}. These robust and reliable reagents have been successfully applied to define protein-protein interactions both *in vitro* [51,

86, 89, 90] and *in vivo* [50]. To probe structural dynamics of protein complexes, stable isotope-labeled cross-linking reagents (usually deuterium labeled) are often used to permit pair-wise comparisons of the two selected conformational states in a single experiment [90, 164, 175, 177]. To allow unambiguous identification and quantification of cross-linked peptides simultaneously, we had developed a pair of sulfoxide-containing MS-cleavable, deuterium-labeled cross-linking reagents allowing quantitative comparison of cross-links identified by either light- or heavy-labeled reagent [88, 90]. Although successful, the usage of isotope-labeled cross-linkers is currently limited to binary comparisons. In addition, deuterated and non-deuterated cross-linked peptides do not co-elute together perfectly, making their automated quantitation challenging [88, 178]. Lastly, the synthesis of stable isotope-labeled cross-linkers can be burdensome. As an alternative, SILAC-based quantitation has been incorporated with non-labeled cross-linkers for quantitative comparison of cross-linked peptides through labeling of targeting amino acids such as lysine [67], eliminating the need for stable isotope-labeled cross-linkers. In contrast to deuterium-labeled cross-linking reagents, $^{13}C/^{12}C$ and $^{15}N/^{14}N$ labeled amino acids are typically used for SILAC labeling, which permits the chromatographic co-elution of labeled peptides. Although SILAC-based methods can be implemented for three-way comparisons, they are best suited for binary comparisons due to the limited variety of isotope-labeled amino acids that can produce sufficient mass differences among compared peptides. Regardless, when stable isotope labels are introduced through labeled amino acids in SILAC experiments or isotope-coded cross-linkers, quantitation is carried out based on isotopic peptide pairs detected at the MS^1 level. Unfortunately, this doubling of peptide species has the adverse effect of increasing sample complexity, thereby decreasing the likelihood of detecting low abundance cross-linked peptides.

For this reason, it remains technically challenging to compare more than two cross-linked samples simultaneously, particularly for complex peptide mixtures.

In recent years, isobaric labeling strategies such as isobaric tags for relative and absolute quantification (iTRAQ) [179] and tandem mass tags (TMT) [180, 181] have emerged as powerful quantitation methods for proteomics due to their unique multiplexing capability. Currently, commercially-available TMT reagents have multiplexing capacity up to 10-plex, and have been widely used for various applications including proteome-wide expression profiling [182]. Isobaric label-based multiplexed quantitation methods permit the simultaneous analysis of multiple proteome experiments, significantly increasing throughput without increasing sample complexity. This is because isobaric labeled peptides carry the same *m/z* value and are measured as one mass spectral peak during MS^1 analysis, even if they originate from different samples. Peptide/protein quantitation is achieved through the detection of unique reporter ions resulting from the fragmentation of each isobaric label at the MS^2 level. However, it has been reported that quantitation accuracy and precision from such experiments are often compromised due to contaminating near-isobaric ions being isolated and fragmented together with the target ions, thus skewing reporter ion intensities [183]. Such interference often results in erroneous quantitation among compared samples, which can be effectively eliminated using triple-stage mass spectrometry (MS^3) [183]. Recent advancements in instrumentation and software have ushered the development of more accurate and reproducible workflows, such as MS^3-level synchronous precursor selection (SPS) to increase TMT reporter ion detection while minimizing reporter ion ratio distortion [184, 185]. Given the fact that similar MS^n analysis has been successfully implemented for unambiguous identification of peptides cross-linked by MS-cleavable cross-linking reagents [50, 73, 86, 88], we hypothesize that isobaric reagents can be

perfectly integrated with such XL-MS^n workflows, resulting in a novel multiplexed quantitative XL-MS strategy for comparing multiple cross-linked samples simultaneously. To test this, we have coupled our previously reported MS-cleavable, cross-linking reagent disuccinimidyl sulfoxide (DSSO) with the isobaric Tandem Mass Tag^{TM} duplex (TMT2) labeling reagents for a proof-of-principle comparative cross-linking analysis using a model protein. This combinatory approach represents the first report on isobaric reagent-based quantitative cross-linking mass spectrometry. The results presented here demonstrate the feasibility of the proposed method and its potential for multiplexed quantitative XL-MS analysis to dissect structural and interaction dynamics at the protein complex and the proteome-wide level in the future.

4.3 Experimental Procedures

4.3.1 Materials and Reagents

General chemicals were purchased from Fisher Scientific or VWR International, bovine heart cytochrome c (98% purity) from Sigma-Aldrich. Tandem Mass Tag^{TM} reagents purchased from Life Technologies (Thermo Fisher Scientific).

4.3.2 DSSO Cross-linking of Cytochrome C

200 μM cytochrome c in PBS buffer (pH 7.4) was reacted with DSSO in a molar ratio of 1:5 (protein: cross-linker) for 1 h at room temperature and quenched with excess hydroxylamine. Cross-linked proteins were then pelleted via TCA precipitation and re-suspended in 8 M urea. Re-suspended proteins were reduced with 15 mM TCEP for 30 min and alkylated with 30 mM chloroacetamide for 45 min in dark, and then diluted to 5 M urea. Cross-linked proteins were then digested with Lys-C for 4 h at 37° followed by dilution to 1.5 M urea and digestion by

trypsin at 37° overnight. The resulting peptide mixtures were de-salted using Waters C18 Sep-Pak cartridges and fractionated by peptide size exclusion (SEC) as previously described by Leitner et al. [163]. The SEC fractions containing cross-linked peptides were used for subsequent TMT labeling and LC-MS^n analysis.

4.3.3 TMT2 labeling of Cross-linked Cytochrome C Peptides

Approximately 80 μg of cross-linked cytochrome c peptides were used for TMT labeling. Peptides were diluted to 100 μL using 50 mM TEAB (triethyl ammonium bicarbonate) and split into equivalent 50 μL aliquots. To each aliquot was added 20 μL of 20 μg/μL of TMT2-126 or TMT2-127 isobaric labeling reagent in anhydrous ACN and incubated for 1 h at room temperature. 5% hydroxylamine was added to each sample to a final concentration of 0.25% and incubated for 15 min to quench the labeling reaction. Samples were cleaned and de-salted again using Waters C18 Sep-PAK cartridges and concentrated. Prior to LC-MS^n analysis, TMT2-126 and TMT2-127 labeled peptides were mixed at five pre-determined molar ratios (10:1, 5:1, 1:1, 1:5, and 1:10).

4.3.3 Liquid Chromatography-Multistage Tandem Mass Spectrometric (LC-MS^n) Analysis

Mixed peptide samples were analyzed utilizing a Thermo Scientific™ EASY-nLC™ 1000 UPLC system coupled on-line to a Thermo Scientific™ Orbitrap Fusion Lumos™ MS. A Thermo Scientific™ EASY-Spray™ source with a 25 cm x 75 μm PepMap EASY-Spray Column was used to separate peptides over a 55 min acetonitrile gradient of 6% to 35% at a flow rate of 300 nL/min. Each mixed peptide sample was analyzed using three individual acquisition methods: 1) a targeted ID-MS^3 acquisition optimized for DSSO cross-linked peptide identification, 2) a MultiNotch MS^3 acquisition featuring synchronous precursor selection (SPS)

[184], and 3) a combined ID-MS^3 targeted acquisition with additional SPS-MS^3 for all precursor ions selected for ID-MS^3. For methods 1 and 3, mass-difference-dependent HCD-MS^3 acquisitions were triggered if a unique mass difference (Δ=31.9721) was observed between fragment ions in the CID-MS^2 spectrum. MS^1 acquisition was performed in top speed mode with a cycle time of 5 s. MS^1 and MS^2 scans were acquired in the Orbitrap whereas MS^3 scans were detected in the ion trap. For MS^1 scans, the scan range was set from 375 to 1600 *m/z*, resolution set to 120,000, and the AGC target set to 4×10^5. For MS^2 scans, the resolution was set to 30,000, the AGC target was set to 5e4, the precursor isolation width was 1.6 *m/z*, and the maximum injection time was 100 ms for CID. The CID-MS^2 normalized collision energy was 25%. For MS^3 scans, HCD was used with a collision energy of 35%, the AGC target was set to 2×10^4, and the maximum injection time was set to 120 ms. For methods 2 and 3 containing SPS-MS^3, the AGC target was set up to 5e4, with MS^1 isolation window to 1.6 *m/z* and MS^2 isolation window to 2 *m/z* and 10 notches. The maximum injection time was set to 105 ms and resolution to 30,000.

4.3.4 Identification and Quantitation of TMT2 Labeled DSSO Cross-linked Peptides

Monoisotopic masses and charges of parent ions and corresponding fragment ions, and ion intensities from cross-linker and peptide fragmentation in ID-MS^3 spectra were extracted as MGF files using ProteoWizard MSConvert. MS^3 spectra were subjected to protein database searching using a developmental version of Protein Prospector (v. 5.17.0) using Batch-Tag against cytochrome c (SwissProt accession #: P62894) with mass tolerances for parent ions and fragment ions set as ± 20 ppm and 0.6 Da respectively. Trypsin was set as the enzyme with four maximum missed cleavages allowed. Cysteine carbamidomethylation was selected as a constant modification, while protein N-terminal acetylation, methionine oxidation, N-terminal conversion of glutamine to pyroglutamic acid, and asparagine deamidation were selected as variable

modifications. In addition, four defined modifications on uncleaved lysines and free protein N-termini were selected: alkene (A: C_3H_2O, +54 Da), sulfenic acid (S: $C_3H_4O_2S$, +104 Da), and unsaturated thiol (T: C_3H_2OS, +86 Da) modifications due to remnant moieties for DSSO, as well as a single modification for TMT2 labeling (+225 Da). Initial acceptance criteria for peptide identification required a reported expectation value ≤ 0.1.

The in-house software xl-Discoverer, designed to validate and summarize cross-linked peptides based on MS^n data and database searching, was used to automatically generate and summarize identified cross-linked peptide pairs [73]. Peak intensities for TMT2-126 and TMT2-127 reporter ions were extracted directly from Lumos™ RAW files to obtain final TMT ratios after considering isotope purities of each isobaric reagent as instructed in the manufacturer's protocol [180].

4.4 Results and Discussion

4.4.1 Development of A New Multiplexed QXL-MS Strategy

In order to increase throughput and facilitate the simultaneous quantitative analysis of differential protein complex topologies under multiple conditions, we have developed a novel multiplexed QXL-MS strategy called QMIX (Quantitation of Multiplexed, Isobaric-labeled cross (X)-linked peptides), which integrates our MS-cleavable cross-linking reagent-based XL-MS^n workflow with isobaric label-based multiplexed quantitation (Figure 4-1). This strategy is established due to the fact that the identification of peptides cross-linked by MS-cleavable reagents is best achieved through MS^n analysis [50, 73, 86, 88]. Coincidentally, MS^n analysis is most advantageous for multiplexed protein quantitation when using isobaric reagents due to peptide interference [183, 184]. In theory, the QMIX strategy can be accomplished by

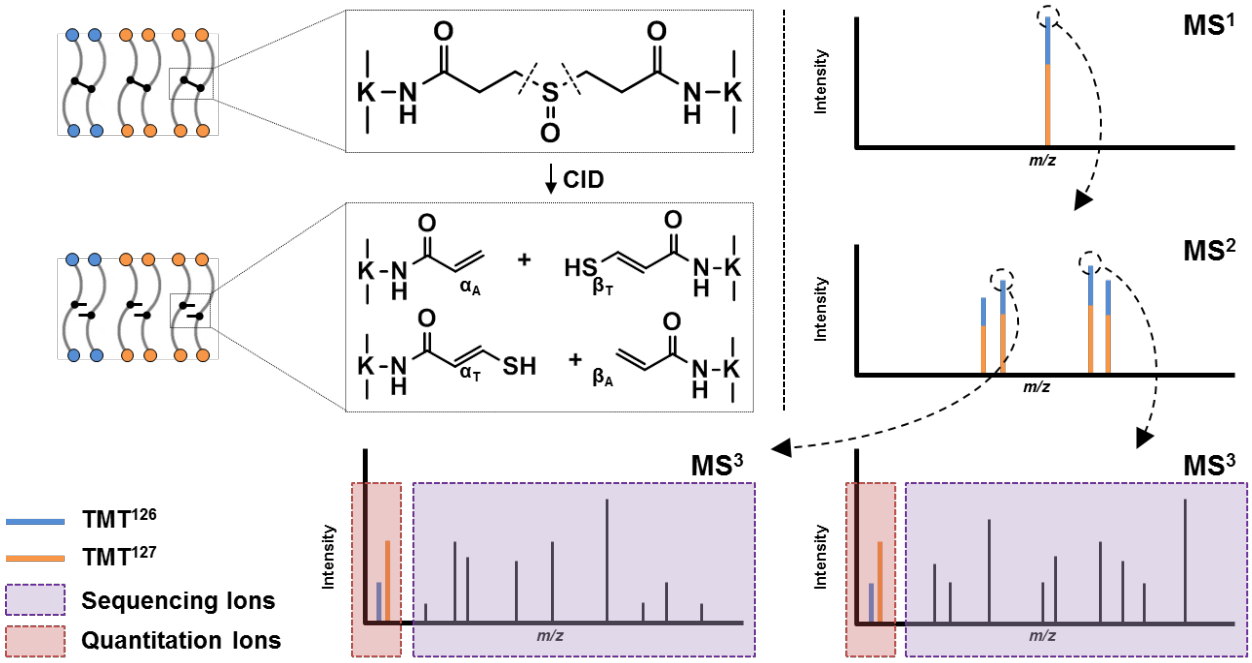

Figure 4-1. The general MS^n analysis workflow for identifying and quantifying TMT-labeled, DSSO cross-linked peptides. Fragment ions from MS^2 are selected for subsequent HCD analysis in MS^3, releasing both b and y ions for sequencing, as well as TMT reporter ions for quantitation.

combining any effective MS-cleavable cross-linker (e.g. sulfoxide-containing MS-cleavable reagents) with any types of isobaric reagents. To demonstrate the feasibility of our multiplexed quantitative strategy for cross-linked peptides, we have employed a sulfoxide-containing, amine-reactive cross-linker, disuccinimidyl sulfoxide (DSSO) and TMT2 labeling reagents. The DSSO-based XL-MS^n workflow has been demonstrated to be effective and robust for fast and unambiguous identification of cross-linked peptides [86, 89], while TMT reagents have been widely and successfully used for multiplexing protein quantitation including proteomes and phosphoproteomes [185, 186]. In contrast to previously reported QXL-MS strategies that rely on isotope-coded cross-linkers or SILAC-labeled lysines [67, 90, 164, 177], our proposed QMIX strategy has a unique multiplexing capability that enables simultaneous quantitation of cross-linked peptides from multiple samples in a similar manner to multiplexed quantitation of non-

cross-linked peptides. The maximum number of cross-linked samples that can be concurrently compared would be limited only by the number of available isobaric tags. Since TMT labeling reagents are isobaric and structurally identical, differentially labeled cross-linked peptides co-elute simultaneously in the LC chromatogram and are measured as a single peak in the survey MS^1 scan, similar to TMT-labeled non-cross-linked peptides. Thus, in contrast to other types of isotope label-based QXL-MS strategies [67, 90, 164, 175], isobaric labeling does not increase sample complexity. In fact, the signal intensities of cross-linked peptides are augmented even if they are contributed through different samples, effectively increasing the detectability of low abundance cross-linked peptides for their identification and quantitation. Moreover, TMT labeling would allow all types of peptides to be quantified within a single run, thus enabling thorough comparison of samples at different levels. Finally, the ability to multiplex would permit the comparative analysis of multiple samples in a single run, significantly improving throughput while providing the flexibility of analyzing biological replicates simultaneously. Collectively, QMIX represents a general strategy that is much more versatile and flexible than any existing QXL-MS strategies.

4.4.2 Fragmentation of TMT-labeled, DSSO-cross-linked peptides

Incubation of TMT2 reagent with DSSO cross-linked peptides results in the covalent labeling of non-cross-linked lysine residues, as well as free N-terminal primary amines generated through enzymatic digestion. We found that the complete labeling of all available primary amines of cross-linked peptides was able to be achieved based on the instructions provided for labeling non-cross-linked peptides. Cross-linked lysine residues were unaffected by TMT labeling reagent, nor did they prevent the efficient labeling of nearby residues. Unambiguous identification of DSSO cross-linked peptides is accomplished through MS^n analysis as

previously described [86]. Because the MS-cleavable C-S bonds adjacent to the sulfoxide within the linker spacer region are significantly more labile than the amide bonds of the peptide backbone, MS^2 fragmentation of a DSSO inter-linked peptide during collision induced dissociation leads to the physical separation of the two covalently linked peptides into single peptide chains. These MS^2 fragments can then be subjected to subsequent MS^3 for peptide sequencing. Along with mass fingerprinting of MS^1 precursor ions and the characteristic fragmentation of cross-linked peptides in MS^2, the sequences of individual peptides determined

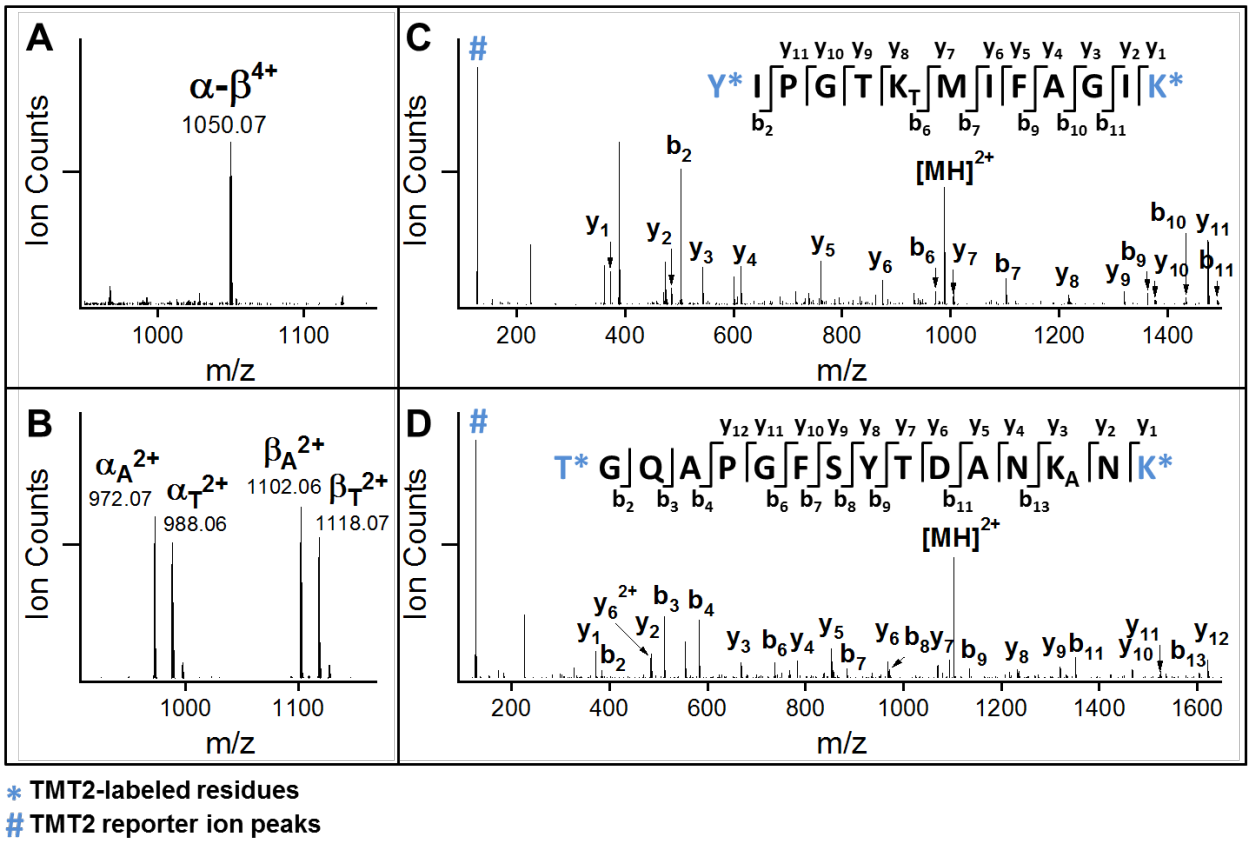

Figure 4-2. MS^n analysis of a selected TMT-labeled, DSSO cross-linked cytochrome c peptide. (**A**) MS^1 spectrum of the TMT-labeled, DSSO cross-linked peptide α-β (*m/z* 1050.0703^{4+}). (**B**) MS^2 spectrum of α-β, in which four dominant fragment ions were detected: $\alpha_A^{2+}/\beta_T^{2+}$ and $\alpha_T^{2+}/\beta_A^{2+}$. (**C-D**) MS^3 spectra of MS^2 fragment ions α_T^{2+} (*m/z* 988.06^{2+}) and β_A^{2+} (*m/z* 1102.06^{2+}), identified as ^{75}Y*IPGTK$_T$MIFAGIK*^{87} and ^{41}T*GQAPGFSYTDANK$_A$NK*^{56}, respectively, and unambiguously confirming a fully TMT-labeled cross-link between Lys54 and Lys80 of cytochrome c. Note: * indicates the TMT2-labeled amino acids, K_A: alkene modified lysine, and K_T: unsaturated thiol modified lysine.

by MS^3 are integrated to confidently determine the identities of cross-linked peptides. To evaluate whether TMT labeling interferes with the MS^n analysis of DSSO cross-linked peptides, cytochrome c was cross-linked with DSSO, and digested prior to TMT labeling. The resulting TMT-labeled peptides were then analyzed by LC-MS^n. As an example, a TMT2-labeled DSSO inter-linked peptide α-β (*m/z* 1050.0703^{4+}) detected in MS^1 (Figure 4-2A) yielded two pairs of dominant fragment ions α_A/β_T (*m/z* 972.07^{2+}/*m/z* 1118.07^{2+}) and α_T/β_A (*m/z* 988.06^{2+}/*m/z* 1102.06^{2+}) during MS^2 analysis (Figure 4-2B). This is expected, as the cleavage of one of the two MS-cleavable C-S bonds in a DSSO inter-linked heterodimeric peptide α-β would result in the observance of two predictive fragment pairs α_A/β_S or α_S/β_A that carry complementary alkene (A, +54.01 Da) or sulfenic acid (S, +103.99 Da) cross-linker remnant moieties [86]. The sulfenic acid moiety often undergoes dehydration to form a more stable unsaturated thiol moiety (T, +85.98 Da), generating dominant α_A/β_T or α_T/β_A peptide ion pairs in the MS^2 spectra. MS^3 sequencing of the α_T and β_A fragment ion pair yielded series of b and y ions that unambiguously identified them as ^{75}Y*IPGTK$_T$MIFAGIK*^{87}, in which Lys80 was modified by a saturated thiol moiety, and ^{41}T*GQAPGFSYTDANK$_A$NK*^{56}, in which Lys54 was modified by the alkene moiety (Figures 4-2C and 4-2D). In addition, MS^3 sequencing confirmed that both peptides were fully labeled by TMT2 reagent on free primary amines at their N-termini and C-terminal lysine residues. Along with mass fingerprinting of the MS^1 precursor and its fragmentation pattern in MS^2, the linkage was determined between Lys54 and Lys80 of cytochrome c (Figure 4-2). Collectively, our results indicate that TMT labeling does not interfere with the characteristic fragmentation of DSSO cross-linked peptides during MS^2 analysis and their subsequent MS^3 sequencing for unambiguous identification [86].

4.4.3 MS^n Analysis of TMT-labeled Cytochrome C Cross-linked Peptides

Previously, data-dependent MS^n acquisition methods were used to identify DSSO cross-linked peptides using an Orbitrap XL mass spectrometer, in which the top 3 MS^2 fragment ions were selected for MS^3 sequencing [50, 86, 90]. This is based on the fact that DSSO inter-linked heterodimeric peptides (α-β) produce four dominant fragment pairs: α_A/β_T and α_T/β_A as illustrated in Figure 4-2B. Therefore, MS^3 sequencing of the three most intense MS^2 fragment ions is typically sufficient for the identification of DSSO cross-linked peptides. We have analyzed our labeled, cross-linked peptide mixtures using an Orbitrap Fusion™ Lumos™ Tribrid™ mass spectrometer, as the Orbitrap XL does not have the capability to perform isobaric labeling-based quantitation due to poor sensitivity in HCD. In comparison, the Lumos™ not only has superior sensitivity, resolution, scanning rate and dynamic range, but also has multiple fragmentation techniques (CID, HCD, ETD and EThcD) and the flexibility of integrating them at any stage of MS^n analysis. Therefore, we sought out the possibility of performing a targeted MS^n method in which alkene- and thiol-modified fragment ion pairs of the same sequence (i.e. α_A/α_T or β_A/β_T) would be chosen on-the-fly based on a defined mass difference (i.e. $\Delta(\alpha_T - \alpha_A)$ or $\Delta(\beta_T - \beta_A)$) equal to the mass of a sulfur atom, 31.9721 Da. The top 2 fragment ion pairs α_A/α_T and β_A/β_T would then be selected for subsequent MS^3 analysis. This approach potentially enables all four predicted MS^2 fragment ions to be sequenced in a selective manner, thus improving identification confidence as well as throughput. During our initial assessment, we found that this targeted MS^n acquisition appears to be more effective than conventional Top N data-dependent MS^n method for these samples. Therefore, we have employed the targeted MS^n acquisition method in this work, resulting in the identification of a redundant total of 652 cytochrome c

cross-linked peptides, representing 79 unique K-K linkages across 5 samples of TMT2-labeled peptides mixed at known concentrations (Appendix 4-1).

4.4.4 Quantitation of TMT-labeled, DSSO Cross-linked Peptides

Next, we investigated whether DSSO cross-linked peptides can be effectively quantified using TMT labeling and MS^n analysis. To test this, we have labeled cross-linked cytochrome c peptides with TMT2-126 and TMT2-127 respectively, and then mixed them in 5 known ratios, (i.e. 10:1, 5:1, 1:1, 1:5; 1:10). To quantify the relative abundances of TMT2-126 and TMT2-127 labeled cross-linked peptides, we have examined three different data acquisition methods as illustrated in Figure 4-3: 1) ID-MS^3, 2) SPS-MS^3, and 3) ID-SPS-MS^3 (Figures 4-3A-C). It is

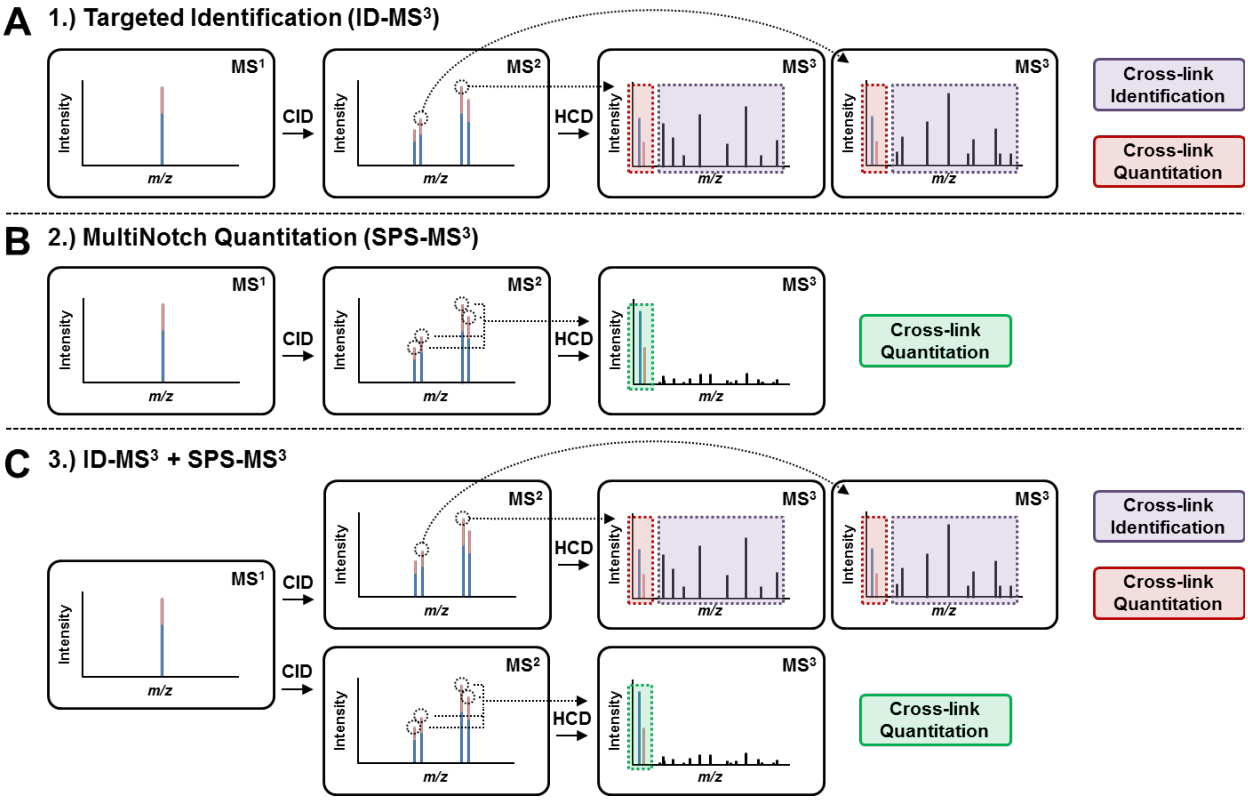

Figure 4-3. Three MS^n acquisition methods utilized for analyzing TMT-labeled, DSSO cross-linked peptides. (A) Method 1: targeted identification method, ID-MS^3. (B) Method 2: MultiNotch quantitation using synchronous precursor selection (SPS), SPS-MS3. (C) Method 3: combined acquisition method consisting of ID-MS^3 with SPS-MS^3, ID-SPS-MS3.

noted that method 3 combines the features of methods 1 and 2. The first method ID-MS^3 involves direct MS^3 analysis in HCD that enables the detection of sequence ions for peptide identification and TMT reporter ions for quantitation simultaneously. Each MS^3 spectrum of the selected MS^2 fragment ions contributes TMT reporter ions for quantitation. For instance, Figure 4-4A depicts the MS^3 spectrum of the α_A (*m/z* 599.70^{2+}) fragment of the inter-linked peptide of cytochrome c [^{7}G*K*KIFVQK*^{14} (α) inter-linked to ^{40}K*TGQAPGFSYTDANK*^{54} (β)] from the 1:1 sample, in which Lys9 is cross-linked to Lys40. As shown, the two TMT2 reporter ions (*m/z* 126 and 127) were detected and used for ratio determination. Due to the abundance of natural ^{13}C isotopes and impurities in TMT2 isobaric labeling reagents, a percentage of TMT2-126 contributes to TMT2-127 reporter ion detection, which must be corrected as previously described [180]. Based on reporter ions detected in MS^3 spectra for each cross-linked peptide, their TMT ratios (126:127) were first calculated, which were then used to obtain the final average ratios for each sample. As a result, their average TMT ratios for the five premixed samples were determined as 11.64, 5.74, 1.11, 0.22, and 0.11 respectively (Figure 4-4C), correlating well with the expected ratios. The results suggest that it is feasible to simultaneously identify and quantify TMT-labeled, DSSO cross-linked peptides using the ID-MS^3 method (i.e. normal MS^n identification analysis). With this method, the ratio deviations in the five selected samples vary from 14% ~ 35%. The larger variations appear to be particularly associated with samples containing more TMT2-126 relative to TMT2-127 (e.g. 10:1). This is likely due to the fact that the observed reporter ions (*m/z* 126 and 127) are much smaller in abundance than sequence ions using the ID-MS^3 method (Figure 4-4A) and different amounts of isotope impurities in TMT2-126 and TMT2-127 reagents contribute to ratio correction. Thus, the relative

quantitation of cross-links in these situations could potentially be compromised when the ratios are skewed in either direction.

To improve the accuracy in TMT-based quantitation, a MultiNotch-based SPS-MS^3 acquisition method has been previously developed to allow the integration of MS^3 signals from up to 10 MS^2 fragment ions, significantly boosting the relative intensities of TMT reporter ions for quantitation [184]. Therefore, we employed a similar SPS-MS^3 acquisition method to evaluate its feasibility for quantitation of cross-linked peptides (Figure 4-3B). However, this type of experiment can only acquire quantitative information, and the correlation with peptide identification has to be done from a separate experiment using an ID-MS^3 method. Figure 4-4B depicts the SPS-MS^3 spectrum of the same cross-linked peptide presented from the 1:1 sample

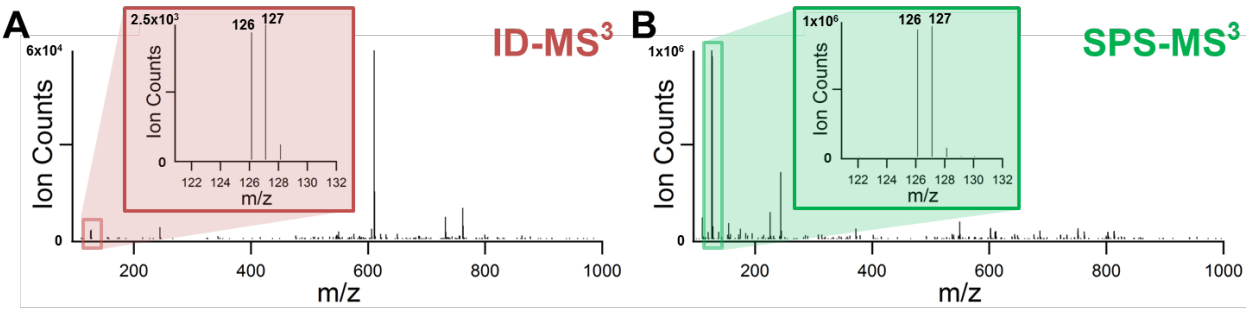

C

Measured TMT ratios (126:127)

Input Ratio (126:127)	Method 1	Method 2	Method 3	
	ID-MS^3	SPS-MS^3	ID-MS^3	SPS-MS^3
10:1	11.64 ± 4.08	11.44 ± 2.49	12.03 ± 4.14	11.01 ± 1.70
5:1	5.74 ± 1.50	5.59 ± 1.28	5.90 ± 1.87	5.32 ± 0.53
1:1	1.11 ± 0.16	1.08 ± 0.09	1.07 ± 0.20	1.05 ± 0.07
1:5	0.22 ± 0.04	0.21 ± 0.02	0.22 ± 0.04	0.20 ± 0.01
1:10	0.11 ± 0.02	0.10 ± 0.01	0.11 ± 0.02	0.10 ± 0.01

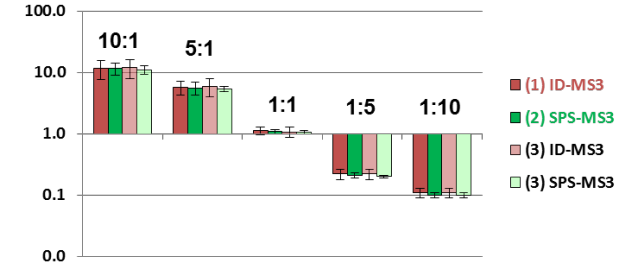

Figure 4-4. Quantitation of TMT-labeled, DSSO cross-linked peptides from five premixed samples. (A) MS^3 spectrum of the α_A (*m/z* 599.70^{2+}) of the cross-linked peptide [^{7}G*K*KIFVQK*^{14} (α) and ^{40}K*TGQAPGFSYTDANK*^{54} (β)] (*m/z* 763.8364^{5+}). α_A sequence was determined as ^{7}G*K*K$_A$IFVQK*^{14}. Inset depicts the two reporter ions. (**B**) SPS-MS^3 spectrum of the same cross-linked peptide (*m/z* 763.8364^{5+}) described in (A). Inset shows the two report ions. (**C**) Average TMT ratios (126:127) for the five pre-mixed samples using the three acquisition methods. (**D**) Corresponding plot of average TMT ratios obtained using three acquisition methods.

(Figure 4-4A). As shown, the intensities of TMT report ions (*m/z* 126 and 127) are significantly enhanced, more than 100-times higher than those obtained using the ID-MS3 method (Figure 4-4A). Using the entirety of the SPS-MS^3 spectra without considering peptide identity, the average TMT ratios for the five samples were determined as 11.44, 5.59, 1.08, 0.21 and 0.10 for 10:1, 5:1, 1:1, 1:5, and 1:10, respectively (Figure 4-4C), corroborating well with the expected values. Importantly, there was a significant decrease in experimental variation compared to ID-MS^3 acquisition, demonstrating the increased accuracy of quantitation via MultiNotch MS^3 analyses.

To enable the identification and quantification of TMT-labeled, DSSO cross-linked peptides simultaneously with better accuracy, we employed an acquisition method, ID-SPS-MS^3, utilizing both ID-MS^3 and SPS-MS^3 for each precursor ion selected for identification and quantification. In comparison to the 652 redundant cross-linked peptides identified from targeted ID-MS^3 analyses, 600 redundant cytochrome c cross-linked peptides were identified from the same samples using ID-SPS-MS^3 acquisition, representing 79 and 70 unique K-K linkages (Appendix 4-1), respectively. This result suggests that the overall increase in duty cycle during the ID-SPS-MS^3 experiment does not significantly impact the total number of identified cross-links. To compare, we have calculated TMT ratios (126:127) of each cross-link obtained from ID-MS^3 and SPS-MS^3 spectra resulted from ID-SPS-MS^3 acquisition. The respective average ratios for the five pre-mixed samples are summarized in Figure 4-4C and plotted in Figures 4-4D and 4-5. As shown, the average ratios determined using the two different acquisition methods in the same experiment are similar to those obtained in the two separate experiments as described above. This demonstrates that it is feasible to use standard MS^3 identification methods to simultaneously identify and quantify DSSO cross-linked peptides. However, SPS-MS^3 method indeed permits TMT-based quantitation of cross-linked peptides with improved accuracy and

less variation (Figure 4-4C-D). This was evidenced by the tight clustering of individual reporter ion ratios from SPS-MS^3 analysis around the average ion ratios, which resulted in lower standard deviations compared to those obtained from ID-MS^3 (Figure 4-5). This observation is consistent with the increase in reporter ion signals from multiple MS^2 ions in SPS-MS^3 experiments, thereby increasing quantitation accuracy. Importantly, these results have shown the effectiveness of integrating ID-MS^3 and SPS-MS^3 acquisition methods, thus permitting simultaneous

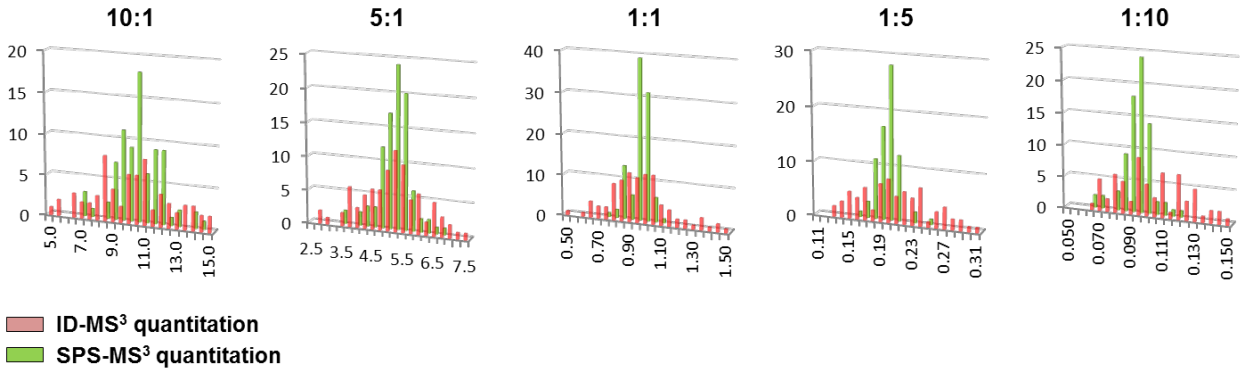

Figure 4-5. Distribution of raw cross-link quantitative ratios across five input mixings. Uncorrected reporter ion ratios for TMT2-126:TMT2-127 as determined by ID-MS^3 (red) and SPS-MS^3 (green). For each mixing, quantitative ratios derived from SPS-MS^3 acquisitions clustered more tightly around average values than those derived from ID-MS^3 acquisitions. As a result, there was a corresponding decrease in standard deviation observed from MultiNotch acquisitions.

identification and quantitation of DSSO cross-linked peptides, and enabling automated multiplexing quantitative analysis of cross-linked peptides. Collectively, these results have demonstrated the capability of quantifying cross-linked peptides using the QMIX approach, combining isobaric, MS-cleavable cross-linking reagents and multistage mass spectrometry.

4.5 Conclusion

Here we present a novel analytical platform QMIX which integrates isobaric labeling with MS-cleavable cross-linking reagents for the identification and multiplexed quantitation of

cross-linked peptides simultaneously using MS^n analysis. The incorporation of isobaric tags enables multiplexed quantitation of cross-linked peptides at a degree that cannot be easily achieved by any existing stable isotope labeling-based quantitative mass spectrometry. In addition, this general strategy is compatible with all cross-linking reagents regardless of their residue-targeting chemistries, or chemical functionalities. Although isobaric labeling in theory can be applied to conventional non-cleavable cross-linkers based XL-MS strategies, coupling this multiplexing strategy with MS-cleavable cross-linking reagents is the optimal combination due to simplified identification of cross-linked peptides using MS^n analysis offered by MS-cleavable cross-linking reagents. With the QMIX strategy, the quantitation of cross-linked peptides is achieved at the MS^3 level, thus eliminating the peptide quantitation interference commonly observed at the MS^1 level using isotope-coded cross-linkers or isotope-labeled residues. Although MS^3 sensitivity is much lower than MS^1 and MS^2, the ultra-high sensitivity in MS^n analysis provided by advanced instrumentation such as the Lumos™ mass spectrometer facilitates the implementation of this strategy. Therefore, any new developments in isobaric labeling for quantitative proteomics, such as DiLeu reagents [187], can also be potentially employed to increase multiplexing ability of quantifying cross-linked peptides in future studies. In summary, this work represents a proof-of-principle of the QMIX strategy and establishes a solid foundation for future studies toward multiplexed comparisons of protein complex conformational dynamics under various biological conditions. This will not only increase experimental throughput, but also advance our capability in QXL-MS studies beyond pair-wise comparisons.

CHAPTER 5: Describing the Molecular Mechanisms of Ubiquitination Inhibition through Targeting of E2 Ubiquitin-Conjugating Enzymes

5.1 Summary

Due to its role in biological processes such as cell cycle progression, oncogenesis, and genome integrity, dysregulation of the ubiquitin-proteasome system is associated with disruption in cell homeostasis and plays a role in a variety of human diseases, including cancers. While proteasome inhibitors (e.g. Bortezomib, Carfilzomib) have been FDA-approved as a treatment for hematopoietic cancers, cell toxicity as a result of proteasomal degradation inhibition prevents their viability as therapies for solid malignancies. However, the UPS still represents an attractive target for cancer treatment, prompting the development of therapeutic options that target the enzymes responsible for selective ubiquitination of substrates for proteasomal degradation, thereby bypassing the need for global proteasome inhibition. E3 Cullin-RING ligases (CRLs) and their associated E2-conjugating enzymes are of particular interest, due to their role in ubiquitinating approximately 20% of all cellular proteins that are degraded via the ubiquitin-proteasome system. In particular, CRL1 (i.e. SCF ligases) and CRL4A E3 ligases have been shown to target proteins involved in cell cycle control and the DNA damage response that normally act as cell cycle inhibitors, pro-apoptotic factors, or DNA damage repair mediators. These CRLs are commonly overexpressed or amplified in malignant neoplasms, contributing to oncogenesis through excessive degradation of tumor suppressors and thereby driving cell proliferation despite genomic instability. Recently, CC0651 has been shown to be effective towards suppressing cancer cell proliferation by blocking the transfer of Ub from Cdc34 to E3-recruited substrates. However, the molecular details underlying its action are lacking. Here we

employ our newly-developed, multiplexed cross-linking platform QMIX to define CC0651-dependent conformational changes in the E2-E3 complex, and thus unravel the structural basis for CC0651-induced inhibition of E2-conjugating enzyme Cdc34. This study establishes the workflow for the utility of QXL-MS in unraveling the molecular mechanisms critical for therapeutic drug development.

5.2 Introduction

Hyperactive proteasomal degradation has been associated with various types of malignancies, including myelomas, lymphomas, breast, lung, and colon cancers. This is largely due to the ubiquitous role that the UPS plays in nearly every biological process—eighty to ninety percent of all intracellular proteins are targeted for proteasomal degradation via the cascade of enzymatic reactions facilitated by E1s, E2s, and E3s, resulting in their poly-ubiquitination and subsequent recognition by the 26S proteasome. Given the myriads of substrates and cellular pathways involved, dysregulation of this degradative pathway leads to aberrations in cell homeostasis and viability. While the clinical efficacy of proteasome inhibitors has established the UPS as a key target in the treatment of multiple myeloma (MM) [188], its dose-limiting toxicity (typically resulting in peripheral neuropathy) limits its effectiveness in the treatment of solid tumors. Compared to general proteasome inhibitors (e.g. Bortezomib, Carfilzomib) that block the entire pathway for proteasomal degradation, drugs that target the enzymes upstream of the proteasome would be expected to have better selectivity with less associated toxicity. As E3 ubiquitin ligases are largely responsible for the specificity of UPS activity through their selective ubiquitination of cognate substrates, they represent the therapeutic targets with the most potential

for counteracting proteasomal hyperactivity while minimizing damage to other essential biological pathways.

Targeting the enzymes upstream of the E3, namely E1s and E2s—as well as the enzymes responsible for cullin neddylation—constitute an approach to modulate CRL activity. While the negative effects on overall protein homeostasis are reduced compared to proteasome inhibitors, they are not likely to be restricted to the precise pathways intended. The human genome encodes two E1s and roughly forty E2s; each E2 associates with their own individual subset of E3 ligases. As a result, E2-conjugating enzyme inhibitors would prevent the ubiquitination of target substrates recognized by its associated E3 ligases, potentially influencing a range of biological pathways. A recent structural and functional study on a small molecule reagent C00651 demonstrated its ability to prevent the ubiquitination of certain SCF substrates [189]. Biochemical studies further indicated that this compound was capable of inhibiting the ubiquitination of multiple CRL1-based substrate/receptor pairs through its targeting of E2-conjugating enzyme Cdc34. Of the approximately three dozen ubiquitin E2s expressed in mammals, Cdc34 is unique in that it functions solely with cullin-RING E3 ligases (CRLs), designating it as an integral component of cell cycle regulation. Allosteric inhibition of Cdc34 by CC0651 prevented the release of its ubiquitin cargo at the E2-E3 step, demonstrating that the inhibition of Cdc34-dependent poly-ubiquitination may represent an avenue of therapeutic intervention. The interactions between the acidic C-terminal tail of Cdc34 with both ubiquitin [190] and the C-terminal domain of Cul1 [191] suggests that Cdc34 plays a role in positioning Ub for transfer to E3 ligase-bound substrates; however, the structural basis for the functional interactions between Cdc34, Rbx1, and Cul1 remain unclear.

Several key questions regarding the specific protein-protein interactions of E2-E3 components and how their structural modulations regulate the ubiquitination process remain unanswered. For instance, titration experiments have shown that free Rbx1 preferentially interacts with Cdc34 in its ubiquitin-charged form. This interaction is favored by over 50-fold compared to unconjugated Cdc34 [192], suggesting that the occupation of Cdc34's catalytic cysteine by ubiquitin plays an important role in its selective recruitment to the SCF. However, it is still unclear whether ubiquitin is directly involved in the Rbx1-Cdc34 interaction, or if it induces a structural reorientation of the E2 that augments its binding efficiency to Rbx1. NMR and subsequent mutational experiments using free Rbx1 with Cdc34 have localized key residues for this interaction to the C terminus of helix a2 (Arg86, Trp87, Lys89) of Rbx1, as well as its subsequent loop (Thr90, Arg91, Gln92, Val93, Leu96, Asp97, Asn98) [192]. However, the structure of Rbx1 is relatively disordered when free compared to its cullin-bound state—and may play a role in the selective nature of this interaction. Other reports have showed that the acidic C-terminal tail of Cdc34 directly associates with a conserved basic "canyon" of the $Cul1^{CTD}$, suggesting that the catalytic domain of Cdc34 may transiently dissociate from the RING interface while remaining tethered by the tail-canyon interaction to Cul1 [191]. This would presumably allow multiple cycles of ubiquitin unloading and reloading to occur without Cdc34 ever fully dissociating from the SCF, which may explain the processivity of ubiquitination by Cdc34. Yet another important distinction is the observation that Cul1 neddylation appears to be a prerequisite for E2 recruitment by SCF ligases [193]; indeed, our previous work suggests that the release of the RING domain may facilitate the interaction between Rbx1 and E2s such as Cdc34 [90]. These observations are certainly likely to play a significant role in mediating the interaction between Cdc34 and CRL E3s. However, because many of these experiments have been

conducted in isolated systems with limited proteins, it remains difficult to visualize the intersection of these interactions—whether they are synergistic, allosteric, or inhibitory. To this end, we aim to employ our newly developed platform for multiplexed cross-linking studies, QMIX, to elucidate specific details of this complex mechanism. Determination of the structural rationale governing these interactions is critical towards understanding the mechanism of processive ubiquitination by Cdc34-CRL complexes, as well as the mechanism behind CC0651 allosteric inhibition of Cdc34-dependent ubiquitination. A comprehensive understanding of the role CC0651 plays in influencing the structure of E2-E3 interactions may provide a structural basis for the design of improved E2 inhibitors.

While we focus here on the anti-tumor potential of CRL-targeting strategies, CRL dysfunction is becoming increasingly associated with a wide range of human diseases, including heart failure and neurodegeneration. Improving our understanding of the assembly and function of these enzymes will provide more opportunities for structure-based design of inhibitors and modulators for therapeutic development. The workflows established here represent versatile strategies that can be employed to study various small molecule-mediated interactions of protein complexes to further facilitate the development of therapeutics targeting protein-protein interactions.

5.3 Experimental Procedures

5.3.1 Materials and Reagents

General chemicals were purchased from Fisher Scientific or VWR International, bovine heart cytochrome c (98% purity) from Sigma-Aldrich. Tandem Mass Tag^{TM} reagents purchased

from Life Technologies (Thermo Fisher Scientific). CC0651 inhibitor was purchased from EMD Millipore, while lenalidomide was purchased from Cayman Chemical.

5.3.2 Preparation of Cullin-RING Protein Complexes

CRL (SCF) protein complexes were purified as described in section 3.3.2. Full-length human DDB1 was subcloned into a pFastBac-GTE vector and recombinant DDB1 was expressed as N-terminal GST fusion in Trichoplusia in High-five insect cells using the Bac-to-Bac baculovirus expression system (Invitrogen). GST-DDB1 was purified by glutathione affinity followed by TEV cleavage and anion exchange chromatography. Cul4-Rbx1 complex was purified from *E. coli* by a similar approach as Cul1-Rbx1. N-terminal unstructured 36 amino acids of Cul4 were truncated to enhance its stability. Nedd8∼Cul4-Rbx1 was prepared by the same approach of Nedd8∼Cul1-Rbx1 purification.

To purify Nedd8∼Cul4-Rbx1-DDB1 complex, DDB1 and Nedd8∼Cul4-Rbx1 were mixed at 1:1.2 (molar ratio) and the mixture was loaded on a Resource Q column to remove extra Nedd8∼Cul4-Rbx1. The full complex was further purified by gel filtration.

5.3.3 Preparation of Cdc34 and Ub-charged Cdc34

Full-length human ubiquitin-conjugating enzyme (E2) Cdc34 was overexpressed and purified from E. coli by a similar approach as Nedd8 purification. Cdc34 was subcloned into a modified pGEX4T1 vector. Cells containing the Cdc34 plasmid were grown for 16 h at 16°C after induction at OD 0.6–0.8 with 200 μM IPTG before harvesting. GST-Cdc34 was purified by glutathione affinity followed by TEV cleavage and anion exchange chromatography.

To prepare stable Ub~Cdc34 conjugate, the cysteine of Cdc34 active site was mutated to lysine [Cdc34(C93K)] to generate isopeptide-linked Ub~Cdc34 conjugate. Conjugation reaction was perfomed by mixing 10 μM human E1, 200 μM His-Ub, 100 μM Cdc34(C93K) in 20 mM Tris-HCl (pH9.0), 2 mM ATP and 10 mM MgCl2, followed by incubation at 37 °C for 6 h. The His-Ub~Cdc34 conjugate was purified from conjugation reactions by a Ni Sepharose affinity column. After TEV on-column cleavage at room temperature overnight, the Ub~Cdc34 conjugate was washed out from the Ni Sepharose column, and further purified by a Resource Q column and a Superdex 75 column (GE Healthcare) equilibrated with 20 mM HEPES (pH 7.5) and 50 mM NaCl.

5.3.4 Preparation of Samples for Analysis of Cdc34-SCF (E2-E3) Intermediates

Purified Cullin-RING complexes were mixed with Cdc34 proteins at 1:1 stoichiometric ratio and diluted in 20 mM HEPES (pH 7.5) to a final concentration of 3.76 μM. For each multiplexed sample set, four individual combinations of proteins were prepared: 1) Cul1-Rbx1 with Cdc34, 2) Cul1-Rbx1 with Ub-Cdc34, 3) Nedd8~Cul1-Rbx1 with Cdc34, and 4) Nedd8~Cul1-Rbx1 with Ub-Cdc34. Each individual combination was cross-linked with DSSO for 1 h at room temperature at a molar ratio of 1:50 (Cul1: DSSO) and reactions were quenched using excess ammonium bicarbonate. Cross-linked proteins were then separated by SDS-PAGE and visualized by Coomassie Blue to access cross-linking efficiency. Higher-order bands corresponding to complexed proteins were then excised, reduced with TCEP for 30 min at RT and alkylated with chloroacetamide for 30 min in dark, and then digested with trypsin at 37°C overnight. Ammonium bicarbonate was replaced in all in-gel digestion buffers with TEAB (triethyl ammonium bicarbonate) to avoid complications with TMT labeling reagents in later steps. Peptide digests were then extracted and vacuum-concentrated to remove acetonitrile. The

pH of resultant peptide samples was then corrected to 7.5 in 40 μL of 50 mM TEAB prior to TMT isobaric labeling.

TMT6plex isobaric labeling reagents in anhydrous ACN were added to each individual cross-linked peptide sample according to the ratio as suggested in product documentation (0.8 mg of labeling reagent for each 100 μg of peptide digest). Each individual sample was incubated with one of six reagents in each set of TMT6plex (i.e. sample 1 with TMT6plex-126, sample 2 with TMT6plex-127, sample 3 with TMT6plex-128, sample 4 with TMT6plex-129) for 1 h at room temperature. Labeling reactions were quenched by the addition of 5% hydroxylamine to a final concentration of 0.25% for 30 minutes. The four individually cross-linked and TMT-labeled samples were then combined equivalently and cleaned using Waters C18 Sep-Pak cartridges to de-salt and remove excess TMT labeling reagent prior to LC-MS^n analysis.

5.3.5 Preparation of Samples for Analysis of CC0651-induced Inhibition of Cdc34

Similar cross-linking schemes were extended to Cul1 and Cul4A to determine the effect of CC0651 on the overall topology of Cdc34-CRL ligase complexes. For each multiplexed sample set, six individual combinations of proteins were prepared: 1) Cul1-Rbx1 with Cdc34, 2) Cul1-Rbx1 with Ub-Cdc34, 3) Cul1-Rbx1 with Ub-Cdc34 and CC0651, 4) Nedd8~Cul1-Rbx1 with Cdc34, 5) Nedd8~Cul1-Rbx1 with Ub-Cdc34, and 6) Nedd8~Cul1-Rbx1 with Ub-Cdc34 and CC0651. Similarly, for Cul4A: 1) Ddb1-Cul4A-Rbx1 with Cdc34, 2) Ddb1-Cul4A-Rbx1 with Ub-Cdc34, 3) Ddb1-Cul4A-Rbx1 with Ub-Cdc34 and CC0651, 4) Ddb1-Nedd8~Cul4A-Rbx1 with Cdc34, 5) Ddb1-Nedd8~Cul4A-Rbx1 with Ub-Cdc34, and 6) Ddb1-Nedd8~Cul4A-Rbx1 with Ub-Cdc34 and CC0651. Each individual combination was cross-linked with DSSO for 1 h at room temperature at a molar ratio of 1:50 (Cul1: DSSO) or 1:100 (Cul4A: DSSO); reactions were quenched using excess ammonium bicarbonate. A small portion of the cross-

linked proteins were then separated by SDS-PAGE and visualized by Coomassie Blue to access cross-linking efficiency. The remaining cross-linked proteins were then loaded onto a similar polyacrylamide gel and subjected to gel electrophoresis for 5 minutes, allowing the proteins to enter the matrix but without sufficient time to separate efficiently. The entire band area corresponding to proteins above 60 kDa were then in-gel digested and processed similarly to the previous section. Selecting a cut-off below the MW of cullin proteins but above the MW of Cdc34 filters the cross-linking products such that the entirety of cullin (and Ddb1) proteins are preserved, but Cdc34 is only extracted if complexed to CRL.

5.3.6 Liquid Chromatography-Multistage Tandem Mass Spectrometric (LC-MS^n) Analysis

Mixed peptide samples were analyzed utilizing a Thermo Scientific™ EASY-nLC™ 1000 UPLC system coupled on-line to a Thermo Scientific™ Orbitrap Fusion Lumos™ MS. A Thermo Scientific™ EASY-Spray™ source with a 25 cm x 75 µm PepMap EASY-Spray Column was used to separate peptides over a 55 min acetonitrile gradient of 6% to 35% at a flow rate of 300 nL/min. As described previously, each mixed peptide sample was analyzed using several types of acquisition methods: 1) targeted ID-MS^3 acquisitions optimized for DSSO cross-linked peptide identification, 2) top 4 data-dependent ID-MS^3 acquisitions, 3) MultiNotch MS^3 acquisitions featuring synchronous precursor selection (SPS) [184], and 4) combinatory ID-MS^3 acquisitions with additional SPS-MS^3 for all precursor ions selected for ID-MS^3. For methods 1 and 4, mass-difference-dependent HCD-MS^3 acquisitions were triggered if a unique mass difference (Δ=31.9721) was observed between fragment ions in the CID-MS^2 spectrum. MS^1 acquisition was performed in top speed mode with a cycle time of 5 s. MS^1 and MS^2 scans were acquired in the Orbitrap whereas MS^3 scans were detected in the ion trap. For MS^1 scans, the scan range was set from 375 to 1600 *m/z*, resolution set to 120,000, and the AGC target set to

4×10^5. For MS^2 scans, the resolution was set to 30,000, the AGC target was set to 5e4, the precursor isolation width was 1.6 *m/z*, and the maximum injection time was 100 ms for CID. The CID-MS^2 normalized collision energy was 25%. For MS^3 scans, HCD was used with a collision energy of 35%, the AGC target was set to 2×10^4, and the maximum injection time was set to 120 ms. For methods 3 and 4 containing SPS-MS^3, the AGC target was set up to 5e4, with MS^1 isolation window to 1.6 *m/z* and MS^2 isolation window to 2 *m/z* and 10 notches. The maximum injection time was set to 105 ms and resolution to 30,000.

5.3.7 Identification and Quantitation of Cross-linked CRL Peptides

Monoisotopic masses and charges of parent ions and corresponding fragment ions, and ion intensities from cross-linker and peptide fragmentation in ID-MS^3 spectra were extracted as MGF files using ProteoWizard MSConvert. MS^3 spectra were subjected to protein database searching using a developmental version of Protein Prospector (v. 5.17.0) using Batch-Tag against Cul1, Cul4A, Ddb1, Rbx1, Nedd8, Ubiquitin, and Cdc34, with mass tolerances for parent ions and fragment ions set as ± 20 ppm and 0.6 Da respectively. Trypsin was set as the enzyme with four maximum missed cleavages allowed. Cysteine carbamidomethylation was selected as a constant modification, while protein N-terminal acetylation, methionine oxidation, N-terminal conversion of glutamine to pyroglutamic acid, and asparagine deamidation were selected as variable modifications. In addition, four defined modifications on uncleaved lysines and free protein N-termini were selected: alkene (A: C_3H_2O, +54 Da), sulfenic acid (S: $C_3H_4O_2S$, +104 Da), and unsaturated thiol (T: C_3H_2OS, +86 Da) modifications due to remnant moieties for DSSO, as well as a single modification for TMT6 labeling (+229.16 Da). Initial acceptance criteria for peptide identification required a reported expectation value ≤ 0.1.

The in-house software xl-Tools, designed to validate and summarize cross-linked peptides based on MS^n data and database searching, was used to automatically generate and summarize identified cross-linked peptide pairs [73]. This software also automatically extracts the peak intensities of TMT6plex reporter ions from Lumos™ RAW files, correlating and generating final TMT ratios for corresponding identified cross-links after considering isotope purities of each isobaric reagent as instructed in the manufacturer's protocol [180].

5.4 Results and Discussion

5.4.1 Application of QMIX to Probe Topologies of Various Cdc34-CRL1 Complexes

We have employed TMT6plex labeling reagent to simultaneously analyze the topologies of various E2-CRL complexes involving Cdc34 and Cul1-Rbx1 (Figure 5-1). This allows us to compare the net structural effect of individual proteins on the overall conformation of the growing E2-E3 intermediate complex. For instance, by comparing the cross-linking profiles of complex 1 with complex 2, we can make observations on the structural impact of Cdc34 ubiquitin-charging on the E2-E3 interaction. By comparing complex 3 and complex 4, we can make the same observation but in the context of neddylated Cul1, which will undoubtedly have its own influence on the conformation of the interaction. Similarly, comparisons between complex 1 and 3 will highlight the influence of Cul1 neddylation on Cdc34 recruitment, while comparisons of complex 2 and 4 will describe the influence on Cul1 neddylation on recruitment of ubiquitin-charged Cdc34.

Our initial attempts on capturing representative E2-E3 interaction complexes using four channels of TMT labeling reagents suggested that unneddylated Cul1-Rbx1 does not readily associate with free Cdc34 (Figure 5-2). Following incubation and DSSO cross-linking of protein

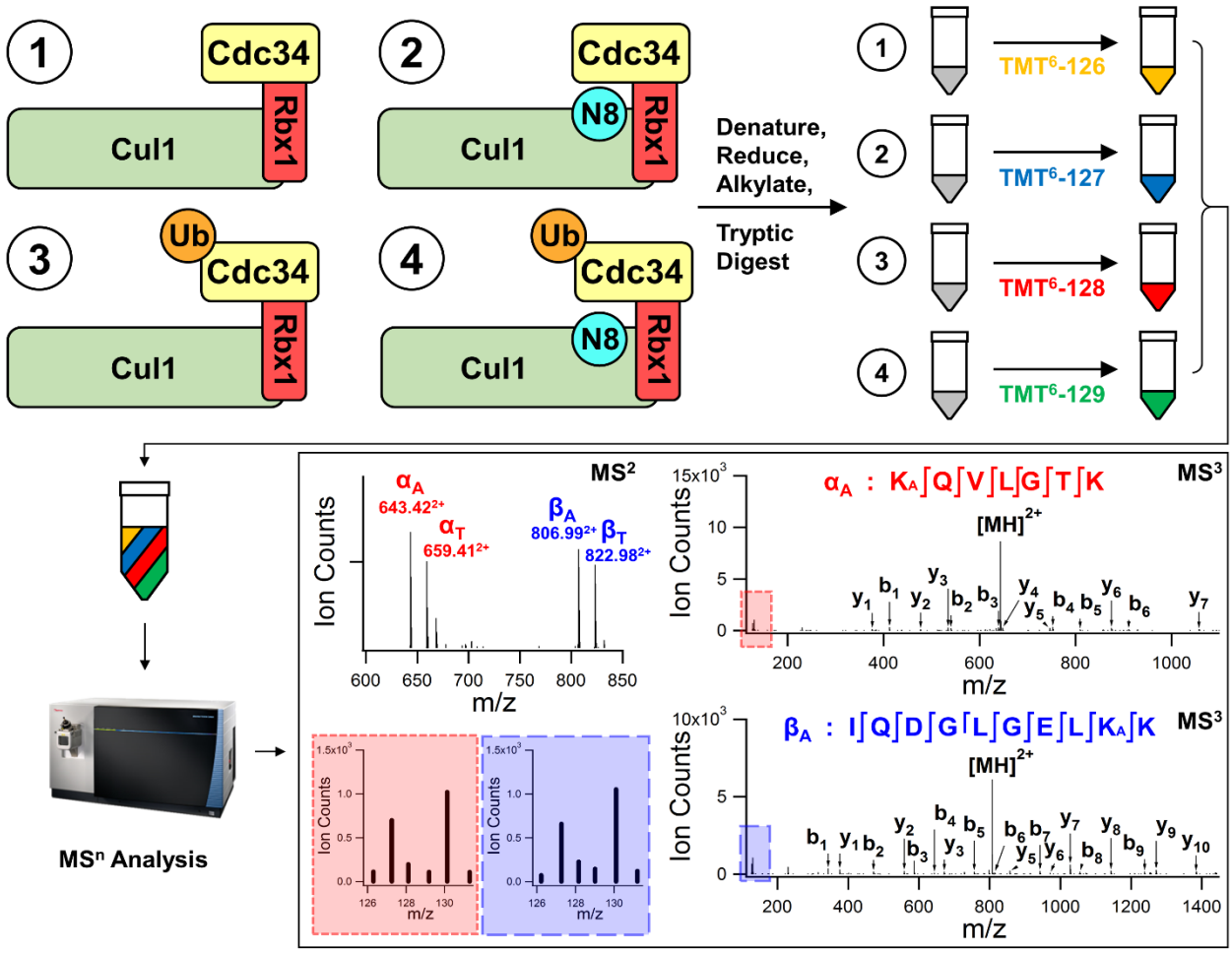

Figure 5-1. General workflow for QMIX sample preparation and MSⁿ analysis. Preparation scheme for samples for analysis of Cdc34-SCF samples. Inset: Example MS^2 and MS^3 spectra for a cross-link identified between Lys167 of Cdc34 (α) and Lys337 of Cul1 (β). Red and blue squares show quantitative reporter ions yielded by each individual peptide during HCD MS^3 analysis.

mixtures, cross-linked proteins were separated via SDS-PAGE and stained using Coomassie Blue. As shown, DSSO cross-linking did not appear to efficiently capture a complex consisting of Cul1-Rbx1 and Cdc34 (Figure 5-2, lane 3). While it is possible that the complex did associate in-solution but was not captured due to lack of proximal lysines, it is more likely that the affinity between Cul1-Rbx1 and Cdc34 are low without the intervention of Nedd8 and Ub. This observation correlates well with published findings, indicating that both Cul1 neddylation and Cdc34 Ub-charging are important in facilitating the interaction between E2 and E3. In

comparison, higher-order bands potentially corresponding to E2-E3 heterodimers were observed for cross-linked protein complexes involving Cul1-Rbx1 with Ub-Cdc34 and Nedd8~Cul1-Rbx1 with Cdc34 (Figure 5-2, lanes 4 and 5). Their presences suggest that both Cul1 neddylation and ubiquitin-conjugation of Cdc34 play independent roles in enhancing the association between Cdc34 and Cul1-Rbx1. Furthermore, their similarity in band intensities suggests that they have a similar net effect on the formation of the E2-E3 complex, even if through different modes of action. Finally, the cross-linked sample representing Nedd8~Cul1-Rbx1 with Ub-Cdc34 yielded the most intense multimer band (Figure 5-2, lane 6). This implies that the individual contributions of Cul1 neddylation and Cdc34 Ub-conjugation towards E2-E3 formation function synergistically—resulting in the most abundant formation of E2-E3 of all protein combinations.

Multimer bands from lanes 4-6 were excised from the gel and digested with trypsin; resultant peptide digests were individually labeled using TMT labeling reagents and mixed equivalently prior to LC-MS^n analysis (Figure 5-1, 5-2). As only three representative E2-E3 complexes were present, we focused on comparing the effects of Cul1 neddylation on the interaction between Cul1 and Ub-Cdc34, and the effects of Ub-conjugation of Cdc34 on neddylated Cul1-Rbx1. So far, we have identified and quantified 124 unique Lys-Lys linkages, describing 70 intra-subunit linkages and 54 inter-subunit linkages

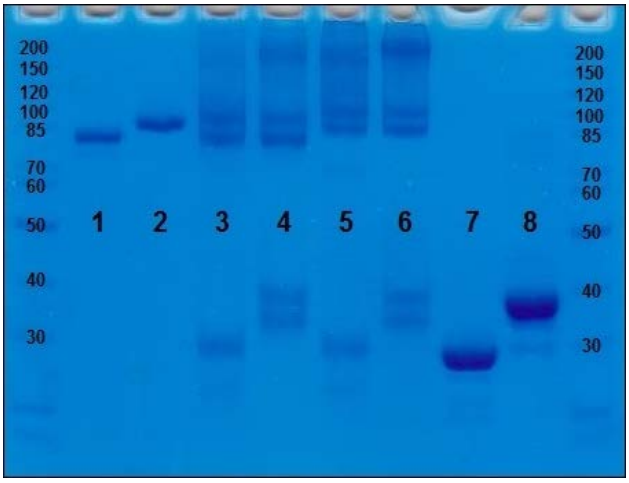

Figure 5-2. SDS-PAGE separation of cross-linked Cul1-Rbx1 and Cdc34 complexes. Lanes 1, 2, 7, and 8 represent un-cross-linked Cul1, Nedd8~Cul1, Cdc34, and Ub-Cdc34, respectively. Lanes 3-6 represent DSSO cross-linked proteins: 3) Cul1-Rbx1 with Cdc34, 4) Cul1-Rbx1 with Ub-Cdc34, 5) Nedd8~Cul1-Rbx1 with Cdc34, and 6) Nedd8~Cul1-Rbx1 with Ub-Cdc34.

(Appendix 5-1). As an example, identification and quantitation of an inter-subunit cross-link between Lys167 of Cdc34 and Lys337 of Cul1 is shown (Figure 5-1). Of the intra-subunit linkages, 6 originated from within Cdc34, 57 from Cul1, 4 from Nedd8, 2 from Ub, and 1 from Rbx1. In general, the majority of Cul1-Cul1 intra-links were not influenced strongly by neddylation or Ub-charging of Cdc34. 85.7% and 87.7% of Cul1 intra-links were unchanged (below 2-fold) when comparing Cul1-Rbx1-Ub-Cdc34 with Nedd8~Cul1-Rbx1-Ub-Cdc34, and Nedd8~Cul1-Rbx1-Cdc34 with Nedd8~Cul1-Rbx1-Ub-Cdc34, respectively (Figures 5-3, 5-4). This suggests that while Cul1 neddylation and ubiquitin-conjugation of Cdc34 contributed to the interaction between Cdc34 and SCF, neither exerted strong influences on the internal structure of Cul1. Similarly, Ub-charging of Cdc34 did not appear to alter the interactions within Nedd8, nor did Cul1 neddylation seem to change the interactions within ubiquitin or Cdc34. These observations suggest that Nedd8 and Ub not only upregulate E2-E3 interactions independently, but also modulate different regions of the complex.

It was generally difficult to discern the structural influence imparted by neddylation on the E2-E3 interaction (Figure 5-3). Just as Cul1 neddylation appeared to have little effect on the abundances of intra-subunit Cul1 cross-links, it also did not have obvious implications on inter-subunit cross-links between Cdc34 and Rbx1, Cdc34 and Ub, Cul1 and Ub, or Cul1 and Rbx1. Interestingly, even the Cul1-Rbx1 cross-links that were observed to change drastically in response to neddylation in our previous study had relatively diminished responses in the same corresponding regions when comparing Nedd8's influence on Ub-Cdc34-Cul1-Rbx1. In fact, inter-subunit cross-links between Cul1 and Rbx1 seemed to be stabilized in the context of the E2-E3 interaction, suggesting that the Ub-Cdc34 interaction with Rbx1 suppresses the flexibility of the RING domain, even when Cul1 is neddylated. Nedd8's lack of effect on the capture of

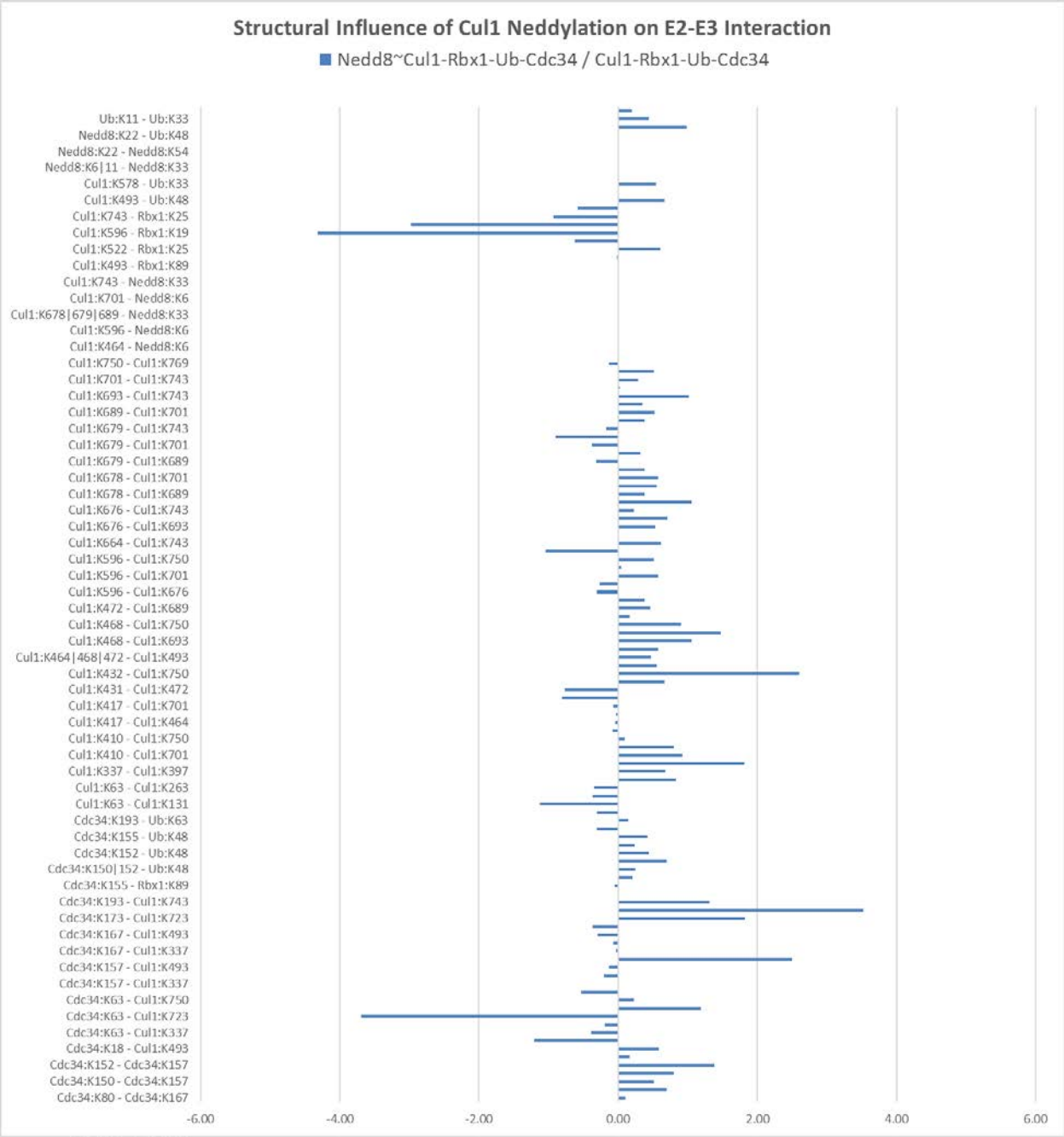

Figure 5-3. Quantitative Analysis on the effect of Cul1 Neddylation on Structure of Cul1-Rbx1-Ub-Cdc34. Degree of change in cross-link abundances following Cul1 neddylation are charted along x-axis. Abundance ratios are represented as log2 values.

cross-links between Cdc34 and Cul1 was particularly surprising. Cul1 neddylation appeared to mediate several cross-links between the WHB domain of Cul1 with the start of the acidic C-terminal tail of Cdc34, while discouraging a specific cross-link between the same region of Cul1

with Lys63 of Cdc34. The most surprising observations were the extensive cross-links identified between Cdc34 and various lysine residues of Cul1 ranging from the C-terminal end of $Cul1^{NTD}$ to the C-terminal end of $Cul1^{CTD}$. These cross-links were identified regardless of Cul1 neddylation, suggesting that the interaction of Cul1-Rbx1 with Ub-Cdc34 conferred a degree of flexibility to Rbx1 in unneddylated Cul1. The range of cross-links formed between Cdc34 and Cul1 were found to be similar regardless of Cul1's neddylation state. Therefore, interaction with Ub-Cdc34 appeared to constrain Rbx1's range of motion in the neddylated "open" state, whereas Rbx1 appeared to be more flexible and dynamic when interacting with Cdc34 than in the "closed", unneddylated state.

On the other hand, ubiquitin conjugation had a considerably more noticeable effect on cross-links involving Cdc34 (Figure 5-4). Cross-links involving Lys155 and Lys157 of Cdc34 to Lys89 of Rbx1 were significantly increased in response to Ub conjugation, confirming the importance of Rbx1's a2 helix as an interaction hotspot to Ub-Cdc34. Ub conjugation was also observed to induce a conformational change within Cdc34, increasing the occurrence of an intra-subunit Cdc34 cross-link between Lys80 and Lys167 that was unperturbed by Cul1 neddylation (Figure 5-4). Ubiquitin conjugation largely discouraged the formation of cross-links between Cdc34 and distant Cul1 residues, instead localizing Cdc34's position nearby to the WHB domain of the $Cul1^{CTD}$. This same observation was observed to a certain extent when comparing the effect of Cul1 neddylation on the topology of the E2-E3 intermediate. However, how these observations align with the notion of a tail-canyon interaction docking the acidic C-terminal tail of Cdc34 to Cul1's basic canyon remains unclear. This tethering effect would likely limit the cross-linking between distant residues of Cul1 and Rbx1, while simultaneously limiting interactions between Cdc34 and Cul1 to a radius originating the Cul1 basic canyon. From this

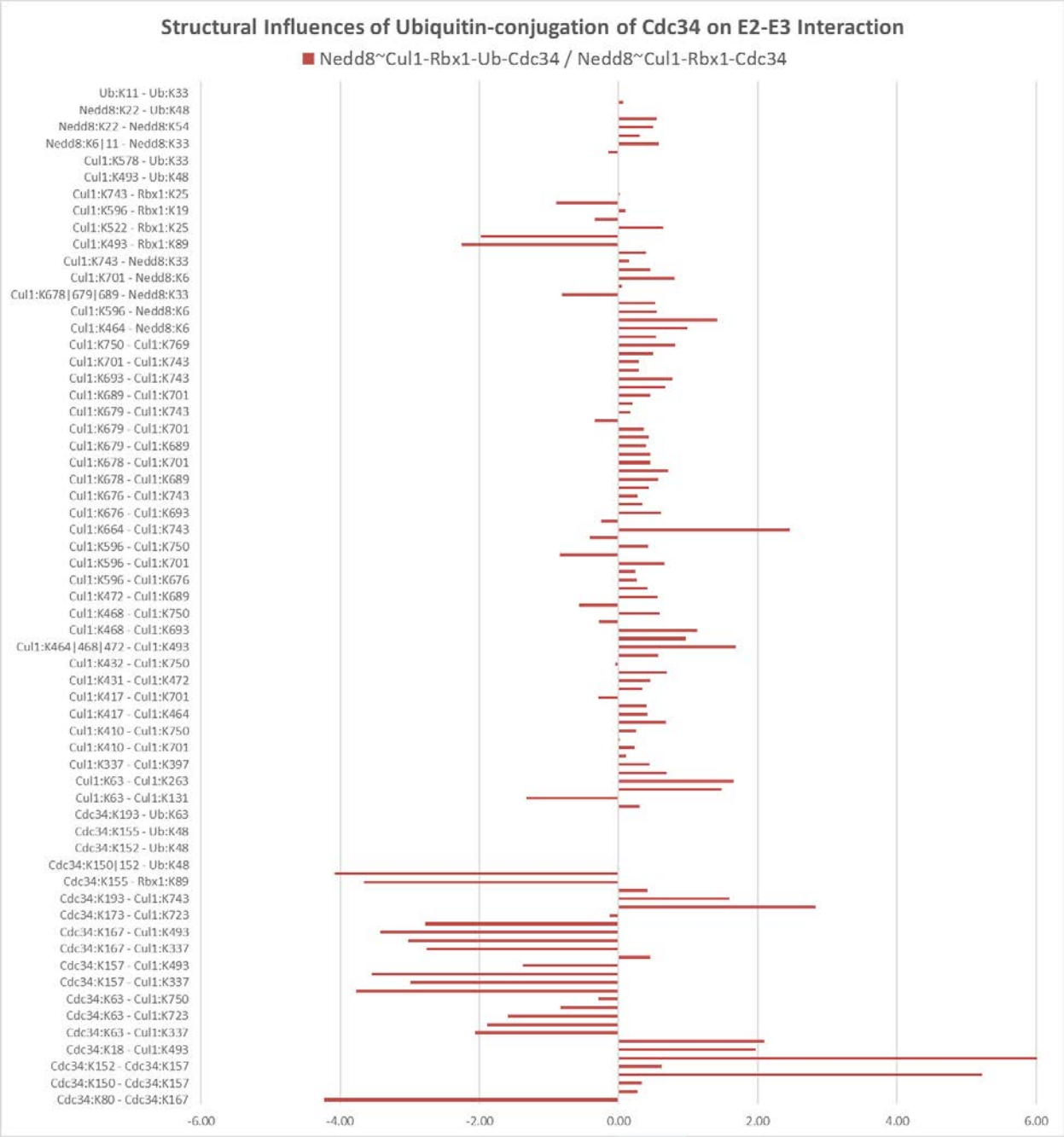

Figure 5-4. Quantitative Analysis on the effect of Ub-charging of Cdc34 on Structure of Nedd8~Cul1-Rbx1-Cdc34. Degree of change in cross-link abundances resulting from interactions involving Ub-Cdc34 compared to free Cdc34 are charted along x-axis. Abundance ratios are represented as log2 values.

perspective, the Cul1 residues identified to participate in cross-links with Cdc34 appear to be equidistant from Cul1's conserved canyon. However, these observations contradict the expected binding mode of Rbx1 to Cdc34 based on the canonical association of RING-domain containing

proteins to E2 ubiquitin-conjugating enzymes, suggesting that Cdc34 may uniquely interact with the Rbx1 in a distinct manner from other E2s. However, short of delineating a structural model for this interaction, we can currently only speculate on the perturbations that cause these changes in cross-link abundances.

5.4.2 Applying QMIX to Study the CC0651-dependent Inhibition of Cdc34

We have expanded the previous QMIX sample preparation to include complexes that represent E2-E3 interactions modulated by Cdc34 inhibitor CC0651. While several reports have been published detailing in high-resolution the structural impact of CC0651 on Cdc34 and Ub-Cdc34 [189, 194], they have been limited to studies on Cdc34 and ubiquitin-charged Cdc34 alone or in the presence of free Rbx1. Therefore, our goal is to determine whether the topological effects induced by CC0651 are identifiable by cross-linking, and whether they correlate with published findings describing the effect of CC0651 on free Cdc34. In addition to Cul1, we have also prepared corresponding samples with Ddb1-Cul4A to interrogate the effect of CC0651-inhibition on the structure of CRL4. While Cdc34 is not the primary E2 for CRL4 E3 ligases, interactions with non-canonical E2's may shed light on various modes of interaction, resulting in distinct responses for different CRL complexes to the same modulator.

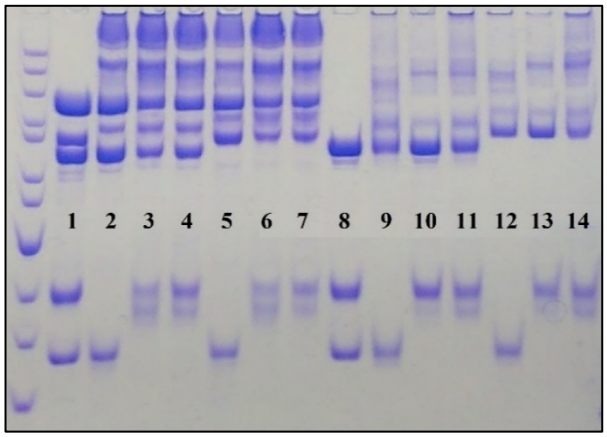

Figure 5-5. SDS-PAGE separation of cross-linked Cul4A- and Cul1-Cdc34 complexes. Lane 1: control Cul4A, Nedd8~Cul4A, Ddb1, Cdc34, and Ub-Cdc34. Lanes 2-7 correspond to six combinations of Cul4A and Cdc34 protein complexes. Lane 8: control Cul1, Nedd8~Cul1, Cdc34, and Ub-Cdc34. Lanes 9-14 correspond to six combinations of Cul1 and Cdc34 protein complexes.

In this experiment, we have cross-linked six combinations of CRL and E2 proteins: 1) CRL + Cdc34, 2) CRL + Ub-Cdc34, 3) CRL + Ub-Cdc34 + CC0651, 4) Nedd8~CRL + Cdc34, 5) Nedd8~CRL + Ub-Cdc34, and 6) Nedd8~CRL + Ub-Cdc34 + CC0651. This scheme has been applied using Cul1-Rbx1 as the CRL, as well as Ddb1-Cul4A-Rbx1. Following cross-linking with DSSO, the resulting cross-linked proteins were separated via SDS-PAGE to access the efficiency of complex capture. Compared to Cul1, CRL4-E2 complexes appeared to form readily regardless of Cul4A's neddylation state or Cdc34's ubiquitin-conjugation state (Figure 5-5, lanes 2-7). In both CRL1 and CRL4A, the incubation of the proteins in-solution with CC0651 prior to cross-linking did not hamper the formation or capture of E2-E3 complex, although a slight increase in intensity of cross-linked products and aggregation was observed in CRL1 complexes following CC0651 incubation (Figure 5-5, lanes 11 and 14); an accompanying decrease in the intensity of monomer products in the same lanes was observed, suggesting that CC0651 may marginally promote the formation of the Cdc34-CRL1 interaction. Similar to previous analyses, cross-linked proteins were subjected to short-duration gel electrophoresis and excised, reduced, alkylated, and digested with trypsin. Following individual labeling with TMT6plex labeling reagents, the peptide samples were combined equally, de-salted, and subjected to LC-MS^n analysis.

Compared to previous analyses, in which only higher MW bands corresponding to individually cross-linked complexes were excised, the entirety of proteins from each lane above 60 kDa were utilized for in-gel digestion for this set of experiments. The rationale for this alteration in sample procedure is largely due to the complexity of band formation resulting when cross-linking Cul4A compared to Cul1. We expect that this will become a common characteristic of cross-linking experiments as more components of full CRL assemblies are introduced.

Therefore, to maintain consistency between individual samples in each mixed set, the entirety of proteins in each condition was extracted for digestion. However, the downside to this approach is the potential suppression/augmentation of quantitative cross-link abundance observations due to the presence of multiple subcomplexes containing the same proteins. This is due to the fact that cross-linking data represents the average state of proteins in a given sample. For instance, quantitative ratios of intra-subunit Cul1 cross-links in the sample containing Cul1-Rbx1 and Ub-Cdc34 represent a distribution of cross-links describing the topologies of Cul1-Rbx1, as well as Ub-Cdc34-complexed Cul1-Rbx1. The relative abundance of an intra-Cul1 cross-link in Cul1-Rbx1-Ub-Cdc34 will be influenced by the presence of the same cross-link in Cul1-Rbx1, depending on the relative abundances of free and Ub-Cdc34-bound Cul1-Rbx1. For this reason, we primarily focus on the inter- and intra-subunit cross-links involving ubiquitin and Cdc34. Because only protein bands above 60 kDa were considered for these comparisons, this guarantees that Ub and Cdc34 cross-links are only detected if they are cross-linked to E3—this prevents the suppression of cross-link abundances for identified cross-links that may occur in both free Cdc34 and CRL-complexed Cdc34.

To determine whether data from single band extraction is comparable to data obtained from simultaneous excision of multiple bands, we examined the relative quantitative abundances of six Cul1-Cdc34 cross-links in Nedd8~Cul1-Rbx1-Ub-Cdc34 compared to Nedd8~Cul1-Rbx1-Cdc34 that were identified with both sample preparation techniques (Figure 5-6). For the dataset obtained from single band extractions, the cross-link abundances were normalized against relative Cul1 concentrations, while in the multiple band extraction, cross-links were normalized against Cdc34. As shown, both preparations yielded similar results indicating that ubiquitin-charging of Cdc34 reduced the cross-linking occurrence between residues localized to a central

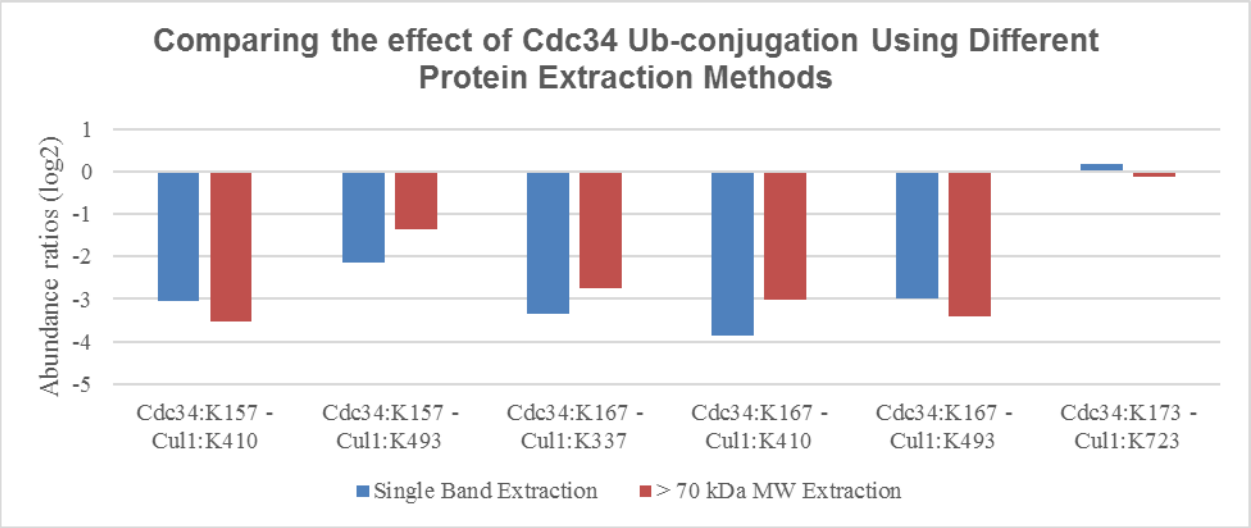

Figure 5-6. Comparison of quantitative data for Cul1-Cdc34 cross-links obtained through single band and multi-band extraction. The effects of Cdc34 conjugation on the occurrence of Cul1-Cdc34 cross-links are shown for **(A)** single band and **(B)** multi-band extraction. Abundance ratios are displayed in log2 values.

helix-loop-helix of Cdc34 (Lys157~Lys167) to those in the 4-HB domain of Cul1. Conversely, ubiquitin-conjugation of Cdc34 did not appear to affect the abundance of a specific cross-link occurring between a lysine located in the WHB of Cul1 and Lys173 of Cdc34, which was observed regardless of the sample preparation method. These results indicate that comparisons made using either extraction can accurately describe the topologies of these protein complexes.

A total of 163 unique Lys-Lys linkages were identified in the mixed Cul1 sample, corresponding to 102 intra-subunit linkages and 61 inter-subunit linkages. In Cul4A, 217 total Lys-Lys linkages were identified, representing 131 intra-subunit and 86 inter-subunit linkages. However, as we are only considering inter-subunit linkages and intra-subunit linkages within Ub and Cdc34, the total number of Lys-Lys linkages quantified in the Cul1 sample was narrowed down to 73, and 100 in Cul4A complexes. We then quantitatively determined the abundances of these cross-links before and after CC0651 inhibition to determine which regions of the proteins reflected a structural change due to CC0651 modulation (Appendix 5-2). These results were

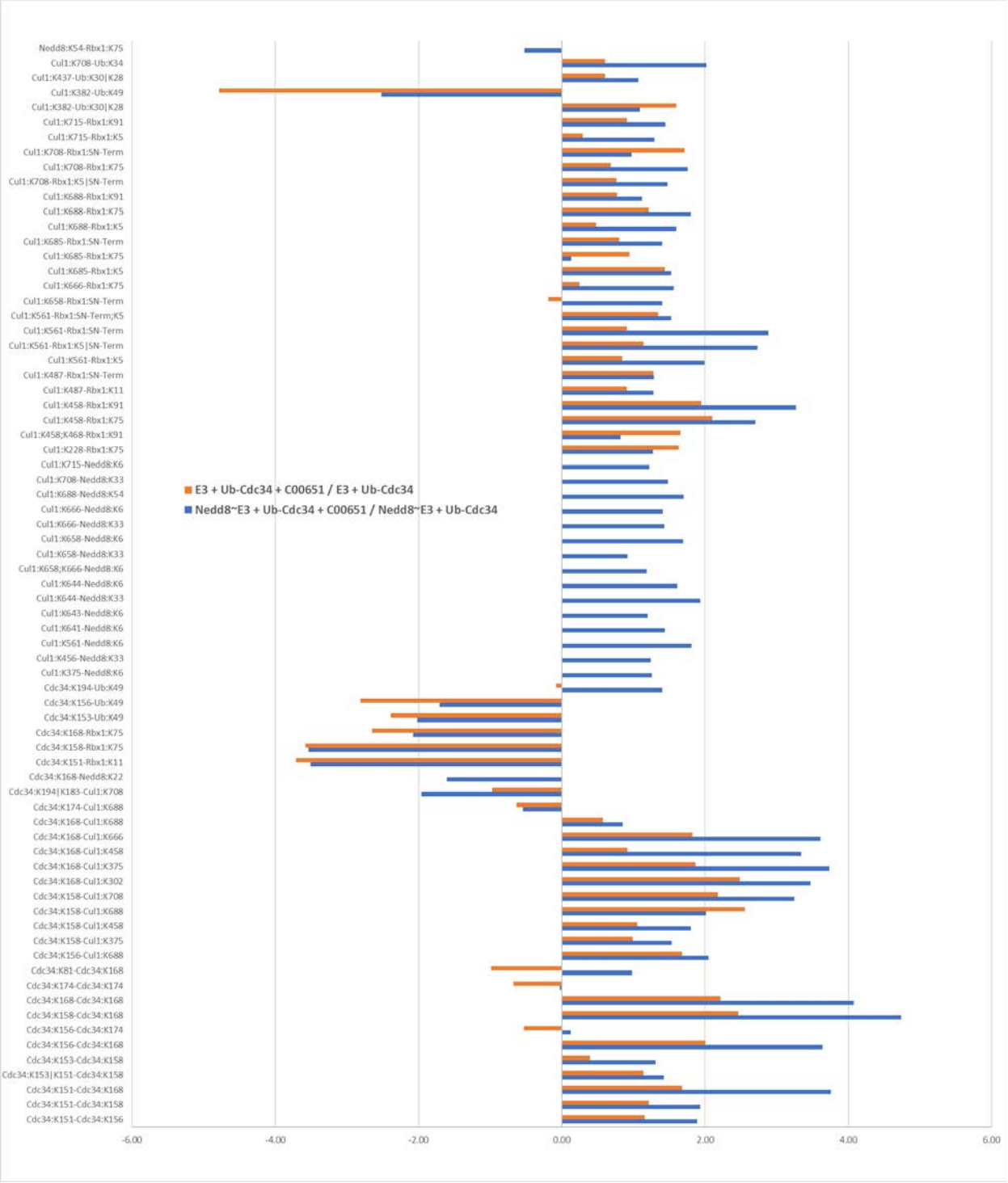

Figure 5-7. Relative abundances of inter- and intra-subunit cross-links identified in CRL1-Cdc34 complexes before and after CC0651 modulation. Orange bars represent the effects of CC0651 on Cul1-Rbx1-Ub-Cdc34, while blue bars represent the effects of CC0651 on neddylated Cul1-Rbx1-Ub-Cdc34. X-axis represents the degree of change (log2). Ratios greater than |2.00| were designed as being significant changes (4-fold increase or decrease).

summarized as bar graphs, which depict the abundance ratios of cross-links in E3-Ub-Cdc34 and Nedd8~E3-Ub-Cdc34 before and after incubation with CC0651. CC0651 modulation induced a range of structural reorientations that were reflected in the abundances of quantified cross-links from the complex formed by Cul1 and Ub-Cdc34 (Figure 5-7). The abundance of cross-links within Cdc34 increased significantly while Ub-Cdc34 cross-links were significantly diminished, suggesting that the CC0651 induces distinct conformational shifts within the structure of Ub-Cdc34. These shifts translated to distinct conformational differences in the topology of the interactions between Rbx1 and Cdc34, which were observed as decreases in the formation of several Cdc34-Rbx1 cross-links, as well as a specific cross-link between Cul1 and Lys48 of ubiquitin. These reductions were accompanied by an increase in cross-links bridging Cul1 to both Rbx1 and Cdc34, showing that CC0651 not only influences the topology of Ub-Cdc34 but also fundamentally changes the nature of the interaction between Cul1-Rbx1 and Ub-Cdc34. Interestingly, many of the observed changes in cross-linked abundances were augmented in the context of the neddylated Cul1 complex, adding yet another layer of complexity to the interpretation of the data analysis.

In comparison, CC0651 did not appear to exhibit the same degree of effect on the topology of the Cul4A-Cdc34 complex as compared to Cul1-Cdc34 (Figure 5-8). Incubation with CC0651 decreased the formation of cross-links between Cdc34 to Ub and Rbx1, as was observed in the Cul1 complex. However, the increase in cross-link formation between Cul1 to both Rbx1 and Cdc34 was not observed for Cul4A, suggesting that CRL4A receives and interacts with Cdc34 in a different manner than CRL1. CC0651 also seemed to facilitate the formation of specific cross-links between Ddb1 and Cdc34, implying an increased degree of flexibility for Rbx1-bound Cdc34. Despite the conservation between Cul1 and Cul4A

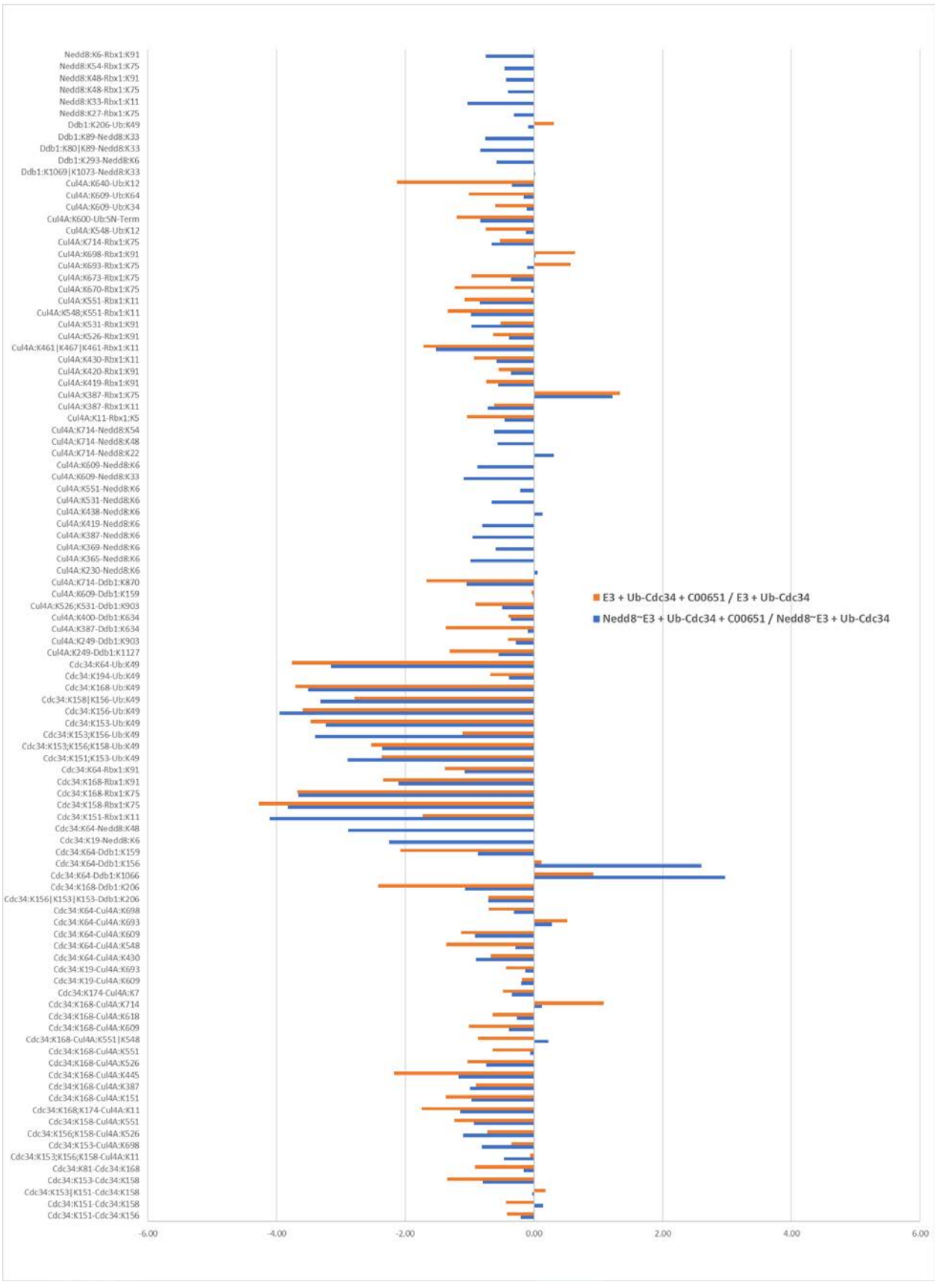
Nedd8:K6-Rbx1:K91
Nedd8:K54-Rbx1:K75
Nedd8:K48-Rbx1:K91
Nedd8:K48-Rbx1:K75
Nedd8:K33-Rbx1:K11
Nedd8:K27-Rbx1:K75
Ddb1:K206-Ub:K49
Ddb1:K89-Nedd8:K33
Ddb1:K80|K89-Nedd8:K33
Ddb1:K293-Nedd8:K6
Ddb1:K1069|K1073-Nedd8:K33
Cul4A:K640-Ub:K12
Cul4A:K609-Ub:K64
Cul4A:K609-Ub:K34
Cul4A:K600-Ub:SN-Term
Cul4A:K548-Ub:K12
Cul4A:K714-Rbx1:K75
Cul4A:K698-Rbx1:K91
Cul4A:K693-Rbx1:K75
Cul4A:K673-Rbx1:K75
Cul4A:K670-Rbx1:K75
Cul4A:K551-Rbx1:K11
Cul4A:K548;K551-Rbx1:K11
Cul4A:K531-Rbx1:K91
Cul4A:K526-Rbx1:K91
Cul4A:K461|K467|K461-Rbx1:K11
Cul4A:K430-Rbx1:K11
Cul4A:K420-Rbx1:K91
Cul4A:K419-Rbx1:K91
Cul4A:K387-Rbx1:K75
Cul4A:K387-Rbx1:K11
Cul4A:K11-Rbx1:K5
Cul4A:K714-Nedd8:K54
Cul4A:K714-Nedd8:K48
Cul4A:K714-Nedd8:K22
Cul4A:K609-Nedd8:K6
Cul4A:K609-Nedd8:K33
Cul4A:K551-Nedd8:K6
Cul4A:K531-Nedd8:K6
Cul4A:K438-Nedd8:K6
Cul4A:K419-Nedd8:K6
Cul4A:K387-Nedd8:K6
Cul4A:K369-Nedd8:K6
Cul4A:K365-Nedd8:K6
Cul4A:K230-Nedd8:K6
Cul4A:K714-Ddb1:K870
Cul4A:K609-Ddb1:K159
Cul4A:K526;K531-Ddb1:K903
Cul4A:K400-Ddb1:K634
Cul4A:K387-Ddb1:K634
Cul4A:K249-Ddb1:K903
Cul4A:K249-Ddb1:K1127
Cdc34:K64-Ub:K49
Cdc34:K194-Ub:K49
Cdc34:K168-Ub:K49
Cdc34:K158|K156-Ub:K49
Cdc34:K156-Ub:K49
Cdc34:K153-Ub:K49
Cdc34:K153;K156-Ub:K49
Cdc34:K153;K156;K158-Ub:K49
Cdc34:K151;K153-Ub:K49
Cdc34:K64-Rbx1:K91
Cdc34:K168-Rbx1:K91
Cdc34:K168-Rbx1:K75
Cdc34:K158-Rbx1:K75
Cdc34:K151-Rbx1:K11
Cdc34:K64-Nedd8:K48
Cdc34:K19-Nedd8:K6
Cdc34:K64-Ddb1:K159
Cdc34:K64-Ddb1:K156
Cdc34:K64-Ddb1:K1066
Cdc34:K168-Ddb1:K206
Cdc34:K156|K153|K153-Ddb1:K206
Cdc34:K64-Cul4A:K698
Cdc34:K64-Cul4A:K693
Cdc34:K64-Cul4A:K609
Cdc34:K64-Cul4A:K548
Cdc34:K64-Cul4A:K430
Cdc34:K19-Cul4A:K693
Cdc34:K19-Cul4A:K609
Cdc34:K174-Cul4A:K7
Cdc34:K168-Cul4A:K714
Cdc34:K168-Cul4A:K618
Cdc34:K168-Cul4A:K609
Cdc34:K168-Cul4A:K551|K548
Cdc34:K168-Cul4A:K551
Cdc34:K168-Cul4A:K526
Cdc34:K168-Cul4A:K445
Cdc34:K168-Cul4A:K387
Cdc34:K168-Cul4A:K151
Cdc34:K168;K174-Cul4A:K11
Cdc34:K158-Cul4A:K551
Cdc34:K156;K158-Cul4A:K526
Cdc34:K153-Cul4A:K698
Cdc34:K153;K156;K158-Cul4A:K11
Cdc34:K81-Cdc34:K168
Cdc34:K153-Cdc34:K158
Cdc34:K153|K151-Cdc34:K158
Cdc34:K151-Cdc34:K158
Cdc34:K151-Cdc34:K156
E3 + Ub-Cdc34 + C00651 / E3 + Ub-Cdc34
Nedd8~E3 + Ub-Cdc34 + C00651 / Nedd8~E3 + Ub-Cdc34
-6.00
-4.00
-2.00
0.00
2.00
4.00
6.00

Figure 5-8. Relative abundances of inter- and intra-subunit cross-links identified in CRL4A-Cdc34 complexes before and after CC0651 modulation. Orange bars represent the effects of CC0651 on Ddb1-Cul4A-Rbx1-Ub-Cdc34, while blue bars represent the effects of CC0651 on neddylated Ddb1-Cul4A-Rbx1-Ub-Cdc34. X-axis represents the degree of change (log2). Ratios greater than |2.00| were designed as being significant changes (4-fold increase or decrease).

(identity ~29%), it is apparent that they associate differently with Cdc34, and thus respond differently to an allosteric inhibitor selective for Cdc34. The fact that Cdc34 is not the primary E2 for CRL4A complexes implies divergent functionalities of various E3 ligases that assemble along cullin family proteins. Mapping of the Cdc34 residues participating in cross-links that were dramatically affected by CC0651 to the published high-resolution structure of Ub-Cdc34-CC0651 indicates that cross-linking is capable of accurately identifying the regions impacted most by structural reconfiguration (Figure 5-9). However, whether this data is sufficient to provide a model for CC0651-bound Ub-Cdc34 interacting with Cul1-Rbx1 or Nedd8~Cul1-Rbx1 remains to be seen.

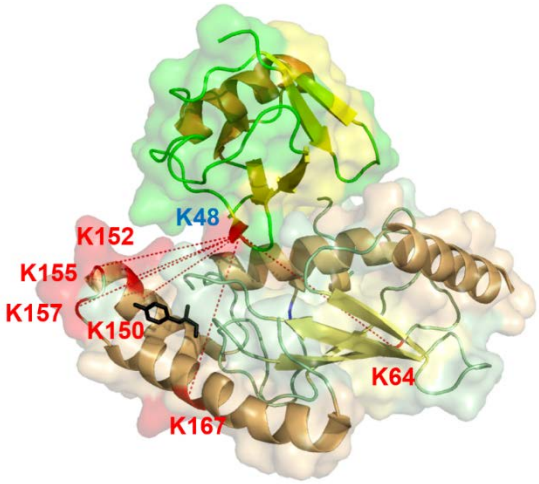

Figure 5-9. Cdc34-Ub cross-links mapped hCdc34-Ub-CC0651. Inter-subunit cross-links between Cdc340 and Ub plotted to known structure (PDB: 4MDK), showing localization of highly changed cross-links relative to CC0651 binding site.

Integration of QXL-MS data represents an ongoing challenge in the field, as current software has not been designed to properly accommodate quantitative data. Most integrative platforms that are able to utilize cross-linking data typically only consider the Euclidean (straight-line) distance between cross-linked residues. While this has been shown to be acceptable for the study of static protein structures, this approach is most likely to be insufficient for analysis of quantitative cross-linking

data. Factors such as solvent accessibility and surface volume can influence residue 'cross-linkability' and subsequently, the likelihood of cross-link formation. Therefore, Euclidean Cα-Cα distances cannot be the only measure in which protein structures are modified to develop derivative conformational models.

We show here that even in the absence of integrative software to properly handle QXL-MS data, quantitative cross-linking can be utilized to study the structural response of protein complexes to post-translational modifications and ligand-binding. Profiling of protein complex topologies through cross-linking is sensitive enough to observe subtle changes in proteins and protein interactions. This work represents an extension of the current XL-MS toolkit to study the conformational dynamics of physiologically important biological assemblies that are difficult to examine using traditional structural techniques. As a result, we expect that the eventual integration of these strategies with existing methods for structure determination will greatly contribute to our understanding of protein dynamics, ultiamtely paving the way for structure-guided therapeutic drug development.

CHAPTER 6: Conclusions and Final Remarks

Protein assemblies represent the workhorses of the cell, forming the basis of all cellular processes. Their biological roles are intimately associated with their topologies, making the structural elucidation of proteins and protein complexes a critical requirement to understanding their function. To this end, traditional biophysical techniques such as X-ray crystallography and NMR spectroscopy (and recently, cryo-EM) have been widely utilized to define the three-dimensional structures of proteins and protein complexes. These high-resolution models have greatly contributed to the plethora of existing knowledge on static protein structures, providing insight on their mechanisms of action (Roughly 85% of entries deposited in the World Wide Protein Data Bank (PDB) were determined by X-ray crystallography, with NMR providing a large portion of the remaining 15%). However, the full functionalities of individual proteins are exerted through their associations and interactions with other proteins, many of which are transient and dynamic. The resulting complexity and conformational heterogeneity of protein complexes is difficult to study using conventional structural biology techniques, due to their demand for pure and highly homologous samples. Thus, there is a pressing need for the development of structural techniques better-suited to describe the dynamic qualities of protein-protein and protein-ligand interactions.

Chemical cross-linking coupled with mass spectrometry (XL-MS) has become a popularized and increasingly utilized component of the structural biologist's toolbox due to its speed, utility, and versatility. What began as an effort towards high-throughput, large-scale identification of protein-protein interactions has, in recent years, evolved into a hybrid structural strategy that permits queries into the composition, stoichiometries, and spatial arrangements of protein networks and assemblies recalcitrant to classical structural techniques [43, 163, 195]. In

this respect, XL-MS methodologies are particularly powerful and informative due to the layers of information that they can provide. Identifying protein-protein contacts through cross-linking confirms the three-dimensional proximity between participating proteins, implying that the distance between cross-linked residues can be constrained to a maximal length depending on the cross-linking reagent employed. These restraints serve as upper limits for distances between specific residues, which can be integrated for molecular modeling purposes. While not a true structural technique, the “peptide-level” resolution information yielded by XL-MS strategies are often highly complementary and supplementary to other existing methodologies. However, it is the versatility of XL-MS that truly sets the approach apart from other structural techniques. Unlike conventional structural biology tools, cross-linking can be applied towards the study of protein complexes in their native or near-native environments. Furthermore, XL-MS is adept at handling conformational and compositional heterogeneity of dynamic complexes, providing an ensemble of information reflecting the average state of protein complex conformations and interactions. This characteristic naturally beckons the question of whether XL-MS strategies can be used to correlate the conformational dynamics of protein-protein interactions to their biological functions.

Quantitative XL-MS (QXL-MS) effectively extends the capability of these strategies to compare the occurrences of cross-links across experimental conditions and biological states. These quantitative values reflect the structural changes in protein assemblies in response to various forms of stimuli, thereby providing insight on the dynamics of protein conformations, interactions, and compositions. While other methodologies such as hydrogen/deuterium exchange, covalent label or radical foot-printing, and ion-mobility MS have shown the ability to deliver quantitative information on the structural changes within protein assemblies, these

approaches are generally limited to identifying and localizing regions of change, but unable to interpret the extent, directionality, or nature of those perturbations. These techniques are commonly used to study variations in protein complex structures between native (i.e. wild-type, apo, un-treated, healthy) and affected (i.e. mutated, ligand-bound, PTM-modified, diseased) conformations, but individual samples are prepared and analyzed independently, which can be time-consuming and heavily dependent on reproducible instrumentation conditions. From an experimental standpoint, QXL-MS strategies relying on synthetic or metabolic incorporation of isotopic labels permit the simultaneous analysis of protein-protein interactions under multiple conditions, reducing the time requirement for analyses while minimizing experimental variabilities. Furthermore, QXL-MS yields structural information that not only identifies perturbed residues but additionally provides insight on how neighboring regions or tertiary structures are affected. Recent applications of QXL-MS have successfully identified conformational dynamics of protein complexes and protein-protein interactions *in vitro* (Schmidt, 2013; Yu, 2014; Chen, 2016; Tan, 2016) and *in vivo* (Wu, 2015; Chavez, 2016), highlighting the versatility of the approach.

Chapter 2 of this dissertation details the rationale and development of a pair of MS-cleavable cross-linking reagents designed for quantitative cross-linking analyses [88]. These DSSO derivatives, d_0- and d_{10}-DMDSSO, carry the robust functionality exhibited by DSSO that permits reliable and characteristic fragmentation of the cross-linker in CID (i.e. the central sulfoxide functional group)—while incorporating alkyl moieties that enable the synthesis of an isotopic variant containing easily-substituted deuteriums into the spacer arm. The characteristic cleavage of cross-linked peptides at the MS^2 level and subsequent fragmentation of individual peptides carrying cross-linker remnant moieties in MS^3 were analyzed and compared to the

patterns yielded by DSSO-cross-linked peptides and proteins. Those results indicated that the MS^n fragmentation patterns occurred as expected, despite the alterations in chemical design in DMDSSO compared to DSSO. Furthermore, in a proof-of-principle study, we showed that the ion intensity ratios of d_0- and d_{10}-DMDSSO cross-linked peptides accurately reflected their actual relative concentrations in cross-linked peptide sample mixtures [88]. Although these relative concentrations were created through the controlled mixing of individually cross-linked proteins, these tests showed that variations in cross-link abundances that occur because of differential protein conformations could be identified and accurately measured using these reagents. These observations effectively set the stage for us to utilize d_0- and d_{10}-DMDSSO to tackle real-world biological questions of protein conformational dynamics and their associated impacts on protein complex function.

In chapter 3, a pair-wise QXL-MS strategy using d0/d10-DMDSSO was successfully employed to study the Nedd8-dependendent activation of SCF ligases. This set of experiments was important in that it served a dual-purpose: the first, to show that QXL-MS strategies could be used to prove or confirm theories of conformational dynamics that were difficult to study using conventional biophysical structure techniques; the second, to show that QXL-MS strategies could be utilized to probe for unknown conformational differences in protein complex topologies that attributed to variational phenotypes, such as loss- or gain-of-function. Post-translational modification of cullin-RING ligases by a ubiquitin-like protein Nedd8 is essential for the full enzymatic activity of CRL E3s. However, this interaction is difficult to study using conventional means due to the conformational and compositional heterogeneity of CRLs, particularly in the case of neddylated Cul1 [170]. At the time, it was postulated and widely accepted that Nedd8 modification of a specific residue Lys720 of Cul1 induced a distinct structural reorganization of

the SCF catalytic core that resulted in the ejection of the RING domain of Rbx1 from a hydrophobic of Cul1 [157]. In this state, Rbx1 was free to sample the three-dimensional space around the $Cul1^{CTD}$, but remaining tethered to Cul1 by its N-terminal tail. This conferred flexibility was speculated to facilitate the interaction between ubiquitin-bound E2s recruited by Rbx1 to the protein substrates recruited by adapter proteins associating with the N-terminal domain of Cul1. However, proof of this state was difficult to obtain, as the structure of neddylated Cul1 remained recalcitrant to crystallographic methods for over a decade. During that time, a publication on a $Cul5^{CTD}$ complex with Rbx1 and Nedd8 did capture two potential states of Rbx1 following Cul5 neddylation, although the crystal lattices obtained depicted awkward placements for Rbx1 in relation to Cul5 [157, 196]. Despite the high degree of conservation and identity shared by Cul1 and Cul5, however, it still remained to be proven whether neddylation of Cul1 affected Rbx1 in the same manner as was observed for Cul5.

Using d_0- and d_{10}-DMDSSO, we probed the topologies of unneddylated and neddylated Cul1-Rbx1, observing similarities and differences in their ensembles of cross-linking data to identify the conformational dynamics associated with Nedd8-conjugation of Cul1. Although several regions of Cul1 seemed to be marginally impacted or not impacted at all by Nedd8 conjugation, there were also several structural domains that exhibited distinct conformational perturbations after Cul1 neddylation. In particular, these regions also shared cross-links with Rbx1, identifying their proximity to the RING domain following neddylation, but not prior. Among the cross-links identified, several cross-links between Cul1 and Rbx1 would have been otherwise too distant to be cross-linked in the unneddylated complex. These results led us to believe that the flexibility of Rbx1 in the open-state allowed its RING domain to sample lysines in the Cul1 C-terminal domain that would have not been possible without the influence of Nedd8.

We also observed distinct intra-subunit Cul1 cross-links that were enabled or prevented as a result of neddylation, allowing us to conclude that Rbx1 ejection most likely results from a series of internal reorientations beginning at the neddylation site. In addition, the structural change of Rbx1 in the CRL complex has the net effect of displacing secondary structural elements that stabilize the Cul1-Rbx1 interaction in its unneddylated form.

Our foray into the unknown using this QXL-MS strategy was the investigation of the structural dynamics associated with SCF inactivation due to a specific glutamine (Gln40) deamidation on wild-type Nedd8 imparted by certain bacterial cycle-inhibiting factors (Cifs) [90]. We modeled this mutant-neddylated Cul1-Rbx1 using a Nedd8 construct with a Q40E mutation, which changed Gln40 to Glu40. In a similar manner to our studies comparing the effect of neddylation on the structure of Cul1-Rbx1, we examined the differences in Cul1-Rbx1 topology that occurred as a result of wild-type compared to mutant Nedd8 conjugation. During these experiments, we observed a distinct reversal in cross-link abundance variations by mutant Nedd8 compared to those induced by wild-type neddylation. In general, we found that the structure of mutant Nedd8~Cul1-Rbx1 described by cross-linking data was nearly identical to the ensemble described by unneddylated Cul1-Rbx1. Furthermore, we also determined that the predominant cross-links detected between Nedd8 and Cul1 were distinctly unique in wild-type- and mutant-neddylated Cul1-Rbx1. Due to the limitation of current integrative modeling platforms to utilize quantitative cross-linking data, we were unable to procure structural models for the two forms of neddylated Cul1-Rbx1. Nevertheless, we were able to describe the overall conformational dynamics based on the individual linkages. Our results have allowed us to conclude that Q40E-Nedd8~Cul1-Rbx1 did not induce the same structural reconfiguration of Cul1-Rbx1 as wild-type Nedd8, resulting in the inactivation of the SCF [90]. These results show that QXL-MS strategies

can be utilized to probe for the structural bases of protein complexes that underlie disparities in functional phenotypes, even without prior knowledge on conformational details. These results have spurred us to focus on the development of quantitative cross-linking strategies to increase the throughput and scope of studies that can be analyzed using such strategies.

Chapter 4 describes the development of QMIX, a platform for the Quantitation of Multiplexed, Isobaric-labeled Cross (X)-linked Peptides [91]. Our primary initiative for the development of a multiplexed strategy for cross-linking studies was to enable simultaneous comparison of more than two protein structural states. This would increase throughput, decreasing the time spent running MS analysis, while also removing opportunities for technical variation due to instrumentation conditions. However, attempting to multiplex cross-linking studies using conventional isotope label strategies would prove to be problematic—both in terms of the synthesis of cross-linking reagents, as well as the combinations of heavy isotopes necessary for metabolic labeling. Furthermore, the resulting increase in spectral complexity associated with the incorporation of multiple sets of isotopic labels would negatively impact the identification of cross-linked peptides, making conventional approaches ill-suited for comparative structural studies on more than two, or at most three, protein complexes. The advent of isobaric labeling reagents such as DiLeu [197] and Tandem Mass Tags [198] revolutionized quantitative proteomics, permitting the simultaneous analysis of multiple samples without increasing the spectral complexity of MS analysis. This was achieved through the usage of isotopomeric labeling reagents, that is, isobaric labeling reagents that share the same mass and chemical structure, but varying in the positions of isotopic atoms. These reagents are designed such that the same peptide labeled with different isobaric labels are chemically identical, not only co-eluting perfectly chromatographically, but contributing to the detection of the same ion

peak at the MS^1 level. In subsequent stages of MS^2 or MS^3, HCD fragmentation can be utilized to cleave the labels, which results in the yield of an individual unique reporter ion for each isobaric reagent. Therefore, the quantitation of ions is conducted at the MS^n level, which has the added advantages of maintaining the sample complexity and also decreasing the interference by similar mass ions on the abundance ratios of peptides during MS analysis. Because TMT reporter ions are detected most cleanly at the MS^3 level [183] and that our MS-cleavable cross-linking workflow utilizes MS^n peptide sequencing of cross-linked peptides [50, 86, 90], we hypothesized that the two strategies could be efficiently integrated to allow multiplexed quantitative cross-linking studies. To this end, we developed a methodology utilizing DSSO in conjunction with the TMT labeling reagents commercialized by Thermo Fisher. In a fashion similar to our previous experiments characterizing DMDSSO, we showed that TMT-labeling of cross-linked peptides did not interfere with the cross-linker fragmentation at MS^2, nor the peptide sequencing at MS^3. Although TMT-labeling did seem to increase the abundance of sulfenic-modified compared to thiol-modified peptides in MS^2, it did not impact the identification process as both sulfenic- and thiol-modified peptides are equally suited for identification. Similarly, we also showed that quantitation of reporter ions at the MS^3 level accurately reflected the relative concentrations of cross-linked peptides in solution. During this time we also experimented with various acquisition methodologies on the state-of-the-art mass spectrometer, i.e., the Orbitrap Fusion Lumos Tribrid MS (Thermo Fisher Scientific), which allowed us to identify and quantify cross-linked peptides with significantly improved efficiency and accuracy. Our success at developing a platform for multiplexed QXL-MS studies [91] enabled us to attempt more comprehensive analyses of CRL E3 assemblies.

Due to the role of targeted degradation by the ubiquitin-proteasome system in regulating nearly all of the diverse biological processes of the cell, E3 complexes represent one of the most highly sought-out targets for the development of therapeutic treatments to combat proteasomal dysregulation. Proteasomal hyperactivity has been associated with a range of human diseases, but particularly in malignancies such as multiple myeloma and mantle cell lymphoma. Proteasome inhibitors such as bortezomib and carfilzomib have shown clinical success in the treatment of such neoplasms; however, targeting of other types of cancers appears to be out of the realm for proteasome inhibitors. This has been hypothesized to be a result of the dose-limiting toxicity of proteasome inhibitors to normal cells, as solid tumors often require larger dosages compared to the treatment of hematopoietic cancers. As an alternative means to targeting aggressive degradation by the UPS, the enzymes responsible for the selective ubiquitination of substrates—in particular, E3 ligases and their associated proteins—have been targets of immense research as of late in order to identify small molecule inhibitors that would selectively prevent the ubiquitination of specific subset of proteins, presumably reducing the occurrence of undesired side-effects associated with general proteasome inhibition. However, the current *modus operandi* for the development of these pharmacological inhibitors typically involves assaying the effect of newly synthesized derivatives against specific pathologies, such as cancer cell proliferation. Usually, only those that show an inhibitory effect are pursued for further research.

We hypothesize that quantitative cross-linking can be utilized to probe for small molecule-induced conformational changes, providing insight on the structural qualities of protein complexes that may be capitalized on for future therapeutic development. To this end, we aim to examine the structural effects associated with CC0651 inhibition of Cdc34 that blocks the

transfer of Ub from E2 to E3-bound substrate. Through these studies we were able to examine the conformational details describing the Cdc34-Cul1-Rbx1 interaction, as well as the topological influences of PTMs and ligand-binding. However, the culmination of QXL-MS data, i.e., structural models delineating the structures of the E2-E3 intermediate at various stages of interaction, remains elusive. While cross-linking strategies in general are becoming more widely accepted, QXL-MS is still ultimately in its infancy and is currently hampered by the lack of software and modeling tools to properly utilize the wealth of data that it can provide.

Although our focus here is the understanding of the enzymatic machinery responsible for selective ubiquitination of proteins, quantitative cross-linking constitutes a versatile strategy that can be utilized to study protein-protein interactions at a speed that is unmatched by other structural approaches. While XL-MS-based methods will likely never replace existing structure determination tools such as cryo-EM and x-ray crystallography, its impact is largest when used in conjunction with other static discovery tools. Its capability to provide supplementary insight on the structural dynamics of protein-protein interactions as they occur within the cell and in near-native environments is a unique contribution that no other current structural technique—traditional or hybrid—can provide, making it an invaluable asset of the structural biologist's arsenal. Half a decade ago, before the prodigious rise of XL-MS to its current prominence, we were confident in its ability to contribute a unique set of structural information that other techniques were unable to provide. Quantitative cross-linking is simply the next step in its evolution towards the common goal of a comprehensive understanding of protein-protein interactions. The development of a multiplexed QXL-MS strategy that permits simultaneous comparative analysis of protein complexes in multiple biological states is a significant

contribution to the structural biology field, and we believe it will be utilized in the future for its potential to determine previously unidentified targets for therapeutic intervention.

Bibliography

1. Alberts, B., *The Cell as a collection of protein machines:preparing the next generation of molecular biologists.* Cell, 1998. **92**: p. 291-294.
2. Nooren, I.M. and J.M. Thornton, *Structural characterisation and functional significance of transient protein-protein interactions.* J Mol Biol, 2003. **325**(5): p. 991-1018.
3. Perkins, J.R., et al., *Transient protein-protein interactions: structural, functional, and network properties.* Structure, 2010. **18**(10): p. 1233-43.
4. Moll, U.M. and O. Petrenko, *The MDM2-p53 interaction.* Mol Cancer Res, 2003. **1**(14): p. 1001-8.
5. Poirier, M.A., H. Jiang, and C.A. Ross, *A structure-based analysis of huntingtin mutant polyglutamine aggregation and toxicity: evidence for a compact beta-sheet structure.* Hum Mol Genet, 2005. **14**(6): p. 765-74.
6. Lim, J., et al., *A protein-protein interaction network for human inherited ataxias and disorders of Purkinje cell degeneration.* Cell, 2006. **125**(4): p. 801-14.
7. Charbonnier, S., O. Gallego, and A.C. Gavin, *The social network of a cell: recent advances in interactome mapping.* Biotechnol Annu Rev, 2008. **14**: p. 1-28.
8. Barabasi, A.L., N. Gulbahce, and J. Loscalzo, *Network medicine: a network-based approach to human disease.* Nat Rev Genet, 2011. **12**(1): p. 56-68.
9. Wells, J.A. and C.L. McClendon, *Reaching for high-hanging fruit in drug discovery at protein-protein interfaces.* Nature, 2007. **450**(7172): p. 1001-9.
10. Shangary, S., et al., *Temporal activation of p53 by a specific MDM2 inhibitor is selectively toxic to tumors and leads to complete tumor growth inhibition.* Proc Natl Acad Sci U S A, 2008. **105**(10): p. 3933-8.
11. Popowicz, G.M., et al., *Structures of low molecular weight inhibitors bound to MDMX and MDM2 reveal new approaches for p53-MDMX/MDM2 antagonist drug discovery.* Cell Cycle, 2010. **9**(6).
12. Basse, M.J., et al., *2P2Idb: a structural database dedicated to orthosteric modulation of.* Nucleic Acids Res, 2013. **41**(Database issue): p. D824-7.
13. Dubrez, L. and J. Berthelet, *IAP proteins as targets for drug development in oncology.* 2013. **6**: p. 1285-304.
14. Arkin, M.R., Y. Tang, and J.A. Wells, *Small-molecule inhibitors of protein-protein interactions: progressing towards the reality.* Chem Biol, 2014. **21**(9): p. 1102-14.
15. Coll, R.C., et al., *A small-molecule inhibitor of the NLRP3 inflammasome for the treatment of inflammatory diseases.* Nat Med, 2015. **21**(3): p. 248-55.
16. Rual, J.F., et al., *Towards a proteome-scale map of the human protein-protein interaction network.* Nature, 2005. **437**(7062): p. 1173-8.
17. Stelzl, U., et al., *A human protein-protein interaction network: a resource for annotating the proteome.* Cell, 2005. **122**(6): p. 957-68.
18. Ewing, R.M., et al., *Large-scale mapping of human protein-protein interactions by mass spectrometry.* Mol Syst Biol, 2007. **3**: p. 89.
19. Gingras, A.C., et al., *Analysis of protein complexes using mass spectrometry.* Nat Rev Mol Cell Biol, 2007. **8**(8): p. 645-54.
20. Sowa, M.E., et al., *Defining the human deubiquitinating enzyme interaction landscape.* Cell, 2009. **138**(2): p. 389-403.

21. Zheng, Y., et al., *Temporal regulation of EGF signalling networks by the scaffold protein Shc1.* Nature, 2013. **499**(7457): p. 166-71.
22. Gavin, A., et al., *Functional organization of the yeast proteome by systematic analysis of protein complexes.* Nature, 2002. **415**(6868): p. 141-7.
23. Krogan, N.J., et al., *Global landscape of protein complexes in the yeast Saccharomyces cerevisiae.* Nature, 2006. **440**(7084): p. 637-43.
24. Kuhner, S., et al., *Proteome organization in a genome-reduced bacterium.* Science, 2009. **326**(5957): p. 1235-40.
25. Guruharsha, K.G., *A Protein Complex Network of Drosophila melanogaster.* 2011. **147**(3): p. 690-703.
26. Rigaut, G., et al., *A generic protein purification method for protein complex characterization and proteome exploration.* Nat. Biotechnol., 1999. **17**(1030-1032).
27. Burckstummer, T., et al., *An efficient tandem affinity purification procedure for interaction proteomics in mammalian cells.* Nat Methods, 2006. **3**(12): p. 1013-9.
28. Wang, X., et al., *Mass spectrometric characterization of the affinity-purified human 26S proteasome complex.* Biochemistry, 2007. **46**(11): p. 3553-65.
29. Li, J., S.R. Powell, and X. Wang, *Enhancement of proteasome function by PA28α overexpression protects against oxidative stress.* Faseb J, 2011. **25**(3): p. 883-93.
30. Nogales, E., *The development of cryo-EM into a mainstream structural biology technique.* Nat Methods, 2016. **13**(1): p. 24-7.
31. Aebersold, R. and M. Mann, *Mass spectrometry-based proteomics.* Nature, 2003. **422**(6928): p. 198-207.
32. Glatter, T., et al., *An integrated workflow for charting the human interaction proteome: insights into the PP2A system.* Mol Syst Biol, 2009. **5**: p. 237.
33. Cox, J. and M. Mann, *Quantitative, high-resolution proteomics for data-driven systems biology.* Annu Rev Biochem, 2011. **80**: p. 273-99.
34. Heck, A.J., *Native mass spectrometry: a bridge between interactomics and structural biology.* Nat Methods, 2008. **5**(11): p. 927-33.
35. Lorenzen, K. and E. van Duijn, *Native mass spectrometry as a tool in structural biology.* Curr Protoc Protein Sci, 2010. **Chapter 17**: p. Unit17.12.
36. Zhang, J., et al., *Native Top-Down Mass Spectrometry for the Structural Characterization of Human Hemoglobin.* Eur J Mass Spectrom (Chichester, Eng), 2015. **21**(3): p. 221-31.
37. Konermann, L., J. Pan, and Y.H. Liu, *Hydrogen exchange mass spectrometry for studying protein structure and dynamics.* Chem Soc Rev, 2011. **40**(3): p. 1224-34.
38. Pirrone, G.F., *Applications of.* 2015. **87**(1): p. 99-118.
39. Fitzgerald, M.C. and G.M. West, *Painting proteins with covalent labels: what's in the picture?* J Am Soc Mass Spectrom, 2009. **20**(6): p. 1193-206.
40. Mendoza, V.L. and R.W. Vachet, *Probing Protein Structure by Amino Acid-Specific Covalent Labeling and Mass Spectrometry.* Mass Spectrom Rev, 2009. **28**(5): p. 785-815.
41. Leitner, A., et al., *Probing native protein structures by chemical cross-linking, mass spectrometry, and bioinformatics.* Mol Cell Proteomics, 2010. **9**(8): p. 1634-49.
42. Rappsilber, J., *The beginning of a beautiful friendship: cross-linking/mass spectrometry and modelling of proteins and multi-protein complexes.* J Struct Biol, 2011. **173**(3): p. 530-40.
43. Herzog, F., et al., *Structural probing of a protein phosphatase 2A network by chemical cross-linking and mass spectrometry.* Science, 2012. **337**(6100): p. 1348-52.

44. Orban, T., et al., *Conformational dynamics of activation for the pentameric complex of dimeric G protein-coupled receptor and heterotrimeric G protein.* Structure, 2012. **20**(5): p. 826-40.
45. Pan, Y., et al., *Conformational dynamics of a membrane transport protein probed by H/D exchange and covalent labeling: the glycerol facilitator.* J Mol Biol, 2012. **416**(3): p. 400-13.
46. Jones, L.M., et al., *Complementary MS methods assist conformational characterization of antibodies with altered S-S bonding networks.* J Am Soc Mass Spectrom, 2013. **24**(6): p. 835-45.
47. Serpa, J.J., et al., *Using multiple structural proteomics approaches for the characterization of prion proteins.* J Proteomics, 2013. **81**: p. 31-42.
48. Politis, A., et al., *A mass spectrometry-based hybrid method for structural modeling of protein complexes.* Nat Methods, 2014. **11**(4): p. 403-6.
49. Guerrero, C., et al., *An integrated mass spectrometry-based proteomic approach: quantitative analysis of tandem affinity-purified in vivo cross-linked protein complexes (QTAX) to decipher the 26 S proteasome-interacting network.* Mol Cell Proteomics, 2006. **5**(2): p. 366-78.
50. Kaake, R.M., et al., *A New In Vivo Cross-linking Mass Spectrometry Platform to Define Protein-Protein Interactions in Living Cells.* Mol Cell Proteomics, 2014. **pii: mcp.M114.042630.**
51. Liu, F., et al., *Proteome-wide profiling of protein assemblies by cross-linking mass spectrometry.* Nat Methods, 2015. **12**(12): p. 1179-84.
52. Fox, C.H., et al., *Formaldehyde fixation.* J Histochem Cytochem, 1985. **33**(8): p. 845-53.
53. Sutherland, B.W., J. Toews, and J. Kast, *Utility of formaldehyde cross-linking and mass spectrometry in the study of protein-protein interactions.* J Mass Spectrom, 2008. **43**(6): p. 699-715.
54. Hall, D.B. and K. Struhl, *The VP16 activation domain interacts with multiple transcriptional components as determined by protein-protein cross-linking in vivo.* J. Biol. Chem., 2002. **277**: p. 46043-46050.
55. Vasilescu, J., X. Guo, and J. Kast, *Identification of protein-protein interactions using in vivo cross-linking and mass spectrometry.* Proteomics, 2004. **4**: p. 3845-3854.
56. Schmitt-Ulms, G., et al., *Time-controlled transcardiac perfusion cross-linking for the study of protein interactions in complex tissues.* Nat Biotechnol., 2004. **22**(6): p. 724-31.
57. Bai, Y., et al., *The in vivo brain interactome of the amyloid precursor protein.* Mol Cell Proteomics, 2008. **7**(1): p. 15-34.
58. Yu, C., et al., *Characterization of Dynamic UbR-Proteasome Subcomplexes by In vivo Cross-linking (X) Assisted Bimolecular Tandem Affinity Purification (XBAP) and Label-free Quantitation.* Mol Cell Proteomics, 2016. **15**(7): p. 2279-92.
59. Tagwerker, C., et al., *A tandem affinity tag for two-step purification under fully denaturing conditions: application in ubiquitin profiling and protein complex identification combined with in vivocross-linking.* Mol Cell Proteomics, 2006. **5**(4): p. 737-48.
60. Guerrero, C., et al., *Characterization of the proteasome interaction network using a QTAX-based tag-team strategy and protein interaction network analysis.* Proc Natl Acad Sci U S A, 2008. **105**(36): p. 13333-8.

61. Young, M.M., et al., *High throughput protein fold identification by using experimental constraints derived from intramolecular cross-links and mass spectrometry.* Proc Natl Acad Sci U S A., 2000. **97**(11): p. 5802-6.
62. Trnka, M.J. and A.L. Burlingame, *Topographic studies of the GroEL-GroES chaperonin complex by chemical cross-linking using diformyl ethynylbenzene: the power of high resolution electron transfer dissociation for determination of both peptide sequences and their attachment sites.* Mol Cell Proteomics, 2010. **9**(10): p. 2306-17.
63. Lasker, K., et al., *Molecular architecture of the 26S proteasome holocomplex determined by an integrative approach.* Proc Natl Acad Sci U S A, 2012. **109**(5): p. 1380-7.
64. Webb, B., et al., *Modeling of proteins and their assemblies with the Integrative Modeling Platform.* Methods Mol Biol, 2014. **1091**: p. 277-95.
65. Wang, X., et al., *Molecular Details Underlying Dynamic Structures and Regulation of the Human 26S Proteasome.* Mol Cell Proteomics, 2017. **16**(5): p. 840-854.
66. Chavez, J.D., et al., *Protein interactions, post-translational modifications and topologies in human cells.* Mol Cell Proteomics, 2013. **12**(5): p. 1451-67.
67. Chavez, J.D., et al., *Quantitative interactome analysis reveals a chemoresistant edgotype.* Nat Commun, 2015. **6**: p. 7928.
68. Kalkhof, S. and A. Sinz, *Chances and pitfalls of chemical cross-linking with amine-reactive N-hydroxysuccinimide esters.* Anal Bioanal Chem, 2008. **392**(1-2): p. 305-12.
69. Madler, S., et al., *Chemical cross-linking with NHS esters: a systematic study on amino acid reactivities.* J Mass Spectrom, 2009. **44**(5): p. 694-706.
70. Soskine, M., S. Steiner-Mordoch, and S. Schuldiner, *Crosslinking of membrane-embedded cysteines reveals contact points in the EmrE oligomer.* Proc Natl Acad Sci U S A, 2002. **99**(19): p. 12043-8.
71. Auclair, J.R., et al., *Strategies for stabilizing superoxide dismutase (SOD1), the protein destabilized in the most common form of familial amyotrophic lateral sclerosis.* Proc Natl Acad Sci U S A, 2010. **107**(50): p. 21394-9.
72. Leitner, A., et al., *Chemical cross-linking/mass spectrometry targeting acidic residues in proteins and protein complexes.* Proc Natl Acad Sci U S A, 2014. **111**(26): p. 9455-60.
73. Gutierrez, C.B., et al., *Developing an Acidic Residue Reactive and Sulfoxide-Containing MS-Cleavable Homobifunctional Cross-Linker for Probing Protein-Protein Interactions.* Anal Chem, 2016.
74. Gomes, A.F. and F.C. Gozzo, *Chemical cross-linking with a diazirine photoactivatable cross-linker investigated by MALDI- and ESI-MS/MS.* J Mass Spectrom, 2010. **45**(8): p. 892-9.
75. Koulov, A.V., et al., *Biological and structural basis for Aha1 regulation of Hsp90 ATPase activity in maintaining proteostasis in the human disease cystic fibrosis.* Mol Biol Cell, 2010. **21**(6): p. 871-84.
76. Tang, X. and J.E. Bruce, *A new cross-linking strategy: protein interaction reporter (PIR) technology for protein-protein interaction studies.* Mol Biosyst, 2010. **6**(6): p. 939-47.
77. Tan, D., et al., *Trifunctional cross-linker for mapping protein-protein interaction networks and comparing protein conformational states.* Elife, 2016. **5**.
78. Chowdhury, S.M., et al., *Identification of Crosslinked Peptides after Click-based Enrichment Using Sequential CID and ETD Tandem Mass Spectrometry.* Anal Chem, 2009. **81**(13): p. 5524-32.

79. Muller, D.R., et al., *Isotope-tagged cross-linking reagents, a new tool in mass spectrometric protein interaction analysis.* Anal. Chem., 2001. **73**(1927-1934).
80. Back, J.W., et al., *Identification of cross-linked peptides for protein interaction studies using mass spectrometry and 18O labeling.* Anal Chem., 2002. **74**(17): p. 4417-22.
81. Seebacher, J., et al., *Protein cross-linking analysis using mass spectrometry, isotope-coded cross-linkers, and integrated computational data processing.* J Proteome Res, 2006. **5**(9): p. 2270-82.
82. Rinner, O., et al., *Identification of cross-linked peptides from large sequence databases.* Nat Methods, 2008. **5**(4): p. 315-8.
83. Petrotchenko, E. and C. Borchers, *ICC-CLASS: isotopically-coded cleavable crosslinking analysis software suite.* BMC bioinformatics, 2010. **11**(1): p. 64.
84. Yang, B., et al., *Identification of cross-linked peptides from complex samples.* Nat Methods, 2012. **9**(9): p. 904-6.
85. Tang, X., et al., *Mass spectrometry identifiable cross-linking strategy for studying protein-protein interactions.* Anal Chem, 2005. **77**(1): p. 311-8.
86. Kao, A., et al., *Development of a novel cross-linking strategy for fast and accurate identification of cross-linked peptides of protein complexes.* Mol Cell Proteomics, 2011. **10**(1): p. M110.002212.
87. Petrotchenko, E.V., J.J. Serpa, and C.H. Borchers, *An isotopically coded CID-cleavable biotinylated cross-linker for structural proteomics.* Mol Cell Proteomics, 2011. **10**(2): p. M110.001420.
88. Yu, C., et al., *Developing new isotope-coded mass spectrometry-cleavable cross-linkers for elucidating protein structures.* Anal Chem, 2014. **86**(4): p. 2099-106.
89. Kao, A., et al., *Mapping the structural topology of the yeast 19S proteasomal regulatory particle using chemical cross-linking and probabilistic modeling.* Mol Cell Proteomics, 2012. **11**(12): p. 1566-77.
90. Yu, C., et al., *Gln40 deamidation blocks structural reconfiguration and activation of SCF ubiquitin ligase complex by Nedd8.* Nat Commun, 2015. **6**: p. 10053.
91. Yu, C., et al., *Developing a Multiplexed Quantitative Cross-Linking Mass Spectrometry Platform for Comparative Structural Analysis of Protein Complexes.* Anal Chem, 2016. **88**(20): p. 10301-10308.
92. Dettmer, U., et al., *In vivo cross-linking reveals principally oligomeric forms of alpha-synuclein and beta-synuclein in neurons and non-neural cells.* J Biol Chem, 2013. **288**(9): p. 6371-85.
93. Hershko, A. and A. Ciechanover, *The ubiquitin system.* Annu Rev Biochem., 1998. **67**: p. 425-79.
94. Kerscher, O., R. Felberbaum, and M. Hochstrasser, *Modification of Proteins by Ubiquitin and Ubiquitin-Like Proteins.* Annu Rev Cell Dev Biol, 2006.
95. Kageshita, T., et al., *Down-regulation of HLA class I antigen-processing molecules in malignant melanoma: association with disease progression.* Am J Pathol, 1999. **154**(3): p. 745-54.
96. McNaught, K.S. and P. Jenner, *Proteasomal function is impaired in substantia nigra in Parkinson's disease.* Neurosci Lett, 2001. **297**(3): p. 191-4.
97. Oh, S., et al., *Amyloid peptide attenuates the proteasome activity in neuronal cells.* Mech Ageing Dev, 2005. **126**(12): p. 1292-9.

98. Cavo, M., *Proteasome inhibitor bortezomib for the treatment of multiple myeloma.* Leukemia, 2006. **20**(8): p. 1341-52.
99. Krause, S., et al., *Immunoproteasome subunit LMP2 expression is deregulated in Sjogren's syndrome but not in other autoimmune disorders.* Ann Rheum Dis, 2006. **65**(8): p. 1021-7.
100. Hershko, A. and A. Ciechanover, *The ubiquitin system for protein degradation.* Annu Rev Biochem, 1992. **61**: p. 761-807.
101. Scheffner, M., U. Nuber, and J.M. Huibregtse, *Protein ubiquitination involving an E1-E2-E3 enzyme ubiquitin thioester cascade.* Nature, 1995. **373**(6509): p. 81-3.
102. Haas, A.L., et al., *Ubiquitin-activating enzyme. Mechanism and role in protein-ubiquitin conjugation.* J Biol Chem, 1982. **257**(5): p. 2543-8.
103. Hershko, A., et al., *Components of ubiquitin-protein ligase system. Resolution, affinity purification, and role in protein breakdown.* J Biol Chem, 1983. **258**(13): p. 8206-14.
104. Pickart, C.M. and I.A. Rose, *Functional heterogeneity of ubiquitin carrier proteins.* J Biol Chem, 1985. **260**(3): p. 1573-81.
105. Peng, J., et al., *A proteomics approach to understanding protein ubiquitination.* Nat Biotechnol, 2003. **21**(8): p. 921-6.
106. Pickart, C.M. and M.J. Eddins, *Ubiquitin: structures, functions, mechanisms.* Biochim Biophys Acta, 2004. **1695**(1-3): p. 55-72.
107. Bremm, A. and D. Komander, *Emerging roles for Lys11-linked polyubiquitin in cellular regulation.* Trends Biochem Sci, 2011. **36**(7): p. 355-63.
108. Jura, N., et al., *Differential modification of Ras proteins by ubiquitination.* Mol Cell, 2006. **21**(5): p. 679-87.
109. Wang, X., et al., *Ubiquitination of tumor necrosis factor receptor-associated factor 4 (TRAF4) by Smad ubiquitination regulatory factor 1 (Smurf1) regulates motility of breast epithelial and cancer cells.* J Biol Chem, 2013. **288**(30): p. 21784-92.
110. Chastagner, P., A. Israel, and C. Brou, *Itch/AIP4 mediates Deltex degradation through the formation of K29-linked polyubiquitin chains.* EMBO Rep, 2006. **7**(11): p. 1147-53.
111. Zhang, Z., et al., *Ter94 ATPase complex targets k11-linked ubiquitinated ci to proteasomes for partial degradation.* Dev Cell, 2013. **25**(6): p. 636-44.
112. Dammer, E.B., et al., *Polyubiquitin linkage profiles in three models of proteolytic stress suggest the etiology of Alzheimer disease.* J Biol Chem, 2011. **286**(12): p. 10457-65.
113. Voges, D., P. Zwickl, and W. Baumeister, *The 26S proteasome: a molecular machine designed for controlled proteolysis.* Annu Rev Biochem., 1999. **68**: p. 1015-68.
114. Finley, D., *Recognition and processing of ubiquitin-protein conjugates by the proteasome.* Annu Rev Biochem, 2009. **78**: p. 477-513.
115. Löwe, J., et al., *Crystal structure of the 20S proteasome from the archaeon T. acidophilum at 3.4 Å resolution.* Science, 1995. **268**: p. 533-539.
116. Groll, M., et al., *Structure of 20S proteasome from yeast at 2.4 A resolution.* Nature, 1997. **386**(6624): p. 463-71.
117. Glickman, M.H., et al., *A subcomplex of the proteasome regulatory particle required for ubiquitin-conjugate degradation and related to the COP9-signalosome and eIF3.* Cell, 1998. **94**(5): p. 615-23.
118. Lander, G.C., et al., *Complete subunit architecture of the proteasome regulatory particle.* Nature, 2012. **482**(7384): p. 186-91.

119. Huang, X., et al., *An atomic structure of the human 26S proteasome.* Nat Struct Mol Biol, 2016. **23**(9): p. 778-85.
120. Schweitzer, A., et al., *Structure of the human 26S proteasome at a resolution of 3.9 A.* Proc Natl Acad Sci U S A, 2016. **113**(28): p. 7816-21.
121. Sohn, D., et al., *The proteasome is required for rapid initiation of death receptor-induced apoptosis.* Mol Cell Biol, 2006. **26**(5): p. 1967-78.
122. Li, L., et al., *Overactivated neddylation pathway as a therapeutic target in lung cancer.* J Natl Cancer Inst, 2014. **106**(6): p. dju083.
123. Cheng, F., et al., *Expression of neddylation-related proteins in melanoma cell lines and the effect of neddylation on melanoma proliferation.* Oncol Lett, 2014. **7**(5): p. 1645-1650.
124. Kisselev, A.F., W.A. van der Linden, and H.S. Overkleeft, *Proteasome inhibitors: an expanding army attacking a unique target.* Chem Biol, 2012. **19**(1): p. 99-115.
125. Richardson, K.S. and W. Zundel, *The emerging role of the COP9 signalosome in cancer.* Mol Cancer Res, 2005. **3**(12): p. 645-53.
126. Argyriou, A.A., G. Iconomou, and H.P. Kalofonos, *Bortezomib-induced peripheral neuropathy in multiple myeloma: a comprehensive review of the literature.* Blood, 2008. **112**(5): p. 1593-9.
127. Nowis, D., et al., *Cardiotoxicity of the anticancer therapeutic agent bortezomib.* Am J Pathol, 2010. **176**(6): p. 2658-68.
128. Bulatov, E. and A. Ciulli, *Targeting Cullin–RING E3 ubiquitin ligases for drug discovery: structure, assembly and small-molecule modulation.* Biochem J, 2015. **467**(Pt 3): p. 365-86.
129. Nakayama, K.I. and K. Nakayama, *Ubiquitin ligases: cell-cycle control and cancer.* Nat Rev Cancer, 2006. **6**(5): p. 369-81.
130. Scheffner, M. and S. Kumar, *Mammalian HECT ubiquitin-protein ligases: biological and pathophysiological aspects.* Biochim Biophys Acta, 2014. **1843**(1): p. 61-74.
131. Metzger, M.B., et al., *RING-type E3 ligases: master manipulators of E2 ubiquitin-conjugating enzymes and ubiquitination.* Biochim Biophys Acta, 2014. **1843**(1): p. 47-60.
132. Spratt, D.E., H. Walden, and G.S. Shaw, *RBR E3 ubiquitin ligases: new structures, new insights, new questions.* Biochem J, 2014. **458**(3): p. 421-37.
133. Deshaies, R.J. and C.A. Joazeiro, *RING domain E3 ubiquitin ligases.* Annu Rev Biochem, 2009. **78**: p. 399-434.
134. Petroski, M.D. and R.J. Deshaies, *Function and regulation of cullin-RING ubiquitin ligases.* Nat Rev Mol Cell Biol, 2005. **6**(1): p. 9-20.
135. Frescas, D. and M. Pagano, *Deregulated proteolysis by the F-box proteins SKP2 and beta-TrCP: tipping the scales of cancer.* Nat Rev Cancer, 2008. **8**(6): p. 438-49.
136. Nalepa, G., M. Rolfe, and J.W. Harper, *Drug discovery in the ubiquitin-proteasome system.* Nat Rev Drug Discov, 2006. **5**(7): p. 596-613.
137. Petroski, M.D., *The ubiquitin system, disease, and drug discovery.* BMC Biochem, 2008. **9 Suppl 1**: p. S7.
138. Bedford, L., et al., *Ubiquitin-like protein conjugation and the ubiquitin-proteasome system as drug targets.* Nat Rev Drug Discov, 2011. **10**(1): p. 29-46.
139. Fang, L., et al., *Mapping the Protein Interaction Network of the Human COP9 Signalosome Complex Using a Label-free QTAX Strategy.* Mol Cell Proteomics, 2012. **11**(5): p. 138-47.

140. Kalisman, N., C.M. Adams, and M. Levitt, *Subunit order of eukaryotic TRiC/CCT chaperonin by cross-linking, mass spectrometry, and combinatorial homology modeling.* Proc Natl Acad Sci U S A, 2012. **109**(8): p. 2884-9.
141. Chu, F., et al., *Isotope-coded and affinity-tagged cross-linking (ICATXL): an efficient strategy to probe protein interaction surfaces.* J Am Chem Soc, 2006. **128**(32): p. 10362-3.
142. Krauth, F., et al., *Heterobifunctional isotope-labeled amine-reactive photo-cross-linker for structural investigation of proteins by matrix-assisted laser desorption/ionization tandem time-of-flight and electrospray ionization LTQ-Orbitrap mass spectrometry.* Rapid Commun Mass Spectrom, 2009. **23**(17): p. 2811-8.
143. Chu, F., et al., *Identification of novel quaternary domain interactions in the Hsp90 chaperone, GRP94.* Protein Sci, 2006. **15**(6): p. 1260-9.
144. Singh, P., et al., *Characterization of protein cross-links via mass spectrometry and an open-modification search strategy.* Anal Chem, 2008. **80**(22): p. 8799-806.
145. Soderblom, E.J. and M.B. Goshe, *Collision-induced dissociative chemical cross-linking reagents and methodology: Applications to protein structural characterization using tandem mass spectrometry analysis.* Anal Chem, 2006. **78**(23): p. 8059-68.
146. Lu, Y., et al., *Ionic reagent for controlling the gas-phase fragmentation reactions of cross-linked peptides.* Anal Chem, 2008. **80**(23): p. 9279-87.
147. Leonard, N.M. and J. Brunckova, *In situ formation of N-trifluoroacetoxy succinimide (TFA-NHS): one-pot formation of succinimidyl esters, N-trifluoroacetyl amino acid succinimidyl esters, and N-maleoyl amino acid succinimidyl esters.* J Org Chem, 2011. **76**(21): p. 9169-74.
148. Zimmerman, E.S., B.A. Schulman, and N. Zheng, *Structural assembly of cullin-RING ubiquitin ligase complexes.* Curr Opin Struct Biol, 2010. **20**(6): p. 714-21.
149. Sarikas, A., T. Hartmann, and Z.Q. Pan, *The cullin protein family.* Genome Biol, 2011. **12**(4): p. 220.
150. Duda, D.M., et al., *Structural regulation of cullin-RING ubiquitin ligase complexes.* Curr Opin Struct Biol, 2011. **21**(2): p. 257-64.
151. Deshaies, R.J., *SCF and Cullin/Ring H2-Based Ubiquitin Ligases.* Annu. Rev. Cell Dev. Biol., 1999. **15**: p. 435-67.
152. Cardozo, T. and M. Pagano, *The SCF ubiquitin ligase: insights into a molecular machine.* Nat Rev Mol Cell Biol, 2004. **5**(9): p. 739-51.
153. Zheng, N., et al., *Structure of a c-Cbl-UbcH7 complex: RING domain function in ubiquitin-protein ligases.* Cell, 2000. **102**(4): p. 533-9.
154. Podust, V.N., et al., *A Nedd8 conjugation pathway is essential for proteolytic targeting of p27Kip1 by ubiquitination.* Proc Natl Acad Sci U S A, 2000. **97**(9): p. 4579-84.
155. Read, M.A., et al., *Nedd8 modification of cul-1 activates SCF(beta(TrCP))-dependent ubiquitination of IkappaBalpha.* Mol Cell Biol, 2000. **20**(7): p. 2326-33.
156. Yu, H., et al., *High-quality binary protein interaction map of the yeast interactome network.* Science, 2008. **322**(5898): p. 104-10.
157. Duda, D.M., et al., *Structural insights into NEDD8 activation of cullin-RING ligases: conformational control of conjugation.* Cell, 2008. **134**(6): p. 995-1006.
158. Cui, J., et al., *Glutamine deamidation and dysfunction of ubiquitin/NEDD8 induced by a bacterial effector family.* Science, 2010. **329**(5996): p. 1215-8.

159. Jubelin, G., et al., *Pathogenic bacteria target NEDD8-conjugated cullins to hijack host-cell signaling pathways.* PLoS Pathog, 2010. **6**(9): p. e1001128.
160. Morikawa, H., et al., *The bacterial effector Cif interferes with SCF ubiquitin ligase function by inhibiting deneddylation of Cullin1.* Biochem Biophys Res Commun, 2010. **401**(2): p. 268-74.
161. Toro, T.B., J.I. Toth, and M.D. Petroski, *The cyclomodulin cycle inhibiting factor (CIF) alters cullin neddylation dynamics.* J Biol Chem, 2013. **288**(21): p. 14716-26.
162. Chen, X., et al., *Structure of proteasome ubiquitin receptor hRpn13 and its activation by the scaffolding protein hRpn2.* Mol Cell, 2010. **38**(3): p. 404-15.
163. Leitner, A., et al., *The molecular architecture of the eukaryotic chaperonin TRiC/CCT.* Structure, 2012. **20**(5): p. 814-25.
164. Schmidt, C., et al., *Comparative cross-linking and mass spectrometry of an intact F-type ATPase suggest a role for phosphorylation.* Nat Commun, 2013. **4**: p. 1985.
165. Erzberger, J.P., et al., *Molecular architecture of the 40SeIF1eIF3 translation initiation complex.* Cell, 2014. **158**(5): p. 1123-35.
166. Shi, Y., et al., *Structural characterization by cross-linking reveals the detailed architecture of a coatomer-related heptameric module from the nuclear pore complex.* Mol Cell Proteomics, 2014. **13**(11): p. 2927-43.
167. Zeng-Elmore, X., et al., *Molecular Architecture of Photoreceptor Phosphodiesterase Elucidated by Chemical Cross-Linking and Integrative Modeling.* J Mol Biol, 2014.
168. Walden, H., M.S. Podgorski, and B.A. Schulman, *Insights into the ubiquitin transfer cascade from the structure of the activating enzyme for NEDD8.* Nature, 2003. **422**(6929): p. 330-4.
169. Xing, W., et al., *SCF(FBXL3) ubiquitin ligase targets cryptochromes at their cofactor pocket.* Nature, 2013. **496**(7443): p. 64-8.
170. Zheng, N., et al., *Structure of the Cul1-Rbx1-Skp1-F boxSkp2 SCF ubiquitin ligase complex.* Nature, 2002. **416**(6882): p. 703-9.
171. Busino, L., et al., *SCFFbxl3 controls the oscillation of the circadian clock by directing the degradation of cryptochrome proteins.* Science, 2007. **316**(5826): p. 900-4.
172. Godinho, S.I., et al., *The after-hours mutant reveals a role for Fbxl3 in determining mammalian circadian period.* Science, 2007. **316**(5826): p. 897-900.
173. Siepka, S.M., et al., *Circadian mutant Overtime reveals F-box protein FBXL3 regulation of cryptochrome and period gene expression.* Cell, 2007. **129**(5): p. 1011-23.
174. Wu, K., A. Chen, and Z.Q. Pan, *Conjugation of Nedd8 to CUL1 enhances the ability of the ROC1-CUL1 complex to promote ubiquitin polymerization.* J. Biol. Chem., 2000. **275**(41): p. 32317-32324.
175. Schmidt, M. and D. Finley, *Regulation of proteasome activity in health and disease.* Biochim Biophys Acta, 2014. **1843**(1): p. 13-25.
176. Scott, D.C., et al., *Structure of a RING E3 trapped in action reveals ligation mechanism for the ubiquitin-like protein NEDD8.* Cell, 2014. **157**(7): p. 1671-84.
177. Fischer, L., Z.A. Chen, and J. Rappsilber, *Quantitative cross-linking/mass spectrometry using isotope-labelled cross-linkers.* J Proteomics, 2013. **88**: p. 120-8.
178. Boutilier, J.M., et al., *Chromatographic behaviour of peptides following dimethylation with H2/D2-formaldehyde: implications for comparative proteomics.* J Chromatogr B Analyt Technol Biomed Life Sci, 2012. **908**: p. 59-66.

179. Ross, P.L., et al., *Multiplexed protein quantitation in Saccharomyces cerevisiae using amine-reactive isobaric tagging reagents.* Mol Cell Proteomics, 2004. **3**(12): p. 1154-69.
180. Dayon, L., et al., *Relative quantification of proteins in human cerebrospinal fluids by MS/MS using 6-plex isobaric tags.* Anal Chem, 2008. **80**(8): p. 2921-31.
181. McAlister, G.C., et al., *Increasing the multiplexing capacity of TMTs using reporter ion isotopologues with isobaric masses.* Anal Chem, 2012. **84**(17): p. 7469-78.
182. Isasa, M., et al., *Multiplexed, Proteome-Wide Protein Expression Profiling: Yeast Deubiquitylating Enzyme Knockout Strains.* J Proteome Res, 2015. **14**(12): p. 5306-17.
183. Ting, L., et al., *MS3 eliminates ratio distortion in isobaric multiplexed quantitative proteomics.* Nat Methods, 2011. **8**(11): p. 937-40.
184. McAlister, G.C., et al., *MultiNotch MS3 enables accurate, sensitive, and multiplexed detection of differential expression across cancer cell line proteomes.* Anal Chem, 2014. **86**(14): p. 7150-8.
185. Erickson, B.K., et al., *Evaluating multiplexed quantitative phosphopeptide analysis on a hybrid quadrupole mass filter/linear ion trap/orbitrap mass spectrometer.* Anal Chem, 2015. **87**(2): p. 1241-9.
186. Whiteaker, J.R., et al., *Peptide Immunoaffinity Enrichment and Targeted Mass Spectrometry Enables Multiplex, Quantitative Pharmacodynamic Studies of Phospho-Signaling.* Mol Cell Proteomics, 2015. **14**(8): p. 2261-73.
187. Frost, D.C., T. Greer, and L. Li, *High-resolution enabled 12-plex DiLeu isobaric tags for quantitative proteomics.* Anal Chem, 2015. **87**(3): p. 1646-54.
188. Kane, R.C., et al., *Velcade: U.S. FDA approval for the treatment of multiple myeloma progressing on prior therapy.* Oncologist, 2003. **8**(6): p. 508-13.
189. Ceccarelli, D.F., et al., *An allosteric inhibitor of the human Cdc34 ubiquitin-conjugating enzyme.* Cell, 2011. **145**(7): p. 1075-87.
190. Spratt, D.E. and G.S. Shaw, *Association of the disordered C-terminus of CDC34 with a catalytically bound ubiquitin.* J Mol Biol, 2011. **407**(3): p. 425-38.
191. Kleiger, G., et al., *Rapid E2-E3 assembly and disassembly enable processive ubiquitylation of cullin-RING ubiquitin ligase substrates.* Cell, 2009. **139**(5): p. 957-68.
192. Spratt, D.E., et al., *Selective recruitment of an E2~ubiquitin complex by an E3 ubiquitin ligase.* J Biol Chem, 2012. **287**(21): p. 17374-85.
193. Kawakami, T., et al., *NEDD8 recruits E2-ubiquitin to SCF E3 ligase.* EMBO J., 2001. **20**(15): p. 4003-12.
194. Huang, H., et al., *E2 enzyme inhibition by stabilization of a low-affinity interface with ubiquitin.* Nat Chem Biol, 2014. **10**(2): p. 156-63.
195. Chen, Z.A., et al., *Architecture of the RNA polymerase II-TFIIF complex revealed by cross-linking and mass spectrometry.* Embo J, 2010. **29**(4): p. 717-726.
196. Liu, J. and R. Nussinov, *Rbx1 Flexible Linker Facilitates Cullin-RING Ligase Function Before Neddylation and After Deneddylation.* Biophys J, 2010. **99**(3): p. 736-44.
197. Xiang, F., et al., *N,N-dimethyl leucines as novel isobaric tandem mass tags for quantitative proteomics and peptidomics.* Anal Chem, 2010. **82**(7): p. 2817-25.
198. Thompson, A., et al., *Tandem mass tags: a novel quantification strategy for comparative analysis of complex protein mixtures by MS/MS.* Anal Chem, 2003. **75**(8): p. 1895-904.